NMR AS A TOOL TO QUANTITATIVELY CHARACTERIZE MOLECULAR MECHANISMS GOVERNING ACTIN DYNAMICS AND RICE LATERAL ROOT DEVELOPMENT

A Dissertation

Presented to the Faculty of the Graduate School

of Cornell University

In Partial Fulfillment of the Requirements for the Degree of

Doctor of Philosophy

by

Lucila Andrea Acevedo

August 2018

NMR AS A TOOL TO QUANTITATIVELY CHARACTERIZE MOLECULAR MECHANISMS GOVERNING ACTIN DYNAMICS AND RICE LATERAL ROOT DEVELOPMENT

Lucila Andrea Acevedo, Ph. D.

Cornell University 2018

Protein-Protein interactions are fundamental for varied biological processes. These interactions are governed by different forces between the proteins, which result in a wide range of interaction strengths. Nuclear Magnetic Resonance (NMR) is an atomistic technique commonly used to understand protein-protein interaction mechanisms, especially weak interactions (K_D>μM). In this work, two different biological systems are studied by NMR. The first system that was studied is related to two proteins involved in cytoskeleton dynamics and cell migration, and the second is related to an enzyme-substrate interaction that controls a gene transcription regulation circuit.

In the first case, a novel mechanism for protein-protein interaction between the Ena/VASP Homology 1 (EVH1) domain of the actin polymerize regulator Vasodilator-Stimulated phosphoprotein (VASP) and the cytoskeleton protein Zyxin was determined. This interaction is important for cellular shape, cell motility and stress fiber repair. This study presented a model for a mechanism of action where phosphorylation can act as a stoichiometric switch and can explain the importance of the phosphorylation cycle in the localization of VASP by Zyxin.

The second protein-protein interaction focuses on the prolyl isomerase enzyme LRT2 (lateral rootless2) acting on the repressor protein OsIAA11. This interaction is critical for lateral root initiation in rice. The mechanism of action for this process is through the regulation of the *cis-trans* isomerization of the well conserved ^{104}Trp-Pro^{105} peptide bond in OsIAA11. OsIAA11 plays a role in repressing gene expression in a manner dependent on the amount of the phytohormone Auxin. At high Auxin concentration, OsIAA11 is specifically degraded in the *cis* conformation of the ^{104}W-P^{105} peptide bond. Thus, studies of LRT2 catalysis of OsIAA11 isomerization are essential to understand this fundamental biological process. In this dissertation, the microscopic equilibrium and rate constants of the LRT2 enzymatic cycle acting on OsIAA11 were determined by NMR lineshape analysis and validated by independent NMR exchange measurements. We found that LRT2 is optimally tuned for supplying maximum OsIAA11 in the *cis* isomer into a slower degradation pathway. Moreover, these studies predict that the catalyzed exchange rate is insensitive to concentrations of OsIAA11 at cellular conditions but scales lineally to the LRT2 concentration.

BIOGRAPHICAL SKETCH

Lucila Andrea Acevedo Charry (Andrea) did her undergraduate studies at the National University of Colombia, where she received her B.S. in physics in 2011. At the National University of Colombia, Andrea explored many fields in physics, but her interest sparked during a computer sciences class, where molecular physics was introduced. Under supervision of Professor Ramiro Cardona Cardona, she simulated how geometrical differences in a carbon nanotube could affect its interaction with water molecules for her undergraduate thesis. However, she soon came to realize that for her proteins were the most interesting molecules to study. From this experience and her passion for biochemistry, she found that the structure and dynamics of proteins would be her core research topic.

In 2011, she graduated from college and immigrated to the U.S.A. looking for a brighter future, access to leading-edge research opportunities and to support her husband during his PhD. In order to strengthen her training in biological sciences she obtained an Associate Degree in Biotechnology at Tompkins County Community College. During this time, she was a peer tutor for math, sciences, and Spanish. She also volunteered at professor Robert Oswald's lab at Cornell University and acquired critical wet lab experience.

She joined the Biophysics PhD program at Cornell University in 2014 with a Dean's Excellence Fellowship. Excited to start her work, Andrea contacted Professor Linda Nicholson to do a pay rotation during the summer of 2014. During this rotation Andrea was introduced to Nuclear Magnetic Resonance (NMR) as a tool to understand protein-protein interactions. She enjoyed learning about NMR and decided to join Professor Nicholson lab in January 2015. Some of her work during her time at the Nicholson Lab is described in this dissertation. Andrea received the support of the National Institutes of Health under Ruth L. Kirschstein National Research Service

Award (6T32GM008267) from the National Institute of General Medical Sciences as trainee from August 2015 to 2018.

Andrea is devoted to promoting diversity in the sciences. She constantly shared her time in the lab with being involved and outspoken about this topic. Additionally, Andrea is passionate about teaching basic science concepts to the general public and has participated in several outreach programs while enrolled at Cornell. She is committed to continuing such activities in her future.

To my life companion, Jorge, and my family for always believing in me and supporting me with great love. In loving memory of my mom, Sonia I. Charry B., for her extraordinary example, love, kindness, and cheerfulness.

ACKNOWLEDGMENTS

First, I would like to thank my advisor, Linda Nicholson, for her support and guidance over the years. I am grateful for the many conversations we had about science and many other subjects. I had a great experience during my graduate studies and this is certainly due to Linda's guidance, attention, and the interesting projects that I was able to work on. She supported my ideas, many applications, necessary breaks from the lab, as well as my involvement in outreach. Thanks to her support, I did great advancements during this time, while traveling around the world to meet scientists, learn biophysical techniques, and experience other cultures. Her enthusiasm and interest in my future has built up my confidence and inspired me to keep growing as a scientist and as a human being.

I would also like to thank my committee members, Holger Sondermann and Robert Oswald, for their support on my projects, and on my professional development. I am grateful of having learned so much from them during the short times I worked at their labs, our conversations, as well as many insightful ideas, tips for publishing, and telling good scientific stories and more. I am also grateful to the members in their labs who were great mentors, and lab mates who always made me feel welcomed.

I would like to thank all the previous and current members in the Nicholson Lab. Especially Ross Resnick, Monique Rogals, Carolyn Fischer, Nathan Korson, and Josephine Gonzales, they created a great atmosphere of collaboration that made me enjoy coming to work every day. I also want to thank Alex Greenwood and Jeahoo Kwon for making key advancement in the projects I worked on. I want to thank undergraduates and rotation students who allow me to be their mentor. In particularly, undergraduate student Tori Knapp, who I am fortunate enough to now call friend.

I want to thank the Cornell graduate school staff and the Diversity Program in Engineering staff who opens their doors not only to engineers, but anyone who seeks

their help and support. I have used many of their services during my time at Cornell, as Sara Hernandez says: “nobody goes through a PhD by themselves” In particularly, Sara Hernandez, Jami Joyner, Colleen McLinn, Anitra Douglas-McCarthy, Alyssa Lopez, Michelle Cox, Jan E Allen, and Christine Holmes. My great experience at Cornell is partially due to be able to be myself and to receive great support on career development, and many times, meaningful food that allowed me to keep going.

I would like to thank my many friends during these years, especially to those who help me to feel like I was at home. “Las chicas” (Irma Fernandez, Josephine Gonzales, Mariela Núñez, Azul Pinochet, Oriana Teran), together we built an extended family in Ithaca to share our frustrations, foods, visions, and love. “Latin roots” dancers who took time of their busy schedule to practice and learn together how to perform wonderful dances, and showing to the Ithaca Community that we are also talented outside of academia. Many student organizations that let me be part of them such as: The Colombian Students Association (CUCSA), the Latina/o Graduate Student Coalition (LGSC), Graduates Employing Empathy, Knowledge and Services (GEEKS) and the chapter of the Society for Advancing Chicanos/Hispanics and Native Americans in Sciences (SACNAS).

I would like to thank those who are not physically present in Ithaca but with their long-distance love and support make my life experiences wonderful. Particularly, my family who texts me every day with a “good morning” and keep reminding me that life is more than just work. As well as, many other friends: Distance might keep us apart, but support and love keeps us close.

Last but definitely not least, I would like to thank my husband, Jorge Chaves. There are not enough words to say thank you for all these 12 years together. You and Lupe were the main reasons why I enjoyed my time in Ithaca. I am looking forward to what the future holds for us.

TABLE OF CONTENTS

CHAPTER 1

INTRODUCTION

Proline, the unique amino acid

Amino acids are the building blocks of proteins and therefore of functional biology. Traditionally, there is a set of 20 common amino acids that are incorporated into proteins. Different characteristics can be given to each amino acid type. One amino acid that stands out for its importance in protein architecture is Proline. Proline differs from the others in the fact that its side chain is bound covalently to both the carbon alpha and the nitrogen in the amino group (Figure 1.1a). This cyclic arrangement is important for the structure of proteins, since proline has a remarkably distinct range of allowed conformations, an outcome of the fixed φ dihedral angle of $-60^{o} \pm 15^{o}$ (Creighton, 1993). It is known that proline is unique because the Gibbs free energy for the *trans* isomer (omega torsion angle ω=180°) of the peptidyl-prolyl bond can be similar to the *cis* isomer (ω=0°) which can be used for specific recognition in biological processes. In this dissertation we discuss two cases in which proline has important biological implications. In the first case, the implication of having closely placed poly-proline motifs in a sequence was investigated in the context of a known biological interaction. In the second case, the rate of catalyzed isomerization of a specific peptidyl-prolyl bond regulates a biological process.

Proline lacks a free amide to stabilize an α-helix or beta sheet secondary structure and the bulkiness of the $N\text{-}CH_2$ group restricts the conformation of the preceding residue, thus making proline even less likely to form an α-helix structure

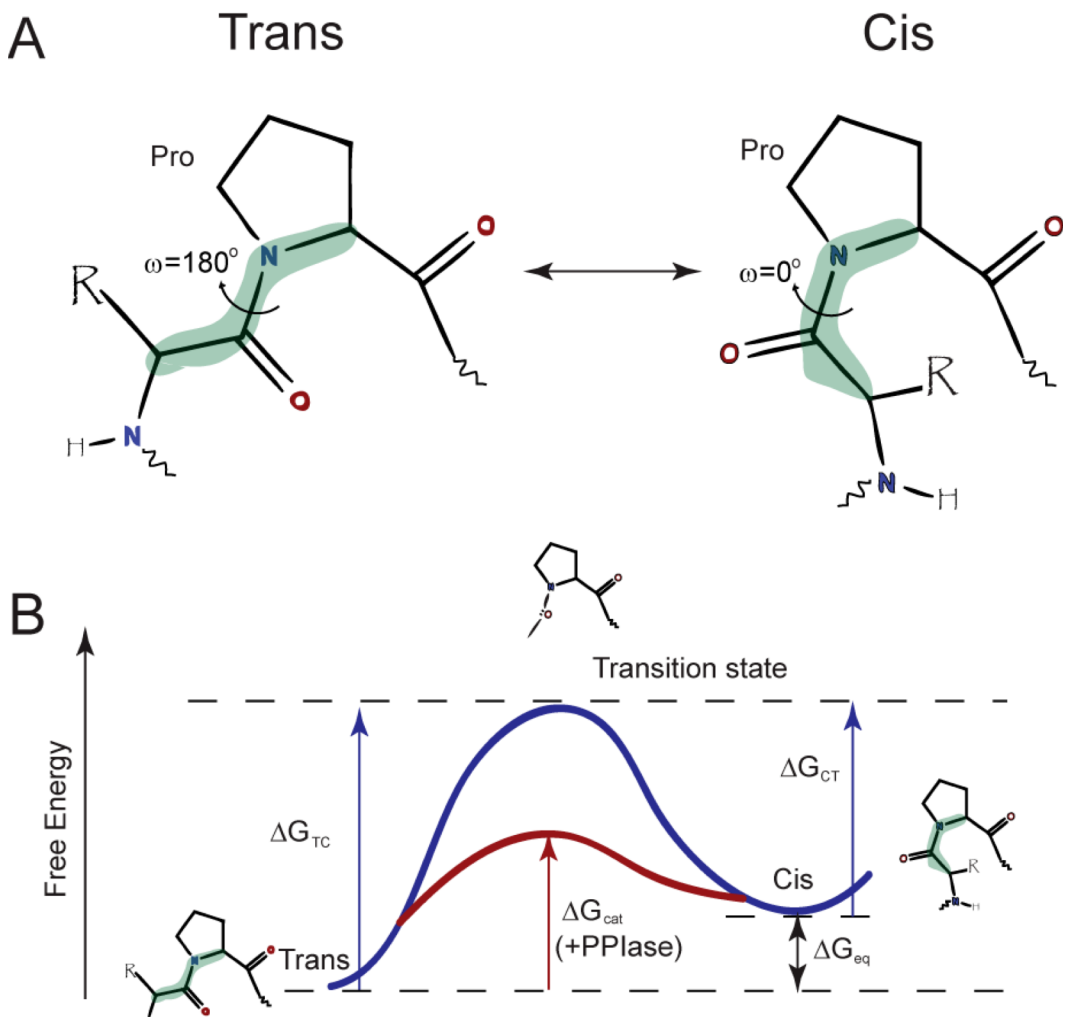

Figure 1.1 A. Structure of X-Proline dipeptide segment. Conformation of the peptidyl prolyl bond in either *Trans*, or *Cis*. R can be any side chain. In the *trans* isomer $\omega=180^{o}$, while in the *cis* isomer $\omega=0^{o}$.**B. Energy diagram for prolyl cis-trans isomerization.** The intrinsic (uncatalyzed) pathway (in blue) has a higher energy barrier than the PPIase catalyzed pathway (in red).

(Richardson, 1981). This restriction makes proline ideal to be part of secondary structures such as type I, II, III, and VIa β-turns and type II poly-prolyl helices (Creighton, 1993). In the case of tandem proline rich repeats, the most stable secondary structure is either the polyproline helix type II (PPII) or type I (Steinberg *et al.*, 1960). For studies in aqueous solvent conditions, the PPII is preferable. This PPII secondary structure is characterized as being left handed. The PPII helix has 3 residues per turn and 3.1Å rise per residue while the α-helix has 3.6 residues per turn and 1.5Å rise per residue, making the PPII narrower and more extended than the α-helix (Creighton, 1993). Nevertheless, both structures are considered to be fairly rigid, which has implications on the thermal resistance of proteins and functionality of protein-protein interactions (Karshikoff *et al.*, 2015). The PPII helix is used in protein-protein (Siligardi *et al.*, 1995; KAY *et al.*, 2000) and protein-nucleic acid (Hicks *et al.*, 2004) interactions. In this dissertation, we discuss the case where multiple poly-proline motifs tandem in the cytoskeleton protein Zyxin have an important role in governing interaction with the Ena/VASP Homology 1 (EVH1) domain of the actin polymerize Vasodilator-Stimulated phosphoprotein (VASP) in Chapter 2.

Another interesting case where proline has importance in biological systems is where the *cis-trans* isomerization can play a role in a biological process. The *cis* isomer of the peptide bond in Xaa-nonPro is found only in about 0.03% of Xaa-nonPro peptide bonds, while the *cis* isomer of the peptide bond in Xaa-Pro is found in 5% of the Xaa-Pro cases. These statistics were found in a study using 571 proteins structures extracted from the Brookhaven protein data base. The authors recognize that this study could be biased since many *cis* peptide bonds could have been unnoticed due to limitations in the

resolution of the structure and refinement protocols (Weiss *et al.*, 1998). However, it is well known that the *cis* isomer of the peptidyl prolyl bond is stabilized by favorable interactions between aromatic groups and the proline ring (W. J. Wu *et al.*, 1998). Nuclear Magnetic Resonance (NMR) spectroscopy studies of a small synthetic peptide Ac-Ala-Trp-Pro-Ala-Lys-NH2 show an equilibrium *cis* population of 38% of the Trp-Pro peptide bond in this unconstrained peptide in aquous solution (Reimer *et al.*, 1998). In data base studies of known protein structures the Trp-Pro *cis* was found in almost 13% of the Trp-Pro peptide bonds (Reimer *et al.*, 1998). Even though both isomers of the peptide bond can exist at similar energetic state, there is a large energetic barrier between the two isomers, with activation energy on the order of 20kcal/mol (Grathwohl *et al.*, 1981) (Figure 1.1b). The rate of interconversion is also dependent on the solvent used in the study, where for non-polar solvent the rate is higher (Y. K. Kang, 2002). For the unassisted case, the isomerization would take minutes or even hours, often making this a rate-limiting step in biological pathways (Fischer *et al.*, 2004). This highlights the necessity of isomerases to accelerate the isomerization transition. In Chapters three to five, we present the case of a Peptidyl-Prolyl *Cis/trans* Isomerase (PPIase) in rice that regulates the level of a key transcription regulator that can fine tune the initiation of lateral root development.

Poly-proline motifs

As mentioned before, poly-proline motifs are typically found in a PPII structure. This structure is usually solvent exposed, which offers an advantage for rapid and reversible binding as well as for presenting backbone carbonyl groups as accessible hydrogen bond acceptors (Siligardi *et al.*, 1995).

In the case of proline rich regions in proteins, it has been suggested that those prolines form a PPII structure (Williamson, 1994). Proline-rich regions bind to multiple proteins and domains, such as Src-homology 3 (SH3) (Yu *et al.*, 1994;Musacchio *et al.*, 1994; and WW Nguyen *et al.*, 1998) domains. It has been determined that some aromatic residues in these domains play a critical role in recognition of PPII (Yu *et al.*, 1994). In a similar way, the EVH1 domain of VASP was proposed to bind to proline rich regions since some of the aromatic residues are conserved, and it was found that indeed the ActA FPPPP motifs binds to the EVH1 domain in a PPII conformation, and aromatic residues in the EVH1 binding surface play an important role in this binding (Carl *et al.*, 1999). There are several binding partners for EVH1 that contains poly-proline motifs such as Zyxin (Drees *et al.*, 2000), ActA (Machner *et al.*, 2001), Lamellipodin (Matthias Krause *et al.*, 2004), Lipoma Prefered Partner (Petit *et al.*, 2000), Vinculin (Harbeck *et al.*, 2000), and Migfilin (Zhang *et al.*, 2006). This opened the question about how selective EVH1 might be toward these different binding partners that have conserved poly-prolyl motifs. In Chapter 2, we discuss this question.

Interaction of EVH1 with poly-prolyl motifs

VASP regulates the polymerization of actin and therefore plays an important role in cellular processes that involve the rearrangement of actin filaments, such as cell migration and cell shape (M. Krause *et al.*, 2003). The VASP structure is divided into three domains: The N-terminal EVH1 domain, the proline rich region and the C-terminal EVH2 domain. The EVH1 domain contributes to the localization of VASP in the cell by binding to the proline rich motif (W/F)PxφP (where x is any amino acid, φ is any aliphatic amino acid, and the motif sequence most commonly FPPPP). This motif

is found in several cytoskeleton proteins including Zyxin, Lamellipodin and Vinculin, as well as the ActA protein associated with the bacteria Listeria (Figure 1.2). The bacteria uses this interaction with VASP for efficient motility in the cell host (Lambrechts *et al.*, 2008). The proline rich domain of VASP is recognized to facilitate actin polymerization by binding to profilin (Reinhard *et al.*, 1995). Profilin binds directly to actin recruiting it to form the actin filaments (Gunning *et al.*, 2015). The EVH2 domains contains a G and F actin binding site (GAB and FAB respectively) and a coiled-coil at the very end of the C-terminus that serves as a tetramerization domain (Kühnel *et al.*, 2004). Hence, the VASP structure is set up to dynamically polymerize actin in regions where it is needed (Bear *et al.*, 2009).

VASP is regulated by multiple phosphorylation events. For instance, Protein Kinase A (PKA) and Protein Kinase G (PKG) mediated phosphorylation of Ser157 changes the subcellular localization of VASP, from being primarily in stress fibers to concentrating at focal adhesions in mouse endothelial cells (Benz *et al.*, 2009). PKA and PKG also mediate phosphorylation at Ser239, which impairs VASP-driven actin filament formation, which curiously, has the same effect as AMPK mediated phosphorylation at Thr278 (Benz *et al.*, 2009). Residue S157 is located between the EVH1 domain and the proline rich region, while S239 and T278 are both located in the EVH2 domain. Importantly for this dissertation, phosphorylation in the EVH1 domain also occurs. Abl tyrosine kinase mediated phosphorylation at Y39 influences VASP localization in leukemic cells, and binding to the cytoskeleton protein Zyxin is diminished (Maruoka *et al.*, 2012).

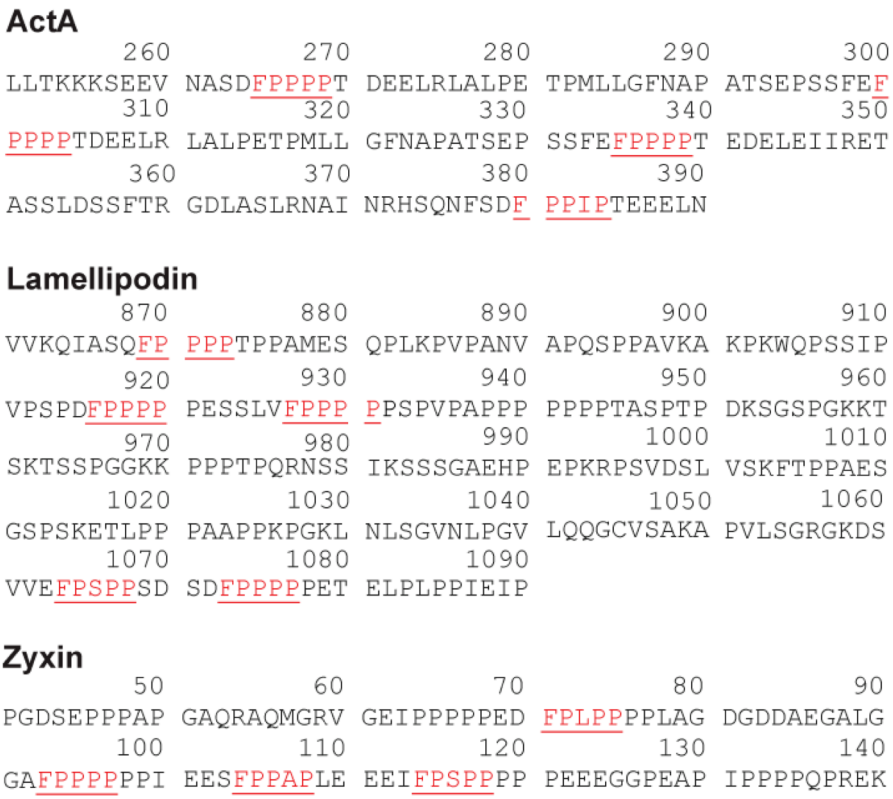

Figure 1.2 Sequences of binding partners to EVH1 domain of VASP. Highlighted in red is the FPxφP motifs in the sequence of ActA, Lamellipodin and Zyxin, which would bind to the EVH1 domain.

NMR studies have mapped the binding site in EVH1, where prominent aromatic and polar residues (M14, Y16, W23, F79, Q81) play a role in binding to the FPPPP motif (Ball *et al.*, 2000). Interestingly, many of the partner proteins of EVH1 contain multiple proline motifs that match the consensus sequence for EVH1 binding. For example, Zyxin has four binding motifs while lamellipodin has five (Figure 1.2). However, binding affinities to the EVH1 domain for individual FPPPP motifs are weak (K_D on the order of 100μM (Ball *et al.*, 2000)), and because VASP is a tetramer, it was expected that there is an avidity effect that increases the affinity between VASP and its partner (Zimmermann *et al.*, 2002). In Chapter 2, we report the NMR-derived binding affinities of the individual motifs in Zyxin as individual peptides and of the full proline rich sequence of Zyxin that contains the four-binding motifs, providing insights regarding the possible biological importance of having multiple proline motifs in one binding partner.

Cis-trans isomerization of the X-P peptide bond has important biological role

As mentioned earlier X-Pro peptide bonds can exist in *cis* and *trans* isomers with a *cis* population higher than that of any other peptide combination. One of the characteristic of these conformations that stand out is that the X-Pro *trans* isomer is quasi planar, where some *cis* X-Pro peptide bonds are highly non-planar (Galat *et al.*, 1998). The structural difference of the isomers creates a specificity for binding with a wide number of proteins hence resulting in a wide number of functions. In this section, we discuss some functions of this peptide bond and, more importantly, how these functions are regulated.

The isomer state of X-pro is crucial for appropriate folding. For instance, bovine pancreatic ribonuclease A (RNase A) has essential X-pro motifs that control the rates of folding to the native structure depending on the isomer state (Wedemeyer *et al.*, 2002). It is thought that for this and other reasons, a diverse group of proteins have evolved to catalyze the *cis/trans* isomerization of X-Pro peptide bonds. These proteins are called Peptidyl-prolyl *cis/trans* isomerases (PPIases) (Fischer *et al.*, 2004).

PPIases are abundant and ubiquitous proteins with a wide phylogenetic distribution (Galat *et al.*, 1998). PPIases have a variety of functions in the cell including: protein folding, stress response, immunosuppression, channel gating, cellular receptors, cell surface binding, chemotaxis, allergic inflammation, DNA binding, Nuclease activity, gene transcription, cell cycle, and more (Galat *et al.*, 1998). In this introduction I focus my discussion on the functions of protein folding, stress response and gene transcription.

With regard to protein folding, some PPIases are crucial for appropriate folding and stability of proteins *in vitro* (Fischer *et al.*, 1985; Gething *et al.*, 1992; Lorenz *et al.*, 2008) and *in vivo*. *In vivo*, final folding and assembly occurs in the lumen of the endoplasmic reticulum (ER). The ER of mammalian cells contains a high level of two PPIases, cyclophilin-B and FKBP-13, and a variety of other PPIases (Zapun *et al.*, 1999). Several studies have confirmed the direct involvement of PPIases in protein folding (Bose *et al.*, 1994; Matouschek *et al.*, 1995; Rassow *et al.*, 1995), making PPIases important chaperones in folding and stability of proteins.

As specific examples of this chaperone role, the expressions of certain PPIases are induced by different stress conditions and play important roles in regulating the

proteome. The level or mRNA of Cyclophilin A and B in yeast increase in response to heat, and disruption to these genes makes yeast more sensitive to a rise in temperature (Sykes *et al.*, 1993). PPIase FkpA improves the biomass yield in *C. glutaicum* at increased growth temperature, a biotech application for the production of the flavor-enhancing amino acid L-glutamate and feed additive L-lysine (Kallscheuer *et al.*, 2015). Another stress condition that elevated the levels of PPIase was the treatment of tunicamycin or A23187 (a Ca^{2+} ionophore). Tunicamycin inhibits the N-linked glycosylation of proteins, and A23187 depletes the cellular reserves of Ca^{2+}. Bush *et al* treated Madin-Darby canine kidney (MDCK) cells with either tunicamycin or A23187. In both cases the mRNA encoding the PPIase FKBP-13 increases (2 and 5 fold respectively) (Bush *et al.*, 1994). In more recent studies, FKBP-13 is suggested to be a protein chaperone that delivers misfolded ER clients to ER-associated degradation, to reduce the proteotoxic stress in ER (Jeong *et al.*, 2017), which explains why it might be important for FKBP-13 to increase under stress conditions (Bush *et al.*, 1994). Together these studies show examples of the importance of increasing the expression of some PPIases under stress conditions, where their chaperone function are needed to assist in the clearance of misfolded proteins.

Finally, there are numerous examples of PPIases that play key regulatory roles in the transcription of genes. These examples include: remodeling RNA-protein complexes during gene expression (Thapar, 2015), controlling transcription regulatory proteins (Hanes, 2015), regulation of RNA polymerase II (pol II) by direct binding to the carboxyl terminal Domain of Rpb1, the largest subunit of pol II (Hani *et al.*, 1999; X. Wu *et al.*, 2000), and alteration of chromatin assembly (Dilworth *et al.*, 2012). In

summary, these studies and reviews show that PPIases can regulate gene transcription at multiple levels.

Chapter 3 to 5 of this dissertation focus on the study of the interaction of a PPIase and its binding partner that contains an X-P epitope important for the degradation pathway of this protein. Interestingly, the target protein for isomerization is a transcription repressor protein that is essential for regulation of specific genes.

Importance of Prolyl Peptidyl Isomerases in the Auxin Circuit.

Auxin is one of the five classes of plant hormone (Davies, 2007). Auxin signaling controls a variety of developmental processes in plants such as cell elongation, bud formation, root initiation, cell division and others (Normanly *et al.*, 2010; Enders *et al.*, 2015). Dynamic regulation is achieved through ubiquitin-mediated proteasomal degradation of the Auxin/Indole-3-Acetic Acid (Aux/IAA) transcription repressor proteins via a negative feedback loop that controls the expression of specific genes (Dinesh *et al.*, 2016). Aux/IAA proteins are short-lived nuclear proteins that have four conserved domains (I through IV) (Abel *et al.*, 1995). Since, domain II is responsible for rapid degradation of Aux/IAA proteins, it is considered the degron domain (Worley *et al.*, 2000). OsIAA11 is one of 31 Aux/IAA proteins in rice (Jain *et al.*, 2006). The *cis* peptide bond of the W-P motif in the degron domain of Aux/IAA is specifically recognized by its cognate E3 ubiquitin ligase enzyme to undergo degradation via the ubiquitin mediated proteasomal pathway (Tan *et al.*, 2007). For OsIAA11, the *trans/cis* isomerization is controlled by LRT2 (Jing *et al.*, 2015), a PPIase that is classified as a cyclophilin (Kumari *et al.*, 2009). This system is the perfect case to study the importance

of rate regulation through isomerase activity and its effects in plant development, a biological process with well-defined output.

Auxin regulates gene expression in developmental processes through the well-studied auxin circuit (Figure 1.3). One of the transcription regulators in plants for development processes is the Aux/IAA repressor protein family (Dinesh *et al.*, 2016). The levels of proteins in this family are highly affected by auxin concentration in the cell. Consequently, the auxin circuit responds to the amount of auxin in the cell. In short, when low concentration of auxin is present in the nucleus, the Aux/IAA binds to the Auxin Responsive Factors (ARF) which at the same time bind to the promoter of the Aux/IAA gene. When Aux/IAA is bound to ARF on the promoter, the transcription activator Auxin Responsive Element (ARE) is repressed, and the expression of Aux/IAA is blocked (Dinesh *et al.*, 2016). Therefore, at low concentrations of auxin there is no expression of Aux/IAA and other genes involved in developmental processes that are controlled by the same promoter (Davies, 2007). However, when there is an increase of auxin in the cell, the degradation of Aux/IAA through the 26s proteasome is activated and the released ARF can then activate the promoter for expression of Aux/IAA and other genes involved in developmental processes (Dinesh *et al.*, 2016). To understand the role of PPIases in the circuit, it is important to understand the mechanism of recognition in the degradation pathway. The Arabidopsis $SCF^{TIR1\text{-}AFB}$ (SKP1, Cullin, F-box protein) complex that mediates entry into the proteasomal degradation pathway has been structurally elucidated by X-ray crystallography (Tan *et al.*, 2007). The SCF complex is an E3 ubiquitin ligase. In this case, the F-box is

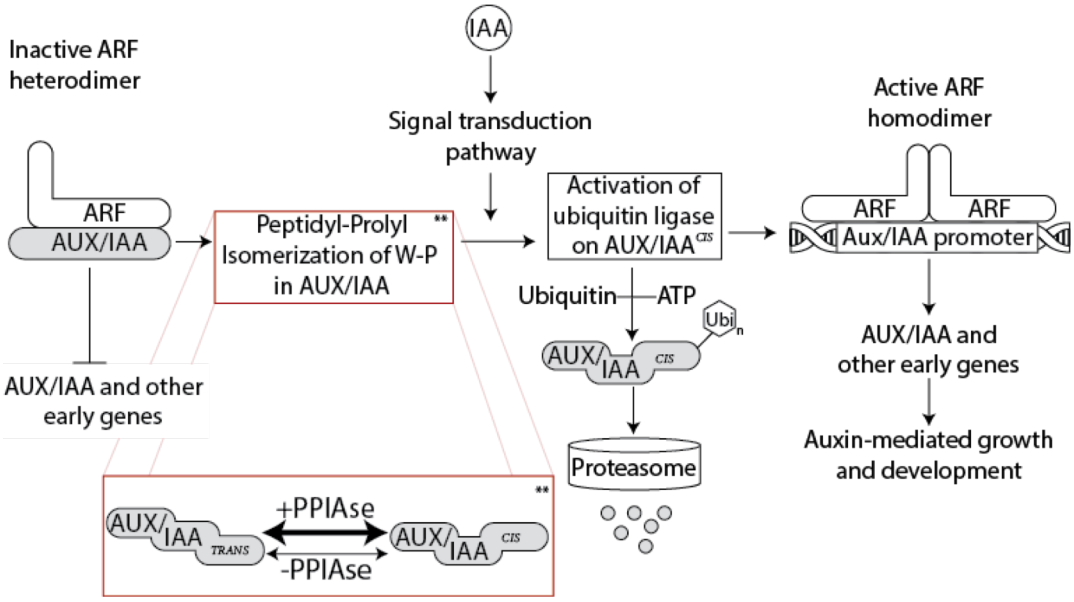

Figure 1.3 Auxin Circuit model. based on Gray *et al.*, 2001 and Su *et al.*, 2015**.** In general, the auxin response factor (ARF), forms inactive heterodimers with AUX/IAA repressor proteins coded by AUX/IAA genes. These heterodimers prevent the transcription of the early auxin genes as well as AUX/IAA genes. In the presence of auxin (IAA), AUX/IAA proteins bind to their cognate E3 ligase and are ubiquitylated and are thereby targeted for destruction by the proteasome. This IAA induces degradation of the AUX/IAA proteins and allows the formation of active ARF homodimers. The active ARF homodimer then promotes expression of early genes and AUX/IAA repressor proteins. Transcription of the early genes initiates the auxin-induced growth. Ubiquitin ligase only recognizes the *cis* isomer of AUX/IAA proteins making a Peptidyl-Prolyl Isomerization step important in the Auxin Circuit (red box). In the case of rice lateral root initiation, the AUX/IAA protein is OsIAA11, and the Peptidyl-Prolyl Isomerase is LRT2.

identified as TIR1 (Transport inhibitor Response1). The crystal structure of the F-Box bound to the degron peptide of IAA7 (conserved through Aux/IAA families) shows a *cis* specific recognition of the peptide bond between the Tryptophan and its following Proline (Tan *et al.*, 2007). This interaction depends on auxin, where auxin acts like a "glue molecule" by filling a gap of the recruitment target box in the Leucine Rich Repeat (LRR) domain in TIR1. Therefore, auxin creates a continuous hydrophobic protein interaction surface allowing the degron domain of Aux/IAA to be recognized for ubiquitination in the rest of the Aux/IAA. The proteasomal complex as well as the SCF^{TIR1} complex have homologs in rice and it is accepted that auxin regulates through this pathway the Aux/IAA family in rice (Nakamura *et al.*, 2008). Moreover, IAA3 and IAA12 in Arabidopsis are poly-ubiquitinated and degraded in response to increase of auxin or TIR1 levels (Dos Santos Maraschin *et al.*, 2009) showing that this system is in general for Aux/IAA proteins. The specific recognition of the *cis* isomer of Aux/IAA proteins means that only the *cis* population of the total Aux/IAA protein can be degraded, and that PPIase activity is necessary for complete degradation of the Aux/IAA proteins in a timely manner.

In vivo and *in vitro* evidence show that LRT2 is the cyclophilin acting in the auxin circuit that functions for lateral root initiation. Mutation screening looking for reduced sensitivity to external auxin 1-Naphthaleneacetic acid (NAA) found two mutant lines. These mutants were selected by the lack of lateral roots, insensitivity to exogenous auxin, and low fertility. Both are single nucleotide mutations, where one has a premature stop codon in LRT2 (called Cyp2-1) that shortens the LRT2 by 21 residues, and the other has a glycine to alanine change in amino acid 72 (Cyp 2-2) (B. Kang *et al.*, 2013).

Also, another genetic screen for auxin-resistant mutants showed a mutant with defective lateral root development. Analysis of the gene confirmed a 50 base-pair deletion in LRT2 (Zheng *et al.*, 2013). Moreover, mutation of Proline 106 to Leucine in OsIAA11 showed a remarkable reduction of lateral root number, an increase in auxin-resistance and a reduction in response to gravity (Zhu *et al.*, 2012). All these mutations show an effect at the initialization phase of lateral root development. The fact that these mutations in two different proteins create the same phenotype suggests that they are acting in the same developmental pathway. Furthermore, LRT2 truncation shows a reduction of degradation of OsIAA11-GFP in protoplasts (B. Kang *et al.*, 2013). This confirms a link in the cell between LRT2 and OsIAA11. It has been reported recently that LRT2 catalyzes isomerization of the degron peptide in OsIAA11, an observation made by the application of NMR (Jing *et al.*, 2015).

Additionally, LRT2 was upregulated during salt-induced stress conditions (Ruan *et al.*, 2011) and studies of LRT2 using a yeast model showed that the inclusion of LRT2 improves the cell growth in stress conditions making it a "suitable candidate" for generation of transgenic plants with abiotic stress tolerance (Kumari *et al.*, 2009). Together, these studies confirm that LRT2 is induced to express under stress conditions, and the fact that it can catalyze a key step in the auxin circuit caught our attention to perform molecular studies aiming to quantify the catalytic cycle for this enzyme-substrate pair and to investigate the impact of this isomerization rate on the auxin circuit and eventually on the initiation of lateral roots directly in the plant.

Experimental approach

The experimental approach in this dissertation is based mostly on protein-protein or protein-peptide interaction observed by NMR spectroscopy. NMR spectroscopy is a powerful atomistic technique to observe local magnetic fields around atomic nuclei. NMR is a strong tool to measure characteristics of biological processes *in vitro*[1](Kleckner *et al.*, 2011). For proteins, the NMR-active nuclei of interest are the 1/2 spin isotopes: ^{1}H, ^{13}C, ^{15}N and ^{31}P which have a dipolar magnetic moment, as well as the nuclei with a spin 1: ^{2}H which has dipolar and quadrupolar moments. The non-naturally abundant isotopes ^{13}C, ^{15}N and ^{2}H can be introduced isotropically to the protein or selectively to specific locations in the protein. Typically, in solution NMR, a soluble protein with a concentration between 0.1-5.0 mM is loaded in a glass tube with volume between 300-600 μL, which is then placed in a strong magnetic field B_0. The bulk magnetic moment of the NMR-active spins prefers to align to the B_0 field (in the z axis of the lab frame). A pulsed of oscillating magnetic field is applied in the x-y plane in the lab frame and subsequently spin precession is allowed to evolve.

The free induction decay (FID) is generated by the precession of nuclear spins, and is recorded at the end of each scan through a given pulse sequence. The observed FID is the sum of the individual FID for each nucleus, which oscillates at a characteristic frequency. The strength of the signal is dependent on the population difference between excited and ground nuclear spin states, which is extremely small. Hence, higher concentration is necessary for signal accumulation. Additionally, signal accumulation

[1] Recent advancements of In-cell NMR has been reported (see Luchinat *et al.*, 2017 for a review on this). For this dissertation, all NMR experiments were performed *in vitro*.

is increased by repeating the identical pulse sequence several times and summing the resulting FIDs (i.e., by signal averaging). The FID loses coherence over time in an inverse exponential way, with a transverse relaxation rate constant R_2 (inverse of the time constant T_2). The intensity of the FID behaves as $I(t)=\exp(-R_2t)$. The FID is Fourier transformed from the time domain to the frequency domain. This process provides the observables of chemical shift ω, intensity *I*, and linewidth λ which can then be measure under different conditions.

The chemical shift is the position of the signal of any given nucleus in the frequency spectrum and reports on the chemical environment of the nucleus. The intensity is the height of the signal peak, and the linewidth is the full peak width at half the maximum signal intensity.

For this dissertation, we used NMR to monitor chemical exchange of nuclei between environments due to chemical reactions or conformational transitions. Chemical exchange can be measured when an NMR probe is exposed to at least two distinct chemical environments or states, for instance, bound to ligand and unbound, folded and unfolded, monomer and dimer, *cis* and *trans* isomer, etc. These can be very dynamic processes that occur in a time-dependent manner, that can correspond to an exchange regime of slow, fast or intermediate exchange. In a slow exchange process, both states are observed reflecting their chemical shifts, intensities and linewidths. From a physical perspective, both states are observed because the interconversion between state 1 and state 2 happens slowly compared to the chemical shift difference (in Hz) between the two states. Therefore, each site reports on the population of that respective species. In fast exchange only one signal is observed, reflecting the averaged chemical

environment, where the single peak has a chemical shift that corresponds to the population weighted average of the chemical shift of each state.

Heteronuclear single quantum coherence (HSQC) is a two-dimensional proton-detected experiment that shows a chemical shift correlation map between directly-bonded ^{1}H and X -heteronuclei (typically ^{13}C or ^{15}N). In proteins, in the case of ^{15}N since each peak represents a specific backbone amide or side chain amine, this experiment can be used to monitor specific chemical exchange processes on the labeled protein. A sequence of well-defined pulses is used to transfer the I spin polarization (I_z) into antiphase heteronuclear single-quantum (SQ) coherence ($2I_zS_y$). The set of pulses is called insensitive nuclei enhanced by polarization transfer (INEPT) (Morris *et al.*, 1979). After this, the antiphase heteronuclear SQ coherence evolves during the subsequent t_1 evolution period, which allows the chemical shift of the heteronucleus to be encoded. Since the detection is in the proton channel, a second INEPT pulse sequence is used to transfer the frequency encoded heteronuclear SQ coherence back to ^{1}H magnetization for detection. We have relied on protein titration using routine ^{15}N-^{1}H-HSQC spectra, where we pay attention to the binding curve trajectory. This allows us to measure moderate to weak binding affinities (K_D> 10uM) at the atomic scale (Carbajo *et al.*, 2013).

Lineshape Analysis is a well-established tool for studying protein interactions at the microsecond to millisecond timescale using NMR (Gunther *et al.*, 2002). Classically this analysis is carried out on a 1D NMR spectrum, but through peak slice extraction, it has been used in 2D experiments (Greenwood *et al.*, 2011). In the studies presented in this dissertation, we used a new software tool (TITAN) that allows for lineshape analysis

directly in 2D experiments (Waudby *et al.*, 2016). Lineshape analysis is performed usually by recording a series of spectra where some physical variable is introduced, in our case unlabeled binding partner protein concentration. In this series of spectra, the data are fitted to the equations governing evolution of magnetization (Binsch, 1969 ; McConnell, 1958) to determine unknown parameters such as the exchange rates between different states and the equilibrium constants between states that characterize the reaction.

For the study of isomerization, we mostly have used EXchange SpectroscopY (EXSY), or ZZ-exchange and Rotating frame Overhause Effect SpectroscopY (ROESY). ZZ-exchange experiment requires a unique signal for each state. Therefore, these experiments can only be performed with slow exchange reactions. ZZ-exchange experiments monitor the exchange of longitudinal magnetization. Since for this experiment, the populations are directly quantified from peak intensity, the recovery time must be longer than the relaxation time T_1 to restore Boltzmann equilibrium magnetization. If this is not the case, then the signal decays due to relaxation being faster than population transfer (Cavanagh *et al.*, 2010). Longitudinal relaxation is much slower for ^{13}C and ^{15}N than for ^{1}H, and their signal is not affected by ^{1}H-^{1}H cross-relaxation, so often isotopically enriched samples are used to perform this type of experiment.

In a two-state case as in *cis-trans* isomerization, cross-peaks (or exchange peaks) are observed. Their intensity can be observed at $T_{mix}=0$, and a series of 2D spectra can be recorded at different values of mixing time T_{mix} (10-5,000ms) which generates "build-up curves" (Figure 1.4). The intensity curves behave according to the following equations (Farrow *et al.*, 1994)

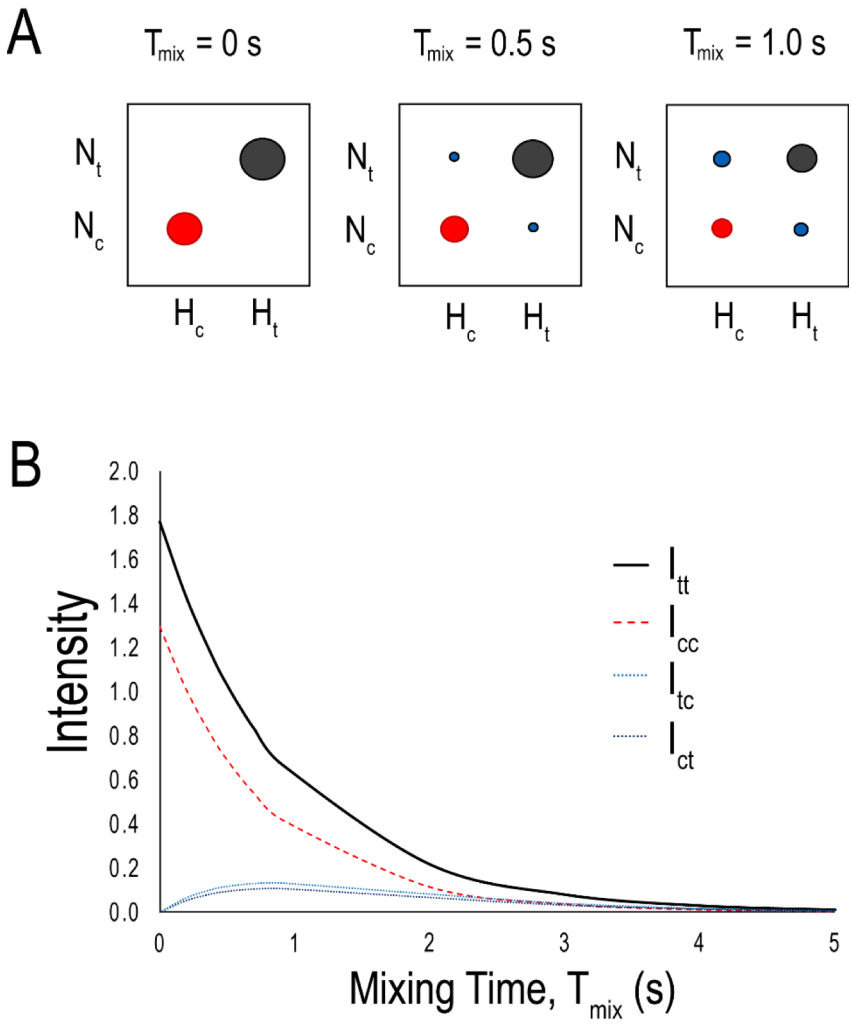

Figure 1.4 The EXSY or ZZ-exchange experiment is used to quantify exchange kinetics. A. At the beginning of the experiment the only two frequencies occupied are the ones labels for the population *trans* isomer (H_t, N_t) and population in the *cis* isomer (H_c, N_c). As time pass, cross peaks intensities build up, showing the interconversion from *trans* to *cis* (H_t, N_c) and from *cis* to *trans* (H_c, N_t). **B.** The "build-up curves" are shown for an exchanging system with an equilibrium constant of 1.1 and isomerization rate of $0.5s^{-1}$.

$$I_{tt} = \left(I_t(0)\left(-(\lambda_2 - a_{11})e^{-\lambda_1 T_{mix}} + (\lambda_1 - a_{11})e^{-\lambda_2 T_{mix}}\right)\right)/(\lambda_1 - \lambda_2)$$

$$I_{cc} = \left(I_c(0)\left(-(\lambda_2 - a_{22})e^{-\lambda_1 T_{mix}} + (\lambda_1 - a_{22})e^{-\lambda_2 T_{mix}}\right)\right)/(\lambda_1 - \lambda_2)$$

$$I_{tc} = \left(I_t(0)\left(a_{21}e^{-\lambda_1 T_{mix}} - a_{21}e^{-\lambda_2 T_{mix}}\right)\right)/(\lambda_1 - \lambda_2)$$

$$I_{ct} = \left(I_c(0)\left(a_{12}e^{-\lambda_1 T_{mix}} - a_{12}e^{-\lambda_2 T_{mix}}\right)\right)/(\lambda_1 - \lambda_2)$$

where $\lambda_{1,2} = \frac{-(a_{11}+a_{22})\pm\sqrt{(a_{11}-a_{22})^2-4k_{ct}k_{tc}}}{2}$, $a_{11} = R_t + k_{tc}$, $a_{12} = -k_{ct}$, $a_{21} = -k_{tc}$, $a_{22} = R_c + k_{ct}$. R_t and R_c are the longitudinal relaxation rates in magnetization for the *trans* and *cis* state. $I_t(0)$ and $I_c(0)$ denote the intensity of the *trans* and *cis* peak at mixing time, T_{mix}=zero. k_{tc} and k_{ct}, denote the exchange rates. This set of equations can be used to fit the intensity data for the auto-peaks and exchange-peaks by a least-square fitting process to obtain the exchange rates.

For small peptides the use of homonuclear methods such as Rotating frame Overhause Effect SpectroscopY (ROESY) allows the study of exchange transitions (Bothner-By *et al.*, 1984). This type of experiment is analyzed in a similar way as for the ZZ-exchange experiment, in this case though, the transverse magnetization is observed instead of the longitudinal magnetization. The Nicholson lab has used this approach for the determination of the complete thermodynamic cycle for the catalytic domain of another PPIase, Pin 1 (Greenwood *et al.*, 2011). In Chapter 4, we show the use of ROESY and ZZ-exchange experiments to confirm the isomerization rates found by line-shape analysis for the thermodynamic cycle of LRT2 acting on OsIAA11. Additionally, we discuss some mutants of LRT2 that change the isomerization rates in Chapter 5.

In conclusion, this dissertation shows the use of NMR to study two interesting biological interactions where proline is the target for binding. In one case, we discuss the advantage of having multiple proline motifs to enhance binding, and report the discovery of a secondary binding site that is regulated by phosphorylation. This secondary binding site can have implications in the stoichiometry of the reaction. In the other case, we report the complete thermodynamic and kinetic characterization of the catalyzed isomerization of a specific W-P epitope with known biological importance, and additionally report the generation and testing of several mutants of this isomerase that tune the isomerization reaction to slower rates.

REFERENCES

Abel, S., Nguyen, M. D., & Theologis, A. (1995). The PS-IAA4/5-like Family of Early Auxin-inducible mRNAs in Arabidopsis thaliana. *Journal of <olecular Biology, 251*(4), 533-549.

Ball, L. J., Kuhne, R., Hoffmann, B., Hafner, A., Schmieder, P., Volkmer-Engert, R., . . . Jarchau, T. (2000). Dual epitope recognition by the VASP EVH1 domain modulates polyproline ligand specificity and binding affinity. *EMBO J, 19*(18), 4903-4914. doi:10.1093/emboj/19.18.4903

Bear, J. E., & Gertler, F. B. (2009). Ena/VASP: towards resolving a pointed controversy at the barbed end. *J Cell Sci, 122*(Pt 12), 1947-1953. doi:122/12/1947 [pii] 10.1242/jcs.038125

Benz, P. M., Blume, C., Seifert, S., Wilhelm, S., Waschke, J., Schuh, K., . . . Renne, T. (2009). Differential VASP phosphorylation controls remodeling of the actin cytoskeleton. *J Cell Sci, 122*(Pt 21), 3954-3965. doi:10.1242/jcs.044537

Binsch, G. (1969). Unified theory of exchange effects on nuclear magnetic resonance line shapes. *J Am Chem Soc, 91*(6), 1304-1309. doi:10.1021/ja01034a007

Bose, S., & Freedman, R. B. (1994). Peptidyl prolyl cis-trans-isomerase activity associated with the lumen of the endoplasmic reticulum. *Biochem J, 300 (Pt 3)*, 865-870.

Bothner-By, A. A., Stephens, R. L., Lee, J., Warren, C. D., & Jeanloz, R. W. (1984). Structure determination of a tetrasaccharide: transient nuclear Overhauser effects in the rotating frame. *J Am Chem Soc, 106*(3), 811-813. doi:10.1021/ja00315a069

Bush, K. T., Hendrickson, B. A., & Nigam, S. K. (1994). Induction of the FK506-binding protein, FKBP13, under conditions which misfold proteins in the endoplasmic reticulum. *Biochem J, 303 (Pt 3)*, 705-708.

Carbajo, R. J., & Neira, J. L. (2013). *NMR for Chemists and Biologists*: Springer Netherlands.

Carl, U. D., Pollmann, M., Orr, E., Gertlere, F. B., Chakraborty, T., & Wehland, J. (1999). Aromatic and basic residues within the EVH1 domain of VASP specify its interaction with proline-rich ligands. *Curr Biol, 9*(13), 715-718.

Cavanagh, J., Fairbrother, W. J., Palmer, A. G., Skelton, N. J., & Rance, M. (2010). *Protein NMR Spectroscopy: Principles and Practice*: Elsevier Science.

Creighton, T. E. (1993). *Proteins: Structures and Molecular Properties*: W. H. Freeman.

Davies, P. J. (2007). *Plant Hormones: Biosynthesis, Signal Transduction, Action!* New York: Springer.

Dilworth, D., Gudavicius, G., Leung, A., & Nelson, C. J. (2012). The roles of peptidyl-proline isomerases in gene regulation. *Biochem Cell Biol, 90*(1), 55-69. doi:10.1139/o11-045

Dinesh, D. C., Calderon Villalobos, L. I. A., & Abel, S. (2016). Structural Biology of Nuclear Auxin Action. *Trends in Plant Science, 21*(4), 302-316.

Dos Santos Maraschin, F., Memelink, J., & Offringa, R. (2009). Auxin-induced, SCF/TIR1-mediated poly-ubiquitination marks AUX/IAA proteins for degradation. *The Plant Journal, 59*(1), 100-109.

Drees, B., Friederich, E., Fradelizi, J., Louvard, D., Beckerle, M. C., & Golsteyn, R. M. (2000). Characterization of the interaction between zyxin and members of the Ena/vasodilator-stimulated phosphoprotein family of proteins. *J Biol Chem, 275*(29), 22503-22511. doi:10.1074/jbc.M001698200

Enders, T., & Strader, L. C. (2015). Auxin Activity: Past, Present, and Future. *American Journal of Botany 102*(2), 180-196.

Farrow, N. A., Zhang, O., Forman-Kay, J. D., & Kay, L. E. (1994). A heteronuclear correlation experiment for simultaneous determination of 15N longitudinal decay and chemical exchange rates of systems in slow equilibrium. *J Biomol NMR, 4*(5), 727-734.

Fischer, G., & Aumüller, T. (2004). Regulation of peptide bond cis/trans isomerization by enzyme catalysis and its implication in physiological processes *Rev Physiol Biochem Pharmacol* (pp. 105-150). Berlin, Heidelberg: Springer Berlin Heidelberg.

Fischer, G., & Bang, H. (1985). The refolding of urea-denatured ribonuclease A is catalyzed by peptidyl-prolyl cis-trans isomerase. *Biochim Biophys Acta, 828*(1), 39-42.

Galat, A., & Riviére, S. (1998). *Peptidyl-prolyl Cis/trans Isomerases*: Oxford University Press.

Gething, M.-J., & Sambrook, J. (1992). Protein folding in the cell. *Nature, 355*(6355), 33-45.

Grathwohl, C., & Wüthrich, K. (1981). Nmr studies of the rates of proline cis–trans isomerization in oligopeptides. *Biopolymers, 20*(12), 2623-2633. doi:10.1002/bip.1981.360201209

Gray, W. M., Kepinski, S., Rouse, D., Leyser, O., & Estelle, M. (2001). Auxin regulates SCFTIR1-dependent degradation of AUX/IAA proteins. *Nature, 414*, 271. doi:10.1038/35104500

Greenwood, A. I., Rogals, M. J., De, S., Lu, K. P., Kovrigin, E. L., & Nicholson, L. K. (2011). Complete determination of the Pin1 catalytic domain thermodynamic cycle by NMR lineshape analysis. *J Biomol NMR, 51*(1-2), 21-34. doi:10.1007/s10858-011-9538-9

Gunning, P. W., Ghoshdastider, U., Whitaker, S., Popp, D., & Robinson, R. C. (2015). The evolution of compositionally and functionally distinct actin filaments. *Journal of Cell Science, 128*(11), 2009.

Gunther, U. L., & Schaffhausen, B. (2002). NMRKIN: simulating line shapes from two-dimensional spectra of proteins upon ligand binding. *J Biomol NMR, 22*(3), 201-209.

Hanes, S. D. (2015). Prolyl isomerases in gene transcription. *Biochim Biophys Acta, 1850*(10), 2017-2034. doi:10.1016/j.bbagen.2014.10.028

Hani, J., Schelbert, B., Bernhardt, A., Domdey, H., Fischer, G., Wiebauer, K., & Rahfeld, J. U. (1999). Mutations in a peptidylprolyl-cis/trans-isomerase gene lead to a defect in 3'-end formation of a pre-mRNA in Saccharomyces cerevisiae. *J Biol Chem, 274*(1), 108-116.

Harbeck, B., Huttelmaier, S., Schluter, K., Jockusch, B. M., & Illenberger, S. (2000). Phosphorylation of the vasodilator-stimulated phosphoprotein regulates its interaction with actin. *J Biol Chem, 275*(40), 30817-30825. doi:10.1074/jbc.M005066200

Hicks, J. M., & Hsu, V. L. (2004). The extended left-handed helix: a simple nucleic acid-binding motif. *Proteins, 55*(2), 330-338. doi:10.1002/prot.10630

Jain, M., Kaur, N., Garg, R., Thakur, J. K., Tyagi, A. K., & Khurana, J. P. (2006). Structure and expression analysis of early auxin-responsive Aux/IAA gene family in rice (Oryza sativa). *Functional and Integrative Genomics, 6*(1), 47-59.

Jeong, M., Jang, E., Choi, S. S., Ji, C., Lee, K., & Youn, J. (2017). The Function of FK506-Binding Protein 13 in Protein Quality Control Protects Plasma Cells from Endoplasmic Reticulum Stress-Associated Apoptosis. *Front Immunol, 8*, 222. doi:10.3389/fimmu.2017.00222

Jing, H., Yang, X., Zhang, J., Liu, X., Zheng, H., Dong, G., . . . Zuo, J. (2015). Peptidyl-prolyl isomerization targets rice Aux/IAAs for proteasomal degradation during auxin signalling. *Nature communications, 6*, 7395-7405.

Kallscheuer, N., Bott, M., van Ooyen, J., & Polen, T. (2015). Single-Domain Peptidyl-Prolyl cis/trans Isomerase FkpA from Corynebacterium glutamicum Improves the Biomass Yield at Increased Growth Temperatures. *Appl Environ Microbiol, 81*(22), 7839-7850. doi:10.1128/aem.02113-15

Kang, B., Zhang, Z., Wang, L., Zheng, L., Mao, W., Li, M., . . . Mo, X. (2013). OsCYP2, a chaperone involved in degradation of auxin-responsive proteins, plays crucial roles in rice lateral root initiation. *Plant J, 74*(1), 86-97.

Kang, Y. K. (2002). Cis−Trans Isomerization and Puckering of Pseudoproline Dipeptides. *The Journal of Physical Chemistry B, 106*(8), 2074-2082. doi:10.1021/jp013608i

Karshikoff, A., Nilsson, L., & Ladenstein, R. (2015). Rigidity versus flexibility: the dilemma of understanding protein thermal stability. *FEBS Journal, 282*(20), 3899-3917. doi:10.1111/febs.13343

KAY, B. K., WILLIAMSON, M. P., & SUDOL, M. (2000). The importance of being proline: the interaction of proline-rich motifs in signaling proteins with their cognate domains. *The FASEB Journal, 14*(2), 231-241.

Kleckner, I. R., & Foster, M. P. (2011). An introduction to NMR-based approaches for measuring protein dynamics. *Biochim Biophys Acta, 1814*(8), 942-968. doi:10.1016/j.bbapap.2010.10.012

Krause, M., Dent, E. W., Bear, J. E., Loureiro, J. J., & Gertler, F. B. (2003). Ena/VASP proteins: regulators of the actin cytoskeleton and cell migration. *Annu Rev Cell Dev Biol, 19*, 541-564. doi:10.1146/annurev.cellbio.19.050103.103356

Krause, M., Leslie, J. D., Stewart, M., Lafuente, E. M., Valderrama, F., Jagannathan, R., . . . Gertler, F. B. (2004). Lamellipodin, an Ena/VASP Ligand, Is Implicated in the Regulation of Lamellipodial Dynamics. *Developmental Cell, 7*(4), 571-583. doi:https://doi.org/10.1016/j.devcel.2004.07.024

Kühnel, K., Jarchau, T., Wolf, E., Schlichting, I., Walter, U., Wittinghofer, A., & Strelkov, S. V. (2004). The VASP tetramerization domain is a right-handed coiled coil based on a 15-residue repeat. *Proc Natl Acad Sci U S A, 101*(49), 17027-17032. doi:10.1073/pnas.0403069101

Kumari, S., Singh, P., Singla-Pareek, S. L., & Pareek, A. (2009). Heterologous Expression of a Salinity and Developmentally Regulated Rice Cyclophilin Gene (OsCyp2) in E. coli and S. cerevisiae confers Tolerance Towards multiple abiotic Stresses. *Mol Biotechnol, 42*, 195-204.

Lambrechts, A., Gevaert, K., Cossart, P., Vandekerckhove, J., & Van Troys, M. (2008). *Listeria* comet tails: the actin-based motility machinery at work. *Trends in Cell Biology, 18*(5), 220-227. doi:10.1016/j.tcb.2008.03.001

Lorenz, T., & Reinstein, J. (2008). The influence of proline isomerization and off-pathway intermediates on the folding mechanism of eukaryotic UMP/CMP Kinase. *J Mol Biol, 381*(2), 443-455. doi:10.1016/j.jmb.2008.06.001

Luchinat, E., & Banci, L. (2017). In-cell NMR: a topical review. *IUCrJ, 4*(Pt 2), 108-118. doi:10.1107/S2052252516020625

Machner, M. P., Urbanke, C., Barzik, M., Otten, S., Sechi, A. S., Wehland, J., & Heinz, D. W. (2001). ActA from Listeria monocytogenes can interact with up to four Ena/VASP homology 1 domains simultaneously. *J Biol Chem, 276*(43), 40096-40103. doi:10.1074/jbc.M104279200

Maruoka, M., Sato, M., Yuan, Y., Ichiba, M., Fujii, R., Ogawa, T., . . . Watanabe, N. (2012). Abl-1-bridged tyrosine phosphorylation of VASP by Abelson kinase impairs association of VASP to focal adhesions and regulates leukaemic cell adhesion. *Biochem J, 441*(3), 889-899. doi:BJ20110951 [pii] 10.1042/BJ20110951

Matouschek, A., Rospert, S., Schmid, K., Glick, B. S., & Schatz, G. (1995). Cyclophilin catalyzes protein folding in yeast mitochondria. *Proc Natl Acad Sci U S A, 92*(14), 6319-6323.

McConnell, H. M. (1958). Reaction Rates by Nuclear Magnetic Resonance. *jcp, 28*, 430-431. doi:10.1063/1.1744152

Morris, G. A., & Freeman, R. (1979). Enhancement of nuclear magnetic resonance signals by polarization transfer. *J Am Chem Soc, 101*(3), 760-762. doi:10.1021/ja00497a058

Musacchio, A., Saraste, M., & Wilmanns, M. (1994). High-resolution crystal structures of tyrosine kinase SH3 domains complexed with proline-rich peptides. *Nat Struct Biol, 1*(8), 546-551.

Nakamura, A., & Matsuoka, M. (2008). Auxin Signaling in Rice *Rice Biology in the Genomics Era* (pp. 129-131). Tokyo: Springer.

Nguyen, J. T., Turck, C. W., Cohen, F. E., Zuckermann, R. N., & Lim, W. A. (1998). Exploiting the basis of proline recognition by SH3 and WW domains: design of N-substituted inhibitors. *Science, 282*(5396), 2088-2092.

Normanly, J., Slovin, J. P., & Cohen, J. D. (2010). Auxin Biosynthesis and Metabolism. In P. J. Davies (Ed.), *Plant Hormones: Biosynthesis, Signal Transduction, Action!* (pp. 36-62). Dordrecht: Springer Netherlands.

Petit, M. M., Fradelizi, J., Golsteyn, R. M., Ayoubi, T. A., Menichi, B., Louvard, D., . . . Friederich, E. (2000). LPP, an actin cytoskeleton protein related to zyxin, harbors a nuclear export signal and transcriptional activation capacity. *Mol Biol Cell, 11*(1), 117-129.

Rassow, J., Mohrs, K., Koidl, S., Barthelmess, I. B., Pfanner, N., & Tropschug, M. (1995). Cyclophilin 20 is involved in mitochondrial protein folding in cooperation with molecular chaperones Hsp70 and Hsp60. *Mol Cell Biol, 15*(5), 2654-2662.

Reimer, U., Scherer, G., Drewello, M., Kruber, S., Schutkowski, M., & Fischer, G. (1998). Side-chain effects on peptidyl-prolyl cis/trans isomerisation. *J Mol Biol, 279*(2), 449-460. doi:10.1006/jmbi.1998.1770

Reinhard, M., Giehl, K., Abel, K., Haffner, C., Jarchau, T., Hoppe, V., . . . Walter, U. (1995). The proline-rich focal adhesion and microfilament protein VASP is a ligand for profilins. *The EMBO Journal, 14*(8), 1583-1589.

Richardson, J. S. (1981). The Anatomy and Taxonomy of Protein Structure. In C. B. Anfinsen, J. T. Edsall, & F. M. Richards (Eds.), *Advances in Protein Chemistry* (Vol. 34, pp. 167-339): Academic Press.

Ruan, S.-L., Ma, H.-S., Wang, S.-H., Fu, Y.-P., Xin, Y., Liu, W.-Z., . . . Chen, H.-Z. (2011). Proteomic identification of OsCYP2, a rice cyclophilin that confers salt tolerance in rice (Oryza sativa L.) seedlings when overexpressed. *BMC Plant Biology, 11*, 34-34. doi:10.1186/1471-2229-11-34

Siligardi, G., & Drake, A. F. (1995). The importance of extended conformations and, in particular, the PII conformation for the molecular recognition of peptides. *Biopolymers, 37*(4), 281-292. doi:10.1002/bip.360370406

Steinberg, I. Z., Harrington, W. F., Berger, A., Sela, M., & Katchalski, E. (1960). The Configurational Changes of Poly-L-proline in Solution. *J Am Chem Soc, 82*(20), 5263-5279. doi:10.1021/ja01505a001

Su, S.-H., Gray, W. M., & Masson, P. H. (2015). Auxin: Shape matters. *Nature Plants, 1*, 15097. doi:10.1038/nplants.2015.97

Sykes, K., Gething, M. J., & Sambrook, J. (1993). Proline isomerases function during heat shock. *Proceedings of the National Academy of Sciences, 90*(12), 5853-5857.

Tan, X., Calderon-Villalobos, L. I. A., Sharon, M., Zheng, C., Robison, C. V., Estelle, M., & Zheng, N. (2007). Mechanism of auxin perception by the TIR1 ubiquitin ligase. *Nature, 446*(7136), 640-645.

Thapar, R. (2015). Roles of Prolyl Isomerases in RNA-Mediated Gene Expression. *Biomolecules, 5*(2), 974-999. doi:10.3390/biom5020974

Waudby, C. A., Ramos, A., Cabrita, L. D., & Christodoulou, J. (2016). Two-Dimensional NMR Lineshape Analysis. *Scientific Reports, 6*, 24826. doi:10.1038/srep24826 http://www.nature.com/articles/srep24826#supplementary-information

Wedemeyer, W. J., Welker, E., & Scheraga, H. A. (2002). Proline cis-trans isomerization and protein folding. *Biochemistry, 41*(50), 14637-14644.

Weiss, M. S., Jabs A Fau - Hilgenfeld, R., & Hilgenfeld, R. (1998). Peptide bonds revisited. (1072-8368 (Print)).

Williamson, M. P. (1994). The structure and function of proline-rich regions in proteins. *Biochemical Journal, 297*(Pt 2), 249-260.

Worley, C. K., Zenser, N., Ramos, J., Rouse, D., Leyser, O., Theologis, A., & Callis, J. (2000). Degradation of Aux/IAA proteins is essential for normal auxin signalling. *The plant Journal, 21*(6), 553-562.

Wu, W. J., & Raleigh, D. P. (1998). Local control of peptide conformation: stabilization of cis proline peptide bonds by aromatic proline interactions. *Biopolymers, 45*(5), 381-394. doi:10.1002/(SICI)1097-0282(19980415)45:5<381::AID-BIP6>3.0.CO;2-H

Wu, X., Wilcox, C. B., Devasahayam, G., Hackett, R. L., Arevalo-Rodriguez, M., Cardenas, M. E., . . . Hanes, S. D. (2000). The Ess1 prolyl isomerase is linked to chromatin remodeling complexes and the general transcription machinery. *EMBO J, 19*(14), 3727-3738. doi:10.1093/emboj/19.14.3727

Yu, H., Chen, J. K., Feng, S., Dalgarno, D. C., Brauer, A. W., & Schreiber, S. L. (1994). Structural basis for the binding of proline-rich peptides to SH3 domains. *Cell, 76*(5), 933-945.

Zapun, A., Jakob, C. A., Thomas, D. Y., & Bergeron, J. J. M. (1999). Protein folding in a specialized compartment: the endoplasmic reticulum. *Structure, 7*(8), R173-R182. doi:https://doi.org/10.1016/S0969-2126(99)80112-9

Zhang, Y., Tu, Y., Gkretsi, V., & Wu, C. (2006). Migfilin interacts with vasodilator-stimulated phosphoprotein (VASP) and regulates VASP localization to cell-matrix adhesions and migration. *J Biol Chem, 281*(18), 12397-12407. doi:10.1074/jbc.M512107200

Zheng, H., Li, S., Ren, B., Zhang, J., Ichii, M., Taketa, S., . . . Wang, H. (2013). LATERAL ROOTLESS2, a cyclophilin protein, regulates lateral root initiation and auxin signaling pathway in rice. *Molecular Plant, 6*(5), 1719-1721.

Zhu, Z.-X., Liu, Y., Liu, S.-J., Mao, C.-Z., Wu, Y.-R., & Wu, P. (2012). A gain-of-function mutation in OsIAA11 affects lateral root development in rice. *Molecular Plant, 5*(1), 154-161.

Zimmermann, J., Labudde, D., Jarchau, T., Walter, U., Oschkinat, H., & Ball, L. J. (2002). Relaxation, Equilibrium Oligomerization, and Molecular Symmetry of the VASP (336-380) EVH2 Tetramer. *Biochemistry, 41*, 11143-11151.

CHAPTER 2

A Noncanonical Binding Site in the EVH1 Domain of VASP Regulates Its Interactions with the Proline Rich Region of Zyxin[2]

Abstract

Vasodilator stimulated phosphoprotein (VASP) is a processive actin polymerase with roles in the control of cell shape and cell migration. Through interaction with the cytoskeletal adaptor protein Zyxin, VASP can localize to damaged stress fibers where it serves to repair and reinforce these structures. VASP localization is mediated by its N-terminal Ena/VASP homology (EVH1) domain, which binds to the (W/F)PxφP motif (most commonly occurring as FPPPP) found in cytoskeletal proteins such as vinculin, lamellipodin, and Zyxin. Sequentially close clusters of four or five of these motifs frequently occur, as in the proline rich region of Zyxin with four such motifs. This suggests that tetrameric VASP might bind very tightly to Zyxin through avidity, with all four EVH1 domains binding to a single Zyxin molecule. Here, quantitative nuclear magnetic resonance titration analysis reveals a dominant bivalent 1:1 (Zyxin:EVH1) interaction between the Zyxin proline rich region and the VASP EVH1 domain that utilizes the EVH1 canonical binding site and a novel secondary binding site on the opposite face of the EVH1 domain. We further show that binding to the secondary binding site is specifically inhibited by mutation of VASP EVH1 domain residue Y39 to E, which mimics Abl-induced phosphorylation of Y39. On the basis of these findings,

[2] Reprinted with permission of Biochemistry ACS publications, 2017, volume 56, pages 4626-4636, "A Noncanonical Binding Site in the EVH1 Domain of VASP Regulates Its Interactions with the Proline Rich Region of Zyxin" by Lucila Andrea Acevedo, Alex I. Greenwood, and Linda K. Nicholson.

we propose a model in which phosphorylation of Y39 acts as a stoichiometry switch that governs binding partner selection by the constitutive VASP tetramer. These results have broader implications for other multivalent VASP EVH1 domain binding partners and for furthering our understanding of the role of Y39 phosphorylation in regulating VASP localization and cellular function.

Introduction[3]

The processive actin polymerase VASP (vasodilator-stimulated phosphoprotein) is an important regulator of the organization of the actin cytoskeleton (Breitsprecher *et al.*, 2008; Breitsprecher *et al.*, 2011; Krause *et al.*, 2003). VASP and its homologues Mena and Evl, are involved in the formation of lamellipodia (Bear *et al.*, 2002) and filopodia (Lebrand *et al.*, 2004; Mejillano *et al.*, 2004) as well as the cellular processes of phagocytosis (Coppolino *et al.*, 2001), cell migration (Bear *et al.*, 2000; Bear *et al.*, 2002; Krause *et al.*, 2003), and neuron axon guidance (Goh *et al.*, 2002). VASP functions both as an actin polymerase and as an anti-capping protein (Barzik *et al.*, 2005; Bear *et al.*, 2009; Bear *et al.*, 2002), by protecting the barbed end of actin filaments from capping proteins. VASP and its homologues localize to specific sites in the cell such as lamellipodia and filopodia as well as focal adhesions and sites of stress fiber damage (Hoffman *et al.*, 2012; Reinhard *et al.*, 1992; Rottner *et al.*, 1999; M. A. Smith *et al.*, 2010; Tokuo *et al.*, 2004) through binding to proline rich sequences with its EVH1 (Ena/VASP homology 1) domain (Ball *et al.*, 2000; Niebuhr *et al.*, 1997).

[3] This introduction section starting above and concluding on page 35, was written by Alexander I. Greenwood, and it appears in his Cornell dissertation dated January 2014 (Greenwood, 2014). It is used here with his permission as well as the approval of my special committee chair and special committee members.

In response to cell mechanical stress, VASP is recruited to actin stress fibers, where it serves to reinforce and repair these highly regulated contractile structures (M. A. Smith *et al.*, 2010). This is partially mediated by an interaction with Zyxin, a cytoskeletal protein involved in the mechanical stress response (Hoffman *et al.*, 2012; M. A. Smith *et al.*, 2010). Zyxin is phosphorylated at S142 in response to mechanical stimulation, which disrupts an inhibitory head tail intramolecular interaction (Call *et al.*, 2011; Moody *et al.*, 2009). Zyxin is then recruited to damaged stress fibers through an interaction between its LIM domains and unknown factors (M. A. Smith *et al.*, 2013). Simultaneously, S142-phosphorylated Zyxin binds via multiple binding motifs in its disordered N-terminus to the proteins VASP and α–actinin (Call *et al.*, 2011).

The interaction between VASP and Zyxin is mediated by both interactions between the N-terminal proline rich region of Zyxin and the EVH1 domain of VASP and an interaction between the LIM domain region of Zyxin and the proline rich region of VASP (Moody *et al.*, 2009). This allows the interaction to be regulated by phosphorylation at multiple sites. First, Zyxin can adopt an inhibited conformation in which its LIM domains obstruct its proline rich region, which can be destabilized by phosphorylation of S142 by Akt (Call *et al.*, 2011; Chan *et al.*, 2007; Moody *et al.*, 2009). Second, although the LIM-VASP interaction can overcome this inhibitory conformation, phosphorylation of VASP at S157 by PKA prevents this (Moody *et al.*, 2009). Third, phosphorylation of Y39 in the EVH1 domain of VASP by Abl inhibits its interaction with Zyxin (Maruoka *et al.*, 2012), though it is not clear why given the placement of Y39 far from the EVH1 canonical binding site (here termed the primary

binding site) known to bind the *Listeria monocytogenes* protein ActA (Prehoda *et al.*, 1999).

The VASP EVH1 domain binds the (W/F)PxφP motif, where x is any amino acid and φ is aliphatic (Ball *et al.*, 2000; Niebuhr *et al.*, 1997). This motif most frequently occurs as FPPPP and very often occurs in clusters of four or five motifs, as in the cytoskeletal proteins lamellipodin and Zyxin, and ActA. This is thought to be a mechanism for enhancing binding between VASP and its binding partners, by combining the individual affinities of each of the four EVH1 domains in a VASP tetramer (Zimmermann *et al.*, 2002). Indeed, deletions in the C-terminal region of the EVH2 domain in Ena (Ena-VASP homology 2 domain) inhibit tetramerization and impair its ability to bind Zyxin in cell lysates (Ahern-Djamali *et al.*, 1998) and to localize VASP to focal adhesions (Haffner *et al.*, 1995). Inconsistent with this, however are the facts that the EVH2 domain is dispensable for *Listeria* motility (Geese *et al.*, 2002) and that there seems to be a linear dependence of the rate of *Listeria* movement on the number of VASP binding sites in Act (G. A. Smith *et al.*, 1996). It has been proposed alternatively that a ligand molecule containing multiple FPPPP sites can be bound by multiple VASP tetramers, which would allow VASP to noncovalently cross-link its binding partners (Zimmermann *et al.*, 2002).

Here, we provide evidence that a secondary binding site is present in the VASP EVH1 domain. This secondary binding site interacts weakly with short peptides containing a single (W/F)PxφP motif but displays enhanced binding to a Zyxin fragment containing all four (W/F)PxφP motifs. This enhancement could be created by Zyxin wrapping around the EVH1 domain in analogy to the structures of the homologous

WASP-EVH1/WIP complexes (Peterson *et al.*, 2007; Volkman *et al.*, 2002 and RanBP2-RanBD1/RanVetter *et al.*, 1999). Analysis of nuclear magnetic resonance (NMR) titrations and of an EVH1 Zyxin chimera reveals a predominant orientation of the interaction, where the second FPPPP motif of Zyxin binds to the canonical binding site and a downstream region binds to the novel secondary binding site. This orientation was not observed when titrations were performed using the phosphomimetic EVH1 mutant Y39E, which demonstrates weakened or abolished binding at the secondary site. The secondary binding site influences the overall stoichiometry of the interaction between Zyxin and VASP, which provides insights regarding the effect of Y39 phosphorylation on the cellular localization of VASP.

Materials and Methods

Protein Purification

EVH1 protein was expressed from a pMW172 vector with the human VASP EVH1 domain encoded (gift from M. Way, London Research Institute, London, UK) to produce cleaved product consisting of EVH1 residues 2-115 with the non-native sequence GPGGRMS at the N-terminus. All proteins were expressed as previously described (Greenwood *et al.*, 2014). The Y39E EVH1 mutant was produced by using site-directed mutagenesis. A pDEST17 plasmid (ampicillin resistance) encoding human Zyxin residues 41-140, with an N-terminal six-His fusion and a TEV cleavage site, was produced using the GATEWAY cloning system (Thermo Fisher Scientific). The Zyxin$^{41\text{-}140}$ sequence was amplified from a RFP-Zyxin expression vector purchased from Addgene (Addgene plasmid 26720, Bhatt *et al.*, 2002). All were purified using native preparations as described previously (Greenwood *et al.*, 2014), and dialyzed into

NMR buffer [20 mM $KHPO_4$, 50 mM KCl (pH 6.7)] following cleavage and removal of the his tag. NMR samples also contained 5 mM NaN_3, 0.05% protease inhibitor cocktail (EDTA-free, Sigma), and 7% D_2O. Unlabeled $Zyxin^{41-140}$ protein used in the [^{15}N]-EVH1 titrations was concentrated to a volume of 600 µl and a sample of 300µl with 10mM DSS was subjected to a one-dimensional NMR experiment to determine by comparison to DSS the stock solution concentration. NMR samples were concentrated with 3000 MWC centrifugal concentrators. The protein concentration was determined by UV absorption at 280 nm, using the theoretical extinction coefficients of 21000 $cm^{-1}M^{-1}$ for VASP EVH1, 19500 $cm^{-1}M^{-1}$ for VASP EVH1 Y39E.

The EVH1 fusion protein with Zyxin was obtained by enzymatic digestion of the pMW172-EVH1 vector with EcoRI and BLP1. Polymerase chain reaction amplification from pDEST17-$Zyxin^{41-140}$ was performed to obtain the SSGSGGGG linker followed by $Zyxin^{82-124}$. After enzyme digestion, ligation to pMW172-EVH1 was performed using the ThermoScientific rapid ligation kit. Expression and purification were performed in the same way as they were for [^{15}N]EVH1 but using media enriched with [^{13}C]glucose.

Peptide Production

Synthetic peptides encompassing the individual motif in Zyxin, $Zyxin^{69-80}$, $Zyxin^{91-102}$, $Zyxin^{102-113}$ and $Zyxin^{112-123}$ were purchased from Genscript (Piscataway, NJ). Peptides were dissolved in NMR buffer, and their pHs were adjusted using NaOH. The peptide concentration was determined using the theoretical extinction coefficient 195 $cm^{-1}M^{-1}$ at 257 nm.

NMR Data Collection and Processing

NMR experiments were performed at 25 ºC using a Varian Inova 600 MHz spectrometer with a (H, C, N) Z-axis gradient probe. Spectra were processed with nmrPipe and analyzed with Sparky. Prior to Fourier transformation, [^{15}N]EVH1 data were processed with an exponential window function. Peak positions and volumes were measured using the Sparky peak detection function.

Resonance Assignments

Resonance assignments for the EVH1 domain were obtained from the BioMagResBank, accession number 18569 (Ball *et al.*, 2000), and incongruent assignments or residues near the N-terminus were clarified by three-dimensional (3D) TOCSY and NOESY spectra of [^{15}N]EVH1. Resonance assignments for the Y39E EVH1 mutant, and EVH1-Zyxin$^{82\text{-}124}$, were obtained by 3D TOCSY and NOESY.

NMR Titration Experiments

Five [^{15}N]EVH1-perspective HSQC and five [^{15}N]Y39E EVH1-perspective HSQC titration experiments were performed. In each experiment the sample with the highest concentration of Zyxin construct was produced first, and subsequent samples were produced by mixing part of the previous sample with a part of a stock of [^{15}N]EVH1 or [^{15}N]Y39E EVH1. The experiments were: titration of the [^{15}N]EVH1 domain with Zyxin$^{41\text{-}140}$, Zyxin$^{69\text{-}80}$, Zyxin$^{91\text{-}102}$, Zyxin$^{102\text{-}113}$ and Zyxin$^{112\text{-}123}$. In the Zyxin$^{41\text{-}140}$ titration, the [^{15}N]EVH1 concentration was held to 0.21 mM, and the Zyxin$^{41\text{-}140}$ concentrations were 0, 0.02, 0.03, 0.06, 0.13, 0.26, 0.52, and 1.03 mM. In the individual motif peptide titrations, the [^{15}N]EVH1 concentration was held at 0.18 mM for all of them. Concentrations of Zyxin$^{69\text{-}80}$ were 0, 0.15, 0.29, 0.59, 1.18, 2.35, 4.71, and 9.41 mM. In the Zyxin$^{91\text{-}102}$ titration the peptide concentrations were 0, 0.08,

0.17, 0.34, 0.67, 1.34, 2.68, and 5.36 mM. For Zyxin$^{102-113}$ the concentrations were 0, 0.14, 0.28, 0.56, 1.11, 2.22, and 4.45 mM and, for Zyxin$^{112-123}$, they were 0, 0.25, 0.51, 1.02, 2.03, and 4.07 mM. The experiments for the phosphomimetic mutant were: titrations of [^{15}N]EVH1 Y39E with Zyxin$^{41-140}$ titration in which the [^{15}N]EVH1 Y39E concentration was held to 0.23 mM and the Zyxin$^{41-140}$ concentrations were 0, 0.01, 0.03, 0.06, 0.12, 0.24, 0.49, and 0.97 mM. For the individual motif titrations, the [^{15}N]EVH1 Y39E concentration was held at 0.18 mM and concentrations of Zyxin$^{69-80}$ were 0, 0.04, 0.08, 0.15, 0.31, 0.61, 1.23, 2.46 and 4.92 mM. The concentrations of Zyxin$^{91-102}$ were 0, 0.10, 0.20, 0.40, 0.80, 1.60, 3.19, and 6.38 mM; those of Zyxin$^{102-113}$ were 0, 0.04, 0.08, 0.16, 0.32, 0.64, 1.28, 2.55, and 5.11 mM, and those of Zyxin$^{112-123}$ were 0, 0.09, 0.19, 0.37, 0.74, 1.49, 2.97, and 5.95 mM.

The [^{15}N]EVH1 and [^{15}N]EVH1 Y39E spectra were recorded with spectral widths of 8 kHz in the proton dimension (2048 complex data points) and 1.8 kHz in the nitrogen dimension (256 complex data points).

Quantification of Motif Binding in the Context of Zyxin$^{41-140}$

TITAN offers a wide range of binding models that can be used for two-dimensional line shape analysis (Waudby *et al.*, 2016). For [^{15}N]Y39E EVH1 titrated with individual motif peptides, we used the simple two-state interaction available in TITAN and simultaneously fit 10 peak profiles. Additionally, TITAN offers the flexibility of including personalized binding models. For the [^{15}N]EVH1 wild type titrated with individual motif peptides, we used the four-state binding model described in detail elsewhere (Rogals *et al.*, 2016), and fit 10 peak profiles in the primary binding site and six in the secondary binding site. Peaks included in these analyses were selected

on the basis of trajectories that displayed maximum Δδ values that exceeded the corresponding error in Δδ by a factor of at least 10. The error in Δδ was determined on the basis of peaks that were insensitive to ligand addition, where the average standard deviations of positions of these "invariant" peaks in each of the proton and nitrogen dimensions were taken as the chemical shift uncertainty for all peaks, and standard error propagation was applied to obtain the corresponding error in Δδ. TITAN also has the option for a model with flexible stoichiometry, which we used to analyze the titration of [^{15}N]EVH1 (WT/Y39E) titrated with Zyxin$^{41\text{-}140}$. An error analysis was performed using 200 repeats to determine the uncertainties of the fitting.

To approximate the distribution of bound motif populations at the primary site for the [^{15}N]EVH1 and [^{15}N]EVH1 Y39E cases at the highest Zyxin$^{41\text{-}140}$ concentration, an analysis of the observed chemical shift relative to the bound chemical shifts for each individual motif peptide was performed. An approximating assumption is that chemical shift perturbations in EVH1 due to binding of a given Zyxin motif are the same in the context of Zyxin$^{41\text{-}140}$ versus the individual motif peptide. For this analysis, the observed chemical shifts ($\Delta\delta_{obs}{}^{max}{}_i$) for 10 residues (separately analyzed in nitrogen and proton dimensions) for which the peak trajectory directions of individual motif titrations differed the most, were used to solve for the bound motif populations using the following equation:

$$\Delta\delta_{obs}{}^{max}{}_i = P_1 * \Delta\delta_{bound}{}^{M1}{}_i + P_2 * \Delta\delta_{bound}{}^{M2}{}_i + P_3 * \Delta\delta_{bound}{}^{M3}{}_i + P_4 * \Delta\delta_{bound}{}^{M4}{}_i + P_5 * \Delta\delta_{apo,i},$$

where P_1, P_2, P_3 and P_4 represent the populations of the EVH1 domain bound to motifs $M1^P$, $M2^P$, $M3^P$ and $M4^P$, respectively, P_5 is the population of free EVH1, $\Delta\delta_{bound}{}^{Mj}{}_i$

represents the fitted chemical shift of the bound state for given residue i determined for titrations with individual motif peptides (j = 1 – 4), and $\Delta\delta_{apo,\,i}$ is the chemical shift of residue i in the primary site of free EVH1. With the additional constraint that the sum of Pi equals 1, Matlab was used to repeatedly solve the system of equations for eight residue-specific data sets selected randomly from a set of 20 data sets corresponding to the N and H_N dimensions of 10 primary binding site residues. The average and standard deviation were obtained from 500 such runs. The same process was performed to approximate the bound motif populations in the most Zyxin$^{41\text{-}140}$-saturated [^{15}N]EVH1 Y39E sample.

Results

The Zyxin Proline Rich Region Induces Chemical Shift Changes at Expected and Unexpected Surfaces on VASP EVH1.

The proline rich region of Zyxin that harbors its four VASP EVH1 binding motifs [Zyxin residues 41-140, Zyxin$^{41\text{-}140}$, (Figure 2.1 A)], was expressed and purified, and its interaction with VASP EVH1 was investigated using NMR spectroscopy. As a first step, the [^{15}N]EVH1 domain was titrated with unlabeled Zyxin$^{41\text{-}140}$ (with the His tag cleaved) and a series of HSQC spectra were recorded. As expected, chemical shift perturbations were observed for residues previously characterized as being important for (W/F)PxφP ligand binding defined by the crystal structure of the Mena EVH1 domain/ActA complex and previous NMR studies of EVH1 titrated with (W/F)PxφP

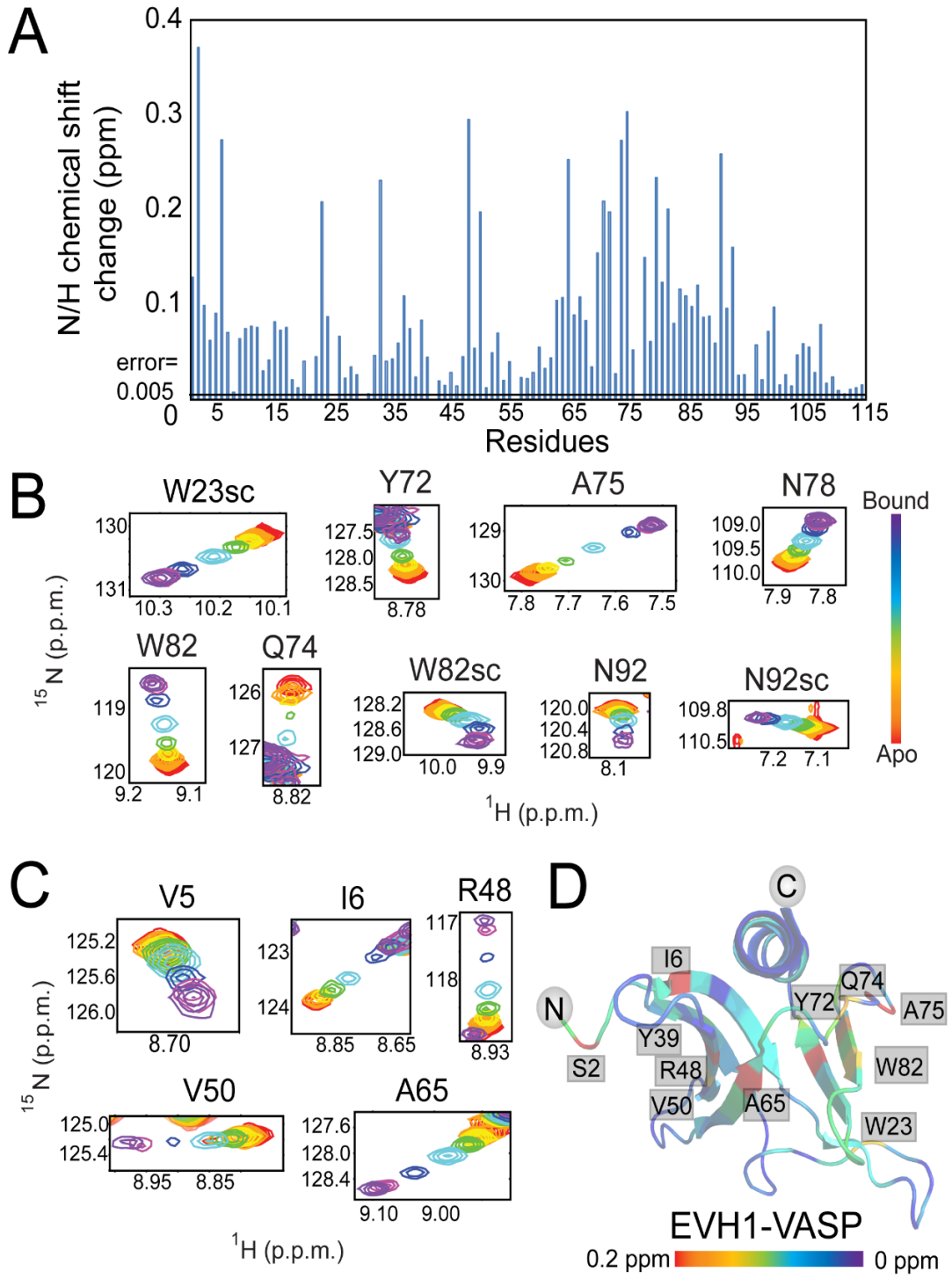
A
N/H chemical shift change (ppm)
0.4
0.3
0.2
0.1
error=
0.005
0
5 15 25 35 45 55 65 75 85 95 105 115
Residues
B
W23sc
Y72
A75
N78
Bound
Apo
W82
Q74
W82sc
N92
N92sc
15N (p.p.m.)
1H (p.p.m.)
C
V5
I6
R48
V50
A65
15N (p.p.m.)
1H (p.p.m.)
D
C
N
I6
Q74
Y72
A75
Y39
S2
R48
W82
V50
A65
W23
EVH1-VASP
0.2 ppm
0 ppm

Figure 2.1 Zyxin$^{41\text{-}140}$ titration provides evidence of a secondary binding site in the EVH1 domain of VASP. (A) Amino acid sequence of the Zyxin$^{41\text{-}140}$ construct, highlighting the four VASP binding motifs (red, bold type). **(B)** Composite chemical shift changes in [^{15}N]EVH1 induced by addition of Zyxin$^{41\text{-}140}$, calculated using the equation $\Delta\boldsymbol{\delta} = \sqrt{(\mathbf{0.154} * \Delta\boldsymbol{\delta_N})^{\mathbf{2}} + \Delta\boldsymbol{\delta_H}^{\mathbf{2}}}$. Extracted regions of overlays of ^{15}N-^{1}H HSQC spectra of [^{15}N]EVH1 titrated with Zyxin$^{41\text{-}140}$ show trajectories for residues in **(C)** the canonical binding site and **(D)** a novel secondary site, all of which show maximum Δδ values in excess of 10 times the error in Δδ (determined to be 0.005). **(E)** Chemical shift changes mapped onto the structure of VASP EVH1(Protein Data Bank entry 1EGX) show that Zyxin$^{41\text{-}140}$ induces chemical shift perturbations for residues in the primary binding site (far right) but also for residues on the opposite face of the EVH1 domain (far left). Red denotates the largest chemical shift perturbation and purple no perturbation.

ligands (Prehoda *et al.*, 1999; Ball *et al.*, 2000; Greenwood *et al.*, 2014). For example, residues W23, Y72, Q74, A75, W82, and N92 displayed large ligand-induced chemical shift changes (Figure 2.1 B,C). Remarkably, chemical shift perturbations were also observed for residues remote from this well-characterized binding site. Namely, residues Ser2, Val5, Ile6, Arg48, Val50, and Ala65 showed perturbations similar in magnitude as to those of residues in the canonical binding site (Figure 2.1 B,D). Mapping these chemical shift changes onto the EVH1 structure shows localization of these noncanonical binding residues on the opposite side of the domain (Figure 2.1 E), suggesting the presence of a secondary binding site. The possibility of slight pH changes being responsible for this observation was ruled out by pH titration (Appendix Figure 2.1). This region has previously been implicated in function, as mutation of the nearby Y39 altered the co-localization of and interaction between VASP and Zyxin (Maruoka *et al.*, 2012)

Quantitative Analysis of the Interaction of [^{15}N]EVH1 with the Zyxin Proline Rich Region Reveals a Bivalent Binding Mechanism.

The detection of two binding sites on EVH1 that potentially interact with the multiple binding motifs on Zyxin$^{41\text{-}140}$ significantly complicates the quantitative interpretation of the Zyxin$^{41\text{-}140}$ titration data. To begin to decipher this interaction, four 12-residue synthetic peptides (M1^{P} = Zyxin$^{69\text{-}80}$, M2^{P} = Zyxin$^{91\text{-}102}$, M3^{P} = Zyxin$^{102\text{-}113}$ and M4^{P} = Zyxin$^{112\text{-}123}$) were used in titrations of wild type [^{15}N]EVH1 to determine the intrinsic affinities of each motif under the same sample conditions, and to determine the chemical shifts of residues in the EVH1 primary site when bound to each of the four Zyxin motifs. As expected, chemical shift perturbations at the primary binding site were

observed. Additionally, chemical shift perturbations at the novel secondary binding site were induced by titration with all four peptides. Therefore, the binding affinity was determined using a four-state model (free [^{15}N]EVH1, only primary site bound, only secondary site bound, and both primary and secondary sites bound) as previously described (Rogals *et al.*, 2016). For all four peptides, this analysis yielded relatively weak affinities for the primary binding site and considerably weaker affinities for the secondary site (Table 2.1). These affinities are mostly weaker than the previously reported values for the same M1^{P} – M4^{P} peptides (74μM, 61μM, 197 μM, and no binding observed, respectively) determined by Trp fluorescence spectroscopy and fitted to a two-state model (free and 1:1 bound) (Ball *et al.*, 2000). It is possible that the affinity differences might be due to the lower pH (6.0) used in the Trp fluorescence measurements (Ball *et al.*, 2000). Importantly, the NMR titration analysis yields motif-specific bound-state chemical shift values for residues in the primary binding site that are critical for characterizing the complex interaction between [^{15}N]EVH1 and Zyxin$^{41-140}$.

Table 2.1 Dissociation Constants Calculated for EVH1 Primary and Secondary Binding Sites Titrated with Different Zyxin Peptides

	$K_d^{primary}$ [μM]	$K_d^{secondary}$ [mM]	X^2_{red}
M1^{P}	237±2	4.5 ±0.1	0.82
M2^{P}	134±2	4.4±0.2	0.96
M3^{P}	235±3	9.8±0.3	1.50
M4^{P}	263±3	2.1±0.1	1.26

The amide proton and nitrogen chemical shifts of a given amino acid residue in a system at equilibrium are a useful readout that can be used to determine the population distribution over multiple states for which distinct chemical shift values are known. With multiple residues serving as observers of the same set of states, complex equilibria can be characterized if the chemical shifts of the different states sampled by a given residue are sufficiently distinct. For the case at hand, several residues in the [^{15}N]EVH1 primary binding site show distinct peak trajectories upon being titrated with M1^{P}, M2^{P}, M3^{P}, and M4^{P} (Figure 2.2 A), enabling populations of the bound Zyxin motifs in the context of Zyxin$^{41\text{-}140}$ to be approximated by assuming the observed [^{15}N]EVH1: Zyxin$^{41\text{-}140}$ chemical shift is a population-weighted average of the apo and individual peptide-bound chemical shifts. This analysis shows a strong preference for binding of M2 in Zyxin$^{41\text{-}140}$ to the primary site [~6.4%, 73.4%, 9.3%, 6.5% and 4.3% occupancy for motifs M1, M2, M3, M4, and apo, respectively (Figure 2.2 B)]. For comparison, Virtual Cell Modeling (VCell) software (Schaff *et al.*, 1997) was used to simulate the expected population distribution for the most saturated [^{15}N]EVH1: Zyxin$^{41\text{-}140}$ sample condition if the four individual motifs in Zyxin were fully accessible and had the same intrinsic affinities as the corresponding short peptides (i.e., a 4:1 EVH1:Zyxin model). These simulations predict a significantly weaker preference of M2 binding [21%, 35%, 21%, 19% and 4% occupancy for motifs M1, M2, M3, M4, and apo, respectively (Figure 2.2 B)], indicating a significant impact of linking the four motifs together. Even if the simultaneous binding of EVH1 to nearest neighbor motifs is prohibited (i.e., all states with M1 and M2, M2 and M3, or M3 and M4 simultaneously bound are eliminated from

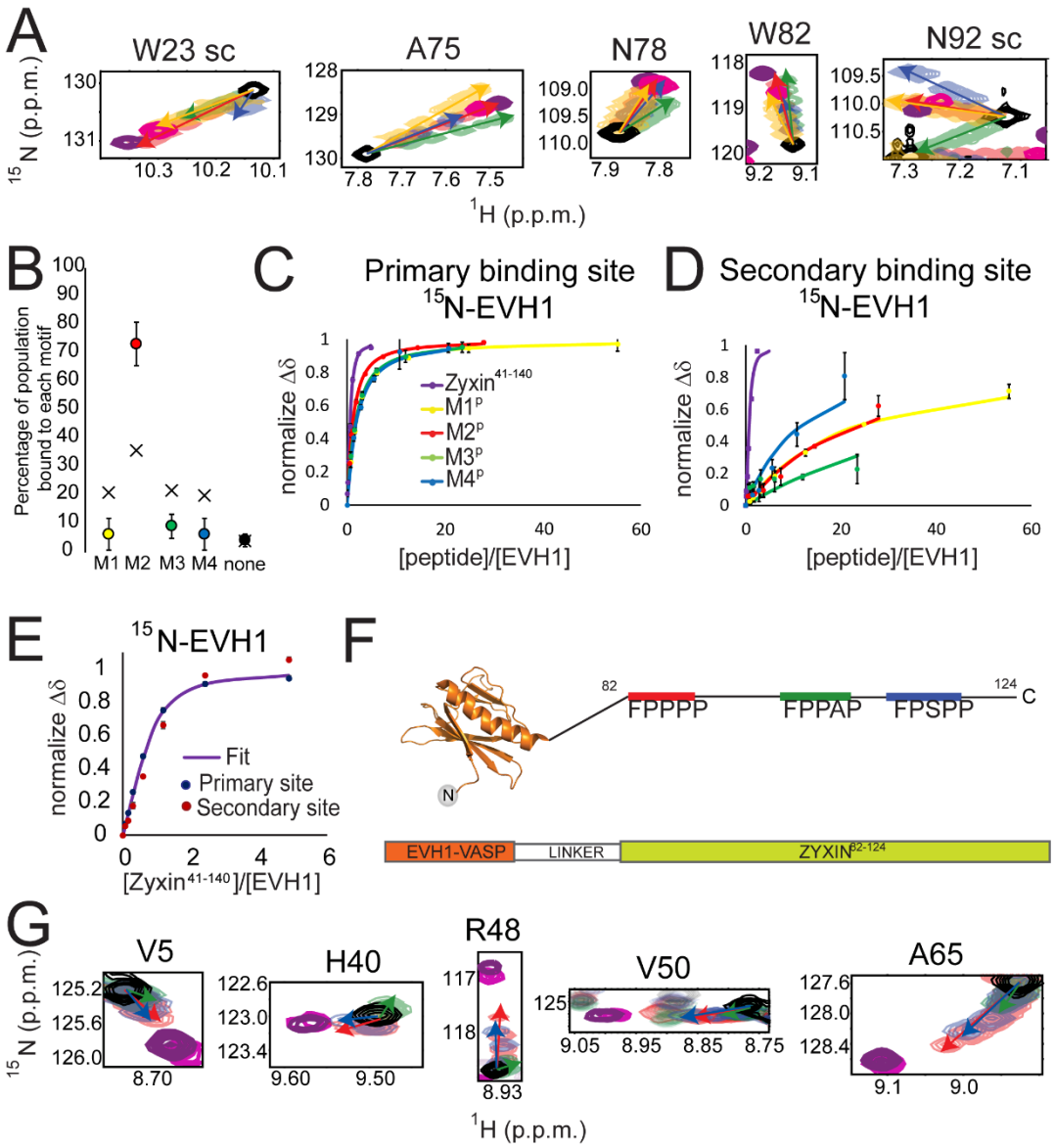
A
W23 sc
A75
N78
W82
N92 sc
15N (p.p.m.)
1H (p.p.m.)
B
Percentage of population bound to each motif
M1 M2 M3 M4 none
C
Primary binding site
15N-EVH1
normalize Δδ
Zyxin41-140
M1P
M2P
M3P
M4P
[peptide]/[EVH1]
D
Secondary binding site
15N-EVH1
E
15N-EVH1
Fit
Primary site
Secondary site
[Zyxin41-140]/[EVH1]
F
FPPPP
FPPAP
FPSPP
EVH1-VASP
LINKER
ZYXIN82-124
G
V5
H40
R48
V50
A65

Figure 2.2 Secondary binding site that creates a larger population of motif 2 bound to the canonical binding site. (A) Titrations show distinct chemical shift peak trajectories upon addition of each motif peptide (yellow, $M1^p$; red, $M2^p$; green, $M3^p$; blue, $M4^p$). The magenta peak shows titration with $Zyxin^{41-140}$ at highest Zyxin concentration. Purple shows the chemical shift of chimeric EVH1-Zyxin). **(B)** Distribution of $Zyxin^{41-140}$ motifs bound at the canonical site of EVH1 deduced from chemical shifts (filled circles) compared with the expected distribution based on K_d values of individual peptides (stars). **(C)** Binding curves from average normalized chemical shift changes of 10 residues in the canonical binding site of EVH1 for individual peptide titrations and for $Zyxin^{41-140}$. The yellow binding curve indicates titration with $M1^p$, the red binding curve titration of EVH1 with $M2^p$, the green binding curve titration of EVH1 with $M3^p$, the blue binding curve titration of EVH1 with $M4^p$, and the purple binding curve titration of EVH1 with $Zyxin^{41-140}$. **(D)** Like panel C, for six residues at the novel secondary binding site of EVH1. **(E)** Binding curve from average normalized chemical shift changes for the primary binding site (blue dots), for the secondary binding site (red dots) and a global fit to both curves (K_d=32.2 μM). **(F)** Chimera of EVH1 and Zyxin (EVH1-$Zyxin^{82-124}$) containing M2 (red), M3 (green), and M4 (blue) motifs. **(G)** Overlays of ^{15}N-^{1}H HSQC spectra for residues in the noncanonical site, titrated with $M2^p$ (red), $M3^p$ (green), $M4^p$ (green), $Zyxin^{41-140}$ (magenta) or in the context of EVH1-$Zyxin^{82-124}$ (purple).

the VCell model), the results are very similar (21%, 35%, 20%, 19%, and 5% occupancy for motifs M1, M2, M3, M4 or apo respectively).

Taken together, the analyses described above demonstrate that Zyxin$^{41\text{-}140}$ binds preferentially via M2 to the primary site, and that this binding mode is stabilized by interaction of another motif on the same Zyxin molecule with the secondary site to generate a bivalent bound state. This hypothesis is supported by an apparent enhancement of the primary site molar affinity compared to the seen with individual peptide titrations (Figure 2.2 C), and an even more pronounced affinity enhancement for the secondary binding site (Figure 2.2 D). Bivalent additivity has been widely studied (Daum *et al.*, 2007; Jencks, 1981; Rogals *et al.*, 2016) and, in this case, could significantly stabilize the 1:1 interaction between Zyxin and the VASP EVH1 domain.

Quantitative interpretation of the binding curves obtained from titration of [^{15}N]EVH1 with Zyxin$^{41\text{-}140}$ is approached by considering a highly simplified two-state model, in which a single Zyxin molecule interacts with a single EVH1 molecule and this interaction involves both primary and secondary sites in one unique Zyxin orientation. In this model, the apparent affinity enhancement of Zyxin$^{41\text{-}140}$ relative to those of individual motif peptides would be due to the combined binding energies of both primary and secondary surfaces. Fitting of the binding data for six residues in the primary and six residues in the secondary binding surface to this model yields an apparent K_d value of 32.2±1.7 μM. (Figure 2.2 E). The goodness of fit, evaluated by a χ^2 analysis as described in detail elsewhere (Rogals *et al.*, 2016), yielded a reduced χ^2 value of 4.19. This χ^2 value is consistent with the two-state bivalent model being an oversimplification, as expected because the population distribution determined above

indicates that multiple bound species are sampled. Separate fitting of just the primary or secondary site residues to the simple two-state model yields apparent K_d values of 21.8±1.3 and 133.3±5.8μM for the primary and secondary sites, respectively, with corresponding χ^2 values of 0.25 and 1.55 indicating good fits. The significant increases in affinity of both independently fitted primary and secondary site K_d values relative to the individual motif peptides, together with the overall affinity enhancement reflected in the highly simplified two-state bivalent fitting, are consistent with a more complex multistate model in which a dominantly populated bivalent state contributes to a significant enhancement of affinity. Additionally, the population distribution deduced from chemical shift perturbations supports a bivalently bound state with M2 bound to the primary site and a downstream epitope bound to the secondary site.

EVH1-Zyxin$^{82-124}$ Fusion Protein Captures the Bivalently Bound State

To confirm that both primary and secondary sites are dominantly bound in a 1:1 stoichiometry in a bivalent manner, a fusion protein was constructed in which the C-terminus of EVH1 is fused to the proline rich region of Zyxin containing motifs M2-M4 [EVH1-Zyxin$^{82-124}$ (Figure 2.2 F)]. Importantly, no significant changes in [^{15}N]EVH1 peak line widths were observed relative to WT EVH1, indicating the chimera is a monomer and not a domain-swapped dimer. Moreover, no NOESY crosspeaks were detected between the Zyxin and EVH1 components of the chimera, consistent with highly dynamic interfaces as expected from the weak intrinsic affinities characterized above. Resonance assignments for the EVH1 domain segment of the chimera were confirmed by standard triple resonance NMR experiments. The ^{15}N-^{1}H-HSQC spectrum of the ^{15}N- and ^{13}C-labeled EVH1-Zyxin$^{82-124}$ chimera shows peak

positions in both primary and secondary binding sites that are consistent with a more saturated state of the same binding trajectory as observed during titration with Zyxin$^{41-140}$ (Figure 2.2 A,G). This coincidence of the forced 1:1 stoichiometry in the chimera and the titration with Zyxin$^{41-140}$ further justify the bivalent model employed above for quantitative analysis of the Zyxin$^{41-140}$ titration data. While the primary site shows a clear preference for M2 based on chemical shifts, it is not possible to distinguish a motif preference at the secondary site from the [^{15}N]EVH1 perspective due to the lack of distinct chemical shift trajectories and the weak affinities of the individual motif peptides that prevented observation of larger populations of bound states (Figure 2.2 G).

The Phosphomimetic EVH1 Y39E Mutation Induces Changes in the Remote Primary Binding Site and Abolishes Binding to the Secondary Site

It has been reported that phosphorylation of Y39 by Abl reduced the level of VASP accumulation in focal adhesions, and that mutation of Y39 to aspartic acid reduced the level of binding of VASP to Zyxin and altered cellular localization (Maruoka *et al.*, 2012). Because Y39 is located within the secondary binding site described above (Figure 2.1 E), we wondered whether placement of a negative charge at the Y39 position would inhibit binding at the EVH1 secondary site, thereby eliminating bivalent binding. Bacterial expression of EVH1 Y39D was poor (unpublished data), while EVH1 Y39E was robustly expressed and stable in aqueous solution. Therefore, EVH1 Y39E was used for phosphomimetic investigations, and backbone resonance assignments for this mutant (BioMagResBank entry 27193) were determined using a standard suite of 3D NMR experiments (Leopold *et al.*, 1994).

Table 2.2. Dissociation Constants for the Primary Binding Site in Y39E EVH1.

	$K_d^{primary}$ [μM]	X^2_{red}
M1^P	176±2	0.91
M2^P	126±2	0.99
M3^P	182±2	0.84
M4^P	240±1	0.54

To investigate whether the Y39E mutation alters the interaction of EVH1 with the Zyxin proline rich region, we first performed titrations with each of the four individual Zyxin motif peptides. Notably, significant chemical shift perturbations were only observed for only residues of [^{15}N]EVH1 Y39E in the primary binding site and not in the secondary site, indicating that indeed placement of a negative charge at residue 39 inhibits binding at the secondary site. Primary site binding affinities for each peptide, determined using a simple two-state binding model, are again relatively weak as was found in wild-type EVH1 (Table 2.2).

Next, Zyxin$^{41\text{-}140}$ was titrated into [^{15}N]EVH1 Y39E. While significant chemical shift changes in the primary binding site were observed, only minimal chemical shift perturbations were observed for residues at the secondary binding site, indicating a loss of the bivalent bound state (Figure 2.3). Consistent with this, the resulting binding curves for residues in the primary site could not be adequately fit to a simple two-state (1:1 stoichiometry) model (reduced χ^2 value of 36.47), suggesting two or more EVH1 domains may bind to a single Zyxin molecule if a dominant 1:1 state is not achievable.

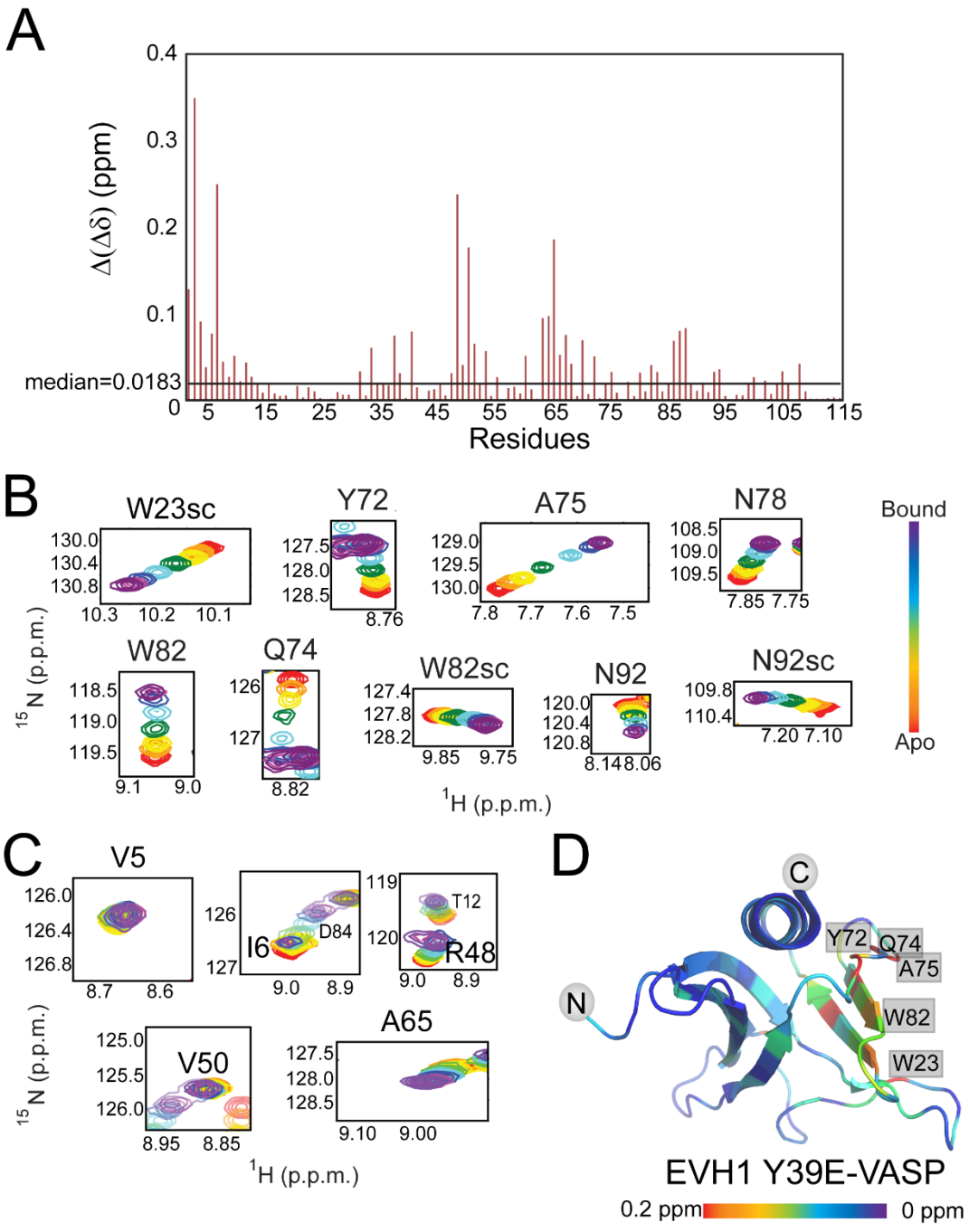
A
Δ(Δδ) (ppm)
median=0.0183
Residues
B
W23sc
Y72
A75
N78
W82
Q74
W82sc
N92
N92sc
Bound
Apo
15N (p.p.m.)
1H (p.p.m.)
C
V5
I6
D84
T12
R48
V50
A65
15N (p.p.m.)
1H (p.p.m.)
D
C
N
Y72
Q74
A75
W82
W23
EVH1 Y39E-VASP
0.2 ppm
0 ppm

Figure 2.3 Phosphomimetic mutation abolishes secondary site binding. (A) Bar plot showing differences between composite chemical shift perturbations of the ^{1}H and ^{15}N resonances upon addition of $Zyxin^{41-140}$ to EVH1 WT and EVH1 Y39E. Those residues with the largest perturbation differences are located in the novel secondary binding site. Overlays of ^{15}N-^{1}H HSQC spectra for residues in **(B)** the canonical binding site and **(C)** the secondary site show binding for the primary but not secondary sites. **(D)** Mapping chemical shift changes induced by titration of [^{15}N]EVH1 Y39E with $Zyxin^{41-140}$ onto the structure of VASP-EVH1 (PDB 1EGX) shows large perturbations for residues in the primary binding site (far right) but almost no perturbations for residues on the opposite face of the EVH1 Y39E domain (far left). Red = highest chemical shift perturbation, purple = no perturbation.

A key difference between the titrations of [^{15}N]EVH1 WT and [^{15}N]EVH1 Y39E is that the chemical shift trajectories differ (Figure 2.3 B compared to Figure 2.1 C). This difference can be explained by an altered population distribution of bound motifs. As was observed for WT EVH1, several residues in the [^{15}N]EVH1 Y39E primary binding site show distinct peak trajectories upon being titrated with M1^{P}-M4^{P}, again enabling populations of the bound Zyxin motifs in the context of [^{15}N]EVH1 Y39E with the most concentrated Zyxin$^{41-140}$ condition to be approximated (Figure 5.4A). Strikingly, the population were 16, 44, 20, 14, and 6% occupancy for motifs M1-M4, and apo, respectively, far more similar to the VCell-simulated population distribution for EVH1 Y39E based on individual motif peptide K_d values (simulation: 22, 32, 23, 18 and 5% occupied by motif M1-M4 and apo respectively). Moreover, chemical shift perturbations induced by titration with Zyxin$^{41-140}$ indicate binding at the primary but not at the secondary binding sites (Figures 2.3 B-D and 2.4 B,C). Together, these results demonstrate that the Y39E phosphomimetic mutation effectively abolishes the bivalent binding mode and enables the four motifs in Zyxin to interact with the primary binding site of EVH1 in a more equal population distribution. These results suggest that Y39 phosphorylation might act as a binding mode switch, where EVH1 domains with unphosphorylated Y39 bind to Zyxin predominantly in a bivalent 1:1 stoichiometry, and upon phosphorylation of tyrosine, up to four EVH1 domains could bind to one molecule of Zyxin.

To investigate potential phosphorylation-induced allostery, we focused our attention on the backbone chemical shift assignments of the phosphomimetic EVH1 Y39E mutant. The peaks corresponding to N-terminal residues S2 – C7 move in

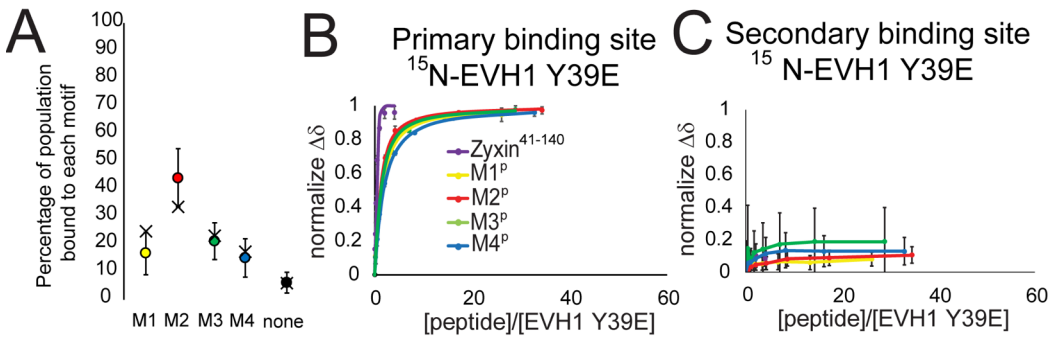

Figure 2.4 Population and binding curves for [15N]EVH1 Y39E (A) Distribution of Zyxin$^{41\text{-}140}$ motifs bound at the canonical site of EVH1 Y39E deduced from chemical shifts (filled circles) compared with the expected distribution based on K_d values of individual peptides (black crosses). **(B)** Binding curves from average normalized chemical shift changes of 10 residues in the canonical binding site of EVH1 Y39E for individual peptide titrations and for Zyxin$^{41\text{-}140}$. The yellow binding curve indicates titration with M1^P, the red binding curve titration of EVH1 Y39E with M2^P, the green binding curve titration of EVH1 Y39E with M3^P, the blue binding curve titration of EVH1 Y39E with M4^P, and the purple binding curve is EVH1 Y39E titrated with Zyxin$^{41\text{-}140}$. **(C)** As in B, for six residues at the novel secondary binding site of EVH1 Y39E.

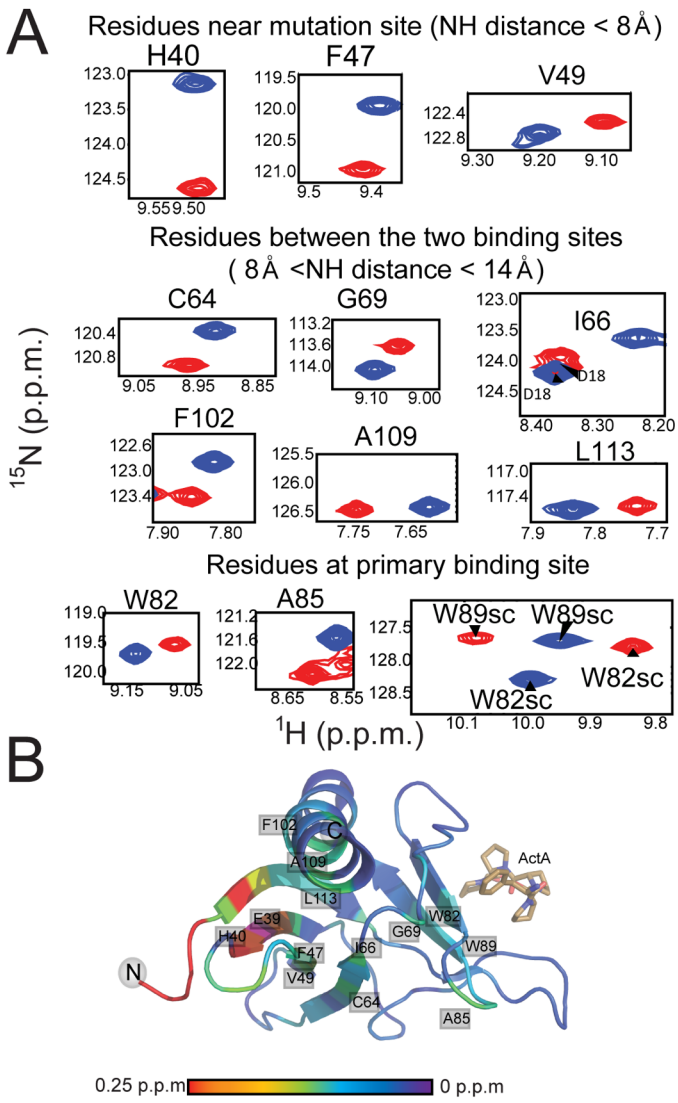

Figure 2.5 ^{1}H-^{15}N chemical shift differences between wild-type EVH1 and mutant Y39E. (A) Chemical shift differences between wild-type EVH1 (blue spectra) and EVH1 Y39E (red spectra). Both spectra were recorded under identical buffer conditions and with the same parameters. All highlighted residues display differences in chemical shift that exceed the error in chemical shift value by a factor of at least 10. **(B)** Mapping of ^{1}H-^{15}N backbone chemical shift differences to the EVH1 structure. Significant changes (>0.25 ppm) are represented by red, and no change is shown as purple

response to the Y39E phosphomimetic mutation, consistent with the structural interaction between Y39 and this region revealed in the NMR structure of human VASP EVH1 (Ball et al., 2000 (1EGX and homologues)). Other residues in sequential or spatial proximity to Y39 also display new peak positions, such as H40, F47, and V49 (Figure 2.5), as expected. However, there are several residues more than 14Å from the mutation site that display altered backbone and/or side chain NH chemical shifts. Striking examples include residues that reside in the primary binding site of EVH1, such as W82, A85, and W89 (Figure 2.5 A). Mapping of the backbone NH chemical shift differences between WT and Y39E EVH1 onto the structure reveals a clear perturbation pathway from the mutation site to these residues (Figure 2.5 B). These long-range perturbations of chemical environment induced by the phosphomimetic Y39E mutation suggest that phosphorylation of Tyr39 could similarly trigger a conformational rearrangement that alters the primary binding site of EVH1.

Discussion.

Understanding protein-protein interaction mechanisms that fine-tune signaling pathways is an important endeavor in biology. Here we studied the interaction between the EVH1 domain of VASP and the proline rich region of Zyxin. This interaction plays a critical role in the localization of VASP in focal adhesions (Nix *et al.*, 2001). Interestingly, VASP mislocalization is achieved only when all four FPxφP motifs of Zyxin are compromised (Drees *et al.*, 2000), showing that indeed these motifs mediate this interaction. VASP differs from MENA and EVL in its regulation by phosphorylation at Y39 (Maruoka *et al.*, 2012). Here, through application of NMR we found a secondary binding site near Y39 in the VASP EVH1 domain that, along with

the canonical EVH1 binding site, contributes to the interaction with the proline rich region of Zyxin. This secondary binding site is abolished by phosphomimetic mutation of Tyr39 to Glu. These studies suggest that Y39 phosphorylation acts as a stoichiometry switch, with one molecule of Zyxin binding to one EVH1 domain in the unphosphorylated state, and one molecule of Zyxin potentially binding to multiple EVH1 domains in the phosphorylated state.

Support for the biological relevance of the secondary binding interaction described here comes from the reported impact of phosphorylation of VASP EVH1 by Abl tyrosine kinase (Maruoka *et al.*, 2012). In Bcr-Abl-positive leukemic cells, Abl phosphorylates Y39 of VASP, which is centrally located in the binding site we describe (Figure 2.1 E). This may regulate the interaction between VASP and Zyxin, because the phosphomimetic mutant Y39D has a weakened ability to bind Zyxin in pull downs. Furthermore, overexpression of the Y39D or Y39F mutant, but not WT VASP, impairs adhesion of K562 cells to fibronectin, implying that a cycle of phosphorylation and dephosphorization is important for the proper regulation of VASP (Maruoka *et al.*, 2012). Here, we provide evidence that the Y39E mutant of VASP EVH1 retains WT binding affinity for its primary site but is incapable of binding in the secondary site. Importantly, we show that this phosphomimetic mutation switches the stoichiometry of the interaction. Taken together, these data suggest that the secondary binding site could play a key role in the phosphorylation and dephosphorization cycle of VASP to regulate interactions with Zyxin and other proline rich binding partners.

EVH1 domains all share a conserved primary binding site that binds proline rich sequences adopting a polyproline type II (PPII)structure. The canonical (primary)

binding site is a concave surface formed by one of the two β-sheetsthat form the domain's β-sandwich fold (Figure 2.6, right). The secondary binding site we define here is a similar concave surface formed by the other β-sheet on the opposite side of the domain. The residues most sensitive to the secondary interaction include the very N-terminal sequence of EVH1 (M0-C7) as well as the side chains of R48, and N63, which are all near each other (Figure 2.6, right). Although interactions beyond the primary site have been reported (Ball *et al.*, 2000; Volkman *et al.*, 2002) these additional EVH1 sites are highly distinct from the secondary binding surface described here.

EVH1 domains are homologous in structure and sequence with RanBDs (Callebaut *et al.*, 1998). The crystal structure of the first RanBD (denoted RanBD1) in RanBP2 bound to the nuclear transport protein Ran demonstrates that key features of the secondary binding site in VASP EVH1 are conserved in RanBDs (Vetter *et al.*, 1999). In this structure, a segment of Ran binds to the face of RanBD1 that corresponds to the secondary binding site we have described (Figure 2.6, left). The side chains of RanBP2 residues R77, R81, and N91 (corresponding to VASP EVH1 residues R48, R52, and N63, respectively) hydrogen bond with the backbone carbonyl groups of residues M179, A181, and L182 in Ran that are part of a PPII segment. Alignment of EVH1 and Ran-binding domains shows that R48 and N63 are highly conserved (Callebaut *et al.*, 1998), suggesting even broader utilization of this secondary binding site (e.g., by EVH1 domains in WASP and Homer). Importantly, the binding of a PPII structure to the corresponding "secondary site" in RanBD1 and the conservation of key interaction residues in EVH1 domains suggest that the EVH1 secondary site identified here might

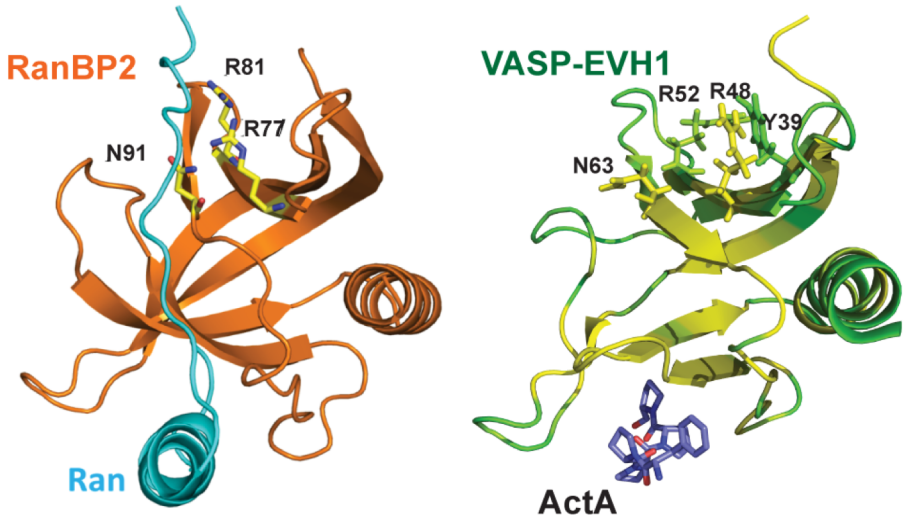

Figure 2.6 Tyr39 is located centrally in the secondary EVH1 binding site. In the left panel, the first Ran binding domain of RanBP2 (orange) binds Ran (cyan) using a secondary binding surface similar to the site we describe, employing residues R77, R81, and N91 that correspond to R48, R52, and N63, respectively, in VASP EVH1 (Protein Data Bank entry 1RRP). In the right panel, VASP EVH1 residue Y39 is located centrally in the secondary binding site. EVH1 is colored according to chemical shift perturbations induced by Zyxin$^{41\text{-}140}$ (green, no perturbation; yellow, largest perturbation). Key residues are shown as sticks. The ActA sequence FPPPP (blue) is shown bound in the primary site.

bind to sequences that adopt the PPII structure without the requirement of the W/FP motif.

VASP EVH1 has several binding partners that contain multiple proline rich motifs, some of which lack the canonical W/FPxφP primary site recognition motif. For instance, the Lipoma preferred partner (LPP), which is implicated in cell shape and motility, has two proline rich motifs (^{66}DFLPPPPPPLD^{76} and ^{87}NFPPPPPLD^{95}, only one of which has the canonical motif) separated by 12 residues, and direct binding of VASP-EVH1 was previously reported (Petit *et al.*, 2000). Similarly, Vinculin, a known EVH1 binding partner (Harbeck *et al.*, 2000) has only one FPxφP motif (^{842}FPPPPP^{847}) but has another proline rich motif nearby (^{859}APPKPPLP^{866}). Even more surprising is Migfilin, a component in cell-matrix adhesions that offers a link with the actin cytoskeleton (Tu *et al.*, 2003). Migfilin regulates localization of VASP to the cell-matrix adhesions via its proline rich region that interacts directly with VASP-EVH1 domain. Deletion of residues 84-112 in Migfillin eliminates VASP binding (Zhang *et al.*, 2006). Interestingly, this deletion contains two proline rich motifs without W or F (^{85}CPPPPP^{90} and ^{104}LPPPPPPPP^{112}) separated by 14 residues. All of these proline rich motifs are expected to adopt PPII structure, which potentially could bind to the secondary binding site. Notably, the presence of neighboring proline rich motifs could enhance dramatically the affinity through bivalent binding as observed here for Zyxin.

It is well established that VASP functions in the cell as a constitutive tetramer (Bachmann *et al.*, 1999). Four VASP polypeptide chains associate via the single-helix tetramerization domain to form a parallel right handed four-helix coiled coil, causing VASP to form a “bouquet-like” tetramer (Kühnel *et al.*, 2004). Truncation of the C-

terminal region of VASP that contains the tetramerization domain causes a decrease in the VASP concentration at focal adhesions, indicating a tetramerization dependence for focal adhesion localization (Haffner *et al.*, 1995). Moreover, the possibility of VASP cross-linking several protein partners has been previously discussed (Zimmermann *et al.*, 2002). Notably, the work presented here suggests that when VASP residue Y39 is not phosphorylated, the bivalent interaction between one EVH1 domain and one multivalent protein ligand could allow a VASP tetramer to tightly localize as many as four different binding partners, effectively achieving reversible cross-linking of these partners (Figure 2.7 A). Moreover, when VASP is phosphorylated at Y39, the resulting loss of secondary site binding would promote interaction of the VASP tetramer with a single multivalent protein partner due to the enhancement of avidity (Figure 2.7 B). We propose a model in which Y39 phosphorylation acts as a molecular switch that governs the stoichiometry of interactions between the VASP tetramer and its binding partners that harbor multiple FPxφP motifs, where the unphosphorylated state acts as a cross linker between multiple partners while the phosphorylated state binds to a single partner (Figure 2.7).

In summary, a secondary binding site in the VASP EVH1 domain was identified and characterized through NMR investigations of the interactions between the proline rich region of Zyxin and [^{15}N]EVH1. By analysis of population distributions over bound states, we determined that this secondary binding site directs the orientation of Zyxin binding through formation of a bivalent interaction between Zyxin and EVH1. In this bivalently bound state, M2 in Zyxin interacts with the primary site and downstream Zyxin regions interact with the secondary site in EVH1. Additionally, we observed that

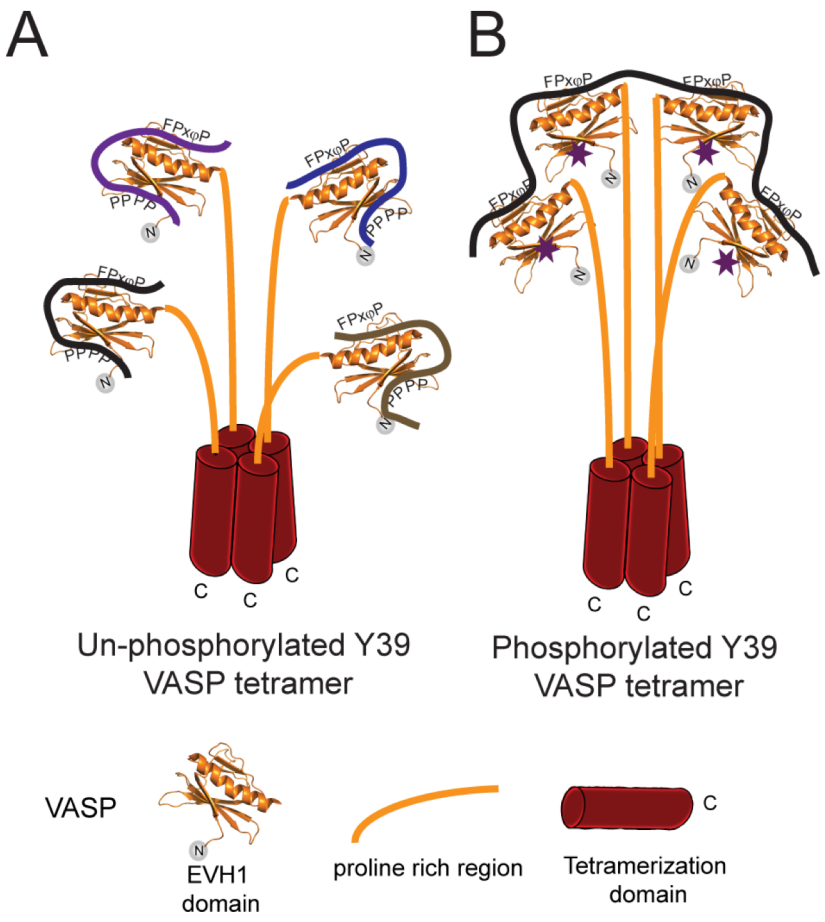

Figure 2.7 Proposed model for stoichiometry switch controlled by phosphorylation of Y39 in VASP tetramers. (A) In the extreme case where all Y39 residues are unphosphorylated, each EVH1 domain in the VASP tetramer could interact with a molecule of Zyxin or any other binding partner. Bivalent interactions could form due to the presence of nearby proline rich motifs. **(B)** In the extreme case where each Y39 residue is phosphorylated (purple stars), one molecule with multiple FPxφP motifs (like Zyxin, ActA, or lammellipodin) could bind to one tetramer of VASP. Phosphorylation of Y39 could recruit VASP exclusively to a specific binding partner with multiple canonical binding sites, while dephosphorylation could cause cross-linking between multiple binding partners

.

the secondary binding site is abolished by phosphomimetic mutation of Y39 to E. Phosphorylation dependence at Y39 for the interaction between VASP and Zyxin has been previously reported (Maruoka *et al.*, 2012). On the basis of our findings, we hypothesize that phosphorylation of Y39 acts as a stoichiometry switch in the interaction between the VASP tetramer and Zyxin. These results have important implications for the regulation of VASP interactions with its other binding partners that contain multiple neighboring proline rich motifs, and more broadly for potential regulation of interactions involving other EVH1 domains in which residues implicated in secondary site function are conserved.

Acknowledgements

This investigation was supported by the National Science Foundation (MCB-1157806 and MCB-1615350) and through graduate student training grant support to LAA by the National Institutes of Health (2T32GM008267).

Supporting Information

Comparison of ^{15}N-^{1}H HSQC chemical shift perturbations of [^{15}N]EVH1 residue H40 induced by pH titration versus by Zyxin$^{41-140}$ titration in Appendix.

REFERENCES

Ahern-Djamali, S. M., Comer, A. R., Bachmann, C., Kastenmeier, A. S., Reddy, S. K., Beckerle, M. C., . . . Hoffmann, F. M. (1998). Mutations in Drosophila enabled and rescue by human vasodilator-stimulated phosphoprotein (VASP) indicate important functional roles for Ena/VASP homology domain 1 (EVH1) and EVH2 domains. *Mol Biol Cell, 9*(8), 2157-2171.

Bachmann, C., Fischer, L., Walter, U., & Reinhard, M. (1999). The EVH2 domain of the vasodilator-stimulated phosphoprotein mediates tetramerization, F-actin binding, and actin bundle formation. *J Biol Chem, 274*(33), 23549-23557.

Ball, L. J., Kuhne, R., Hoffmann, B., Hafner, A., Schmieder, P., Volkmer-Engert, R., . . . Jarchau, T. (2000). Dual epitope recognition by the VASP EVH1 domain modulates polyproline ligand specificity and binding affinity. *EMBO J, 19*(18), 4903-4914. doi:10.1093/emboj/19.18.4903

Barzik, M., Kotova, T. I., Higgs, H. N., Hazelwood, L., Hanein, D., Gertler, F. B., & Schafer, D. A. (2005). Ena/VASP proteins enhance actin polymerization in the presence of barbed end capping proteins. *J Biol Chem, 280*(31), 28653-28662. doi:M503957200 [pii] 10.1074/jbc.M503957200

Bear, J. E., & Gertler, F. B. (2009). Ena/VASP: towards resolving a pointed controversy at the barbed end. *J Cell Sci, 122*(Pt 12), 1947-1953. doi:122/12/1947 [pii] 10.1242/jcs.038125

Bear, J. E., Loureiro, J. J., Libova, I., Fassler, R., Wehland, J., & Gertler, F. B. (2000). Negative regulation of fibroblast motility by Ena/VASP proteins. *Cell, 101*(7), 717-728. doi:S0092-8674(00)80884-3 [pii]

Bear, J. E., Svitkina, T. M., Krause, M., Schafer, D. A., Loureiro, J. J., Strasser, G. A., . . . Gertler, F. B. (2002). Antagonism between Ena/VASP proteins and actin filament capping regulates fibroblast motility. *Cell, 109*(4), 509-521. doi:S0092867402007316 [pii]

Bhatt, A., Kaverina, I., Otey, C., & Huttenlocher, A. (2002). Regulation of focal complex composition and disassembly by the calcium-dependent protease calpain. *J Cell Sci, 115*(Pt 17), 3415-3425.

Breitsprecher, D., Kiesewetter, A. K., Linkner, J., Urbanke, C., Resch, G. P., Small, J. V., & Faix, J. (2008). Clustering of VASP actively drives processive, WH2 domain-mediated actin filament elongation. *EMBO J, 27*(22), 2943-2954. doi:emboj2008211 [pii] 10.1038/emboj.2008.211

Breitsprecher, D., Kiesewetter, A. K., Linkner, J., Vinzenz, M., Stradal, T. E., Small, J. V., . . . Faix, J. (2011). Molecular mechanism of Ena/VASP-mediated actin-filament elongation. *EMBO J, 30*(3), 456-467. doi:emboj2010348 [pii] 10.1038/emboj.2010.348

Call, G. S., Chung, J. Y., Davis, J. A., Price, B. D., Primavera, T. S., Thomson, N. C., . . . Hansen, M. D. (2011). Zyxin phosphorylation at serine 142 modulates the zyxin head-tail interaction to alter cell-cell adhesion. *Biochem Biophys Res Commun, 404*(3), 780-784. doi:S0006-291X(10)02296-5 [pii] 10.1016/j.bbrc.2010.12.058

Callebaut, I., Cossart, P., & Dehoux, P. (1998). EVH1/WH1 domains of VASP and WASP proteins belong to a large family including Ran-binding domains of the RanBP1 family. *FEBS Lett, 441*(2), 181-185. doi:S0014-5793(98)01541-5 [pii]

Chan, C. B., Liu, X., Tang, X., Fu, H., & Ye, K. (2007). Akt phosphorylation of zyxin mediates its interaction with acinus-S and prevents acinus-triggered chromatin condensation. *Cell Death Differ, 14*(9), 1688-1699. doi:4402179 [pii] 10.1038/sj.cdd.4402179

Coppolino, M. G., Krause, M., Hagendorff, P., Monner, D. A., Trimble, W., Grinstein, S., . . . Sechi, A. S. (2001). Evidence for a molecular complex consisting of Fyb/SLAP, SLP-76, Nck, VASP and WASP that links the actin cytoskeleton to Fcgamma receptor signalling during phagocytosis. *J Cell Sci, 114*(Pt 23), 4307-4318.

Daum, S., Lucke, C., Wildemann, D., & Schiene-Fischer, C. (2007). On the benefit of bivalency in peptide ligand/pin1 interactions. *J Mol Biol, 374*(1), 147-161. doi:10.1016/j.jmb.2007.09.019

Drees, B., Friederich, E., Fradelizi, J., Louvard, D., Beckerle, M. C., & Golsteyn, R. M. (2000). Characterization of the interaction between zyxin and members of the Ena/vasodilator-stimulated phosphoprotein family of proteins. *J Biol Chem, 275*(29), 22503-22511. doi:10.1074/jbc.M001698200

Geese, M., Loureiro, J. J., Bear, J. E., Wehland, J., Gertler, F. B., & Sechi, A. S. (2002). Contribution of Ena/VASP proteins to intracellular motility of listeria requires phosphorylation and proline-rich core but not F-actin binding or multimerization. *Mol Biol Cell, 13*(7), 2383-2396. doi:10.1091/mbc.E02-01-0058

Goh, K. L., Cai, L., Cepko, C. L., & Gertler, F. B. (2002). Ena/VASP proteins regulate cortical neuronal positioning. *Curr Biol, 12*(7), 565-569. doi:S096098220200725X [pii]

Greenwood, A. I. (2014). *The interaction between the EVH1 domain of VASP and Proline-rich sequences: significance of isomerization, phosphorylation, and a secondary binding site.* (PhD of Biophysics), Cornell University. (2014-02-25T18:39:59Z)

Greenwood, A. I., Kwon, J., & Nicholson, L. K. (2014). Isomerase-Catalyzed Binding of Interleukin-1 Receptor-Associated Kinase 1 to the EVH1 Domain of Vasodilator-Stimulated Phosphoprotein. *Biochemistry, 53*(22), 3593-3607. doi:10.1021/bi500031e

Haffner, C., Jarchau, T., Reinhard, M., Hoppe, J., Lohmann, S. M., & Walter, U. (1995). Molecular cloning, structural analysis and functional expression of the proline-rich focal adhesion and microfilament-associated protein VASP. *EMBO J, 14*(1), 19-27.

Harbeck, B., Huttelmaier, S., Schluter, K., Jockusch, B. M., & Illenberger, S. (2000). Phosphorylation of the vasodilator-stimulated phosphoprotein regulates its interaction with actin. *J Biol Chem, 275*(40), 30817-30825. doi:10.1074/jbc.M005066200

Hoffman, L. M., Jensen, C. C., Chaturvedi, A., Yoshigi, M., & Beckerle, M. C. (2012). Stretch-induced actin remodeling requires targeting of zyxin to stress fibers and recruitment of actin regulators. *Mol Biol Cell, 23*(10), 1846-1859. doi:mbc.E11-12-1057 [pii] 10.1091/mbc.E11-12-1057

Jencks, W. P. (1981). On the attribution and additivity of binding energies. *Proc Natl Acad Sci U S A, 78*(7), 4046-4050.

Krause, M., Dent, E. W., Bear, J. E., Loureiro, J. J., & Gertler, F. B. (2003). Ena/VASP proteins: regulators of the actin cytoskeleton and cell migration. *Annu Rev Cell Dev Biol, 19*, 541-564. doi:10.1146/annurev.cellbio.19.050103.103356

Kühnel, K., Jarchau, T., Wolf, E., Schlichting, I., Walter, U., Wittinghofer, A., & Strelkov, S. V. (2004). The VASP tetramerization domain is a right-handed coiled coil based on a 15-residue repeat. *Proc Natl Acad Sci U S A, 101*(49), 17027-17032. doi:10.1073/pnas.0403069101

Lebrand, C., Dent, E. W., Strasser, G. A., Lanier, L. M., Krause, M., Svitkina, T. M., . . . Gertler, F. B. (2004). Critical role of Ena/VASP proteins for filopodia

formation in neurons and in function downstream of netrin-1. *Neuron, 42*(1), 37-49. doi:S0896627304001084 [pii]

Leopold, M. F., Urbauer, J. L., & Wand, A. J. (1994). Resonance assignment strategies for the analysis of nmr spectra of proteins. *Mol Biotechnol, 2*(1), 61-93. doi:10.1007/bf02789290

Maruoka, M., Sato, M., Yuan, Y., Ichiba, M., Fujii, R., Ogawa, T., . . . Watanabe, N. (2012). Abl-1-bridged tyrosine phosphorylation of VASP by Abelson kinase impairs association of VASP to focal adhesions and regulates leukaemic cell adhesion. *Biochem J, 441*(3), 889-899. doi:BJ20110951 [pii] 10.1042/BJ20110951

Mejillano, M. R., Kojima, S., Applewhite, D. A., Gertler, F. B., Svitkina, T. M., & Borisy, G. G. (2004). Lamellipodial versus filopodial mode of the actin nanomachinery: pivotal role of the filament barbed end. *Cell, 118*(3), 363-373. doi:10.1016/j.cell.2004.07.019 S0092867404007068 [pii]

Moody, J. D., Grange, J., Ascione, M. P., Boothe, D., Bushnell, E., & Hansen, M. D. (2009). A zyxin head-tail interaction regulates zyxin-VASP complex formation. *Biochem Biophys Res Commun, 378*(3), 625-628. doi:S0006-291X(08)02302-4 [pii] 10.1016/j.bbrc.2008.11.100

Niebuhr, K., Ebel, F., Frank, R., Reinhard, M., Domann, E., Carl, U. D., . . . Chakraborty, T. (1997). A novel proline-rich motif present in ActA of Listeria monocytogenes and cytoskeletal proteins is the ligand for the EVH1 domain, a protein module present in the Ena/VASP family. *EMBO J, 16*(17), 5433-5444. doi:10.1093/emboj/16.17.5433

Nix, D. A., Fradelizi, J., Bockholt, S., Menichi, B., Louvard, D., Friederich, E., & Beckerle, M. C. (2001). Targeting of Zyxin to Sites of Actin Membrane Interaction and to the Nucleus. *Journal of Biological Chemistry, 276*(37), 34759-34767. doi:10.1074/jbc.M102820200

Peterson, F. C., Deng, Q., Zettl, M., Prehoda, K. E., Lim, W. A., Way, M., & Volkman, B. F. (2007). Multiple WASP-interacting protein recognition motifs are required for a functional interaction with N-WASP. *J Biol Chem, 282*(11), 8446-8453. doi:M609902200 [pii] 10.1074/jbc.M609902200

Petit, M. M., Fradelizi, J., Golsteyn, R. M., Ayoubi, T. A., Menichi, B., Louvard, D., . . . Friederich, E. (2000). LPP, an actin cytoskeleton protein related to zyxin, harbors a nuclear export signal and transcriptional activation capacity. *Mol Biol Cell, 11*(1), 117-129.

Prehoda, K. E., Lee, D. J., & Lim, W. A. (1999). Structure of the enabled/VASP homology 1 domain-peptide complex: a key component in the spatial control of actin assembly. *Cell, 97*(4), 471-480.

Reinhard, M., Halbrugge, M., Scheer, U., Wiegand, C., Jockusch, B. M., & Walter, U. (1992). The 46/50 kDa phosphoprotein VASP purified from human platelets is a novel protein associated with actin filaments and focal contacts. *EMBO J, 11*(6), 2063-2070.

Rogals, M. J., Greenwood, A. I., Kwon, J., Lu, K. P., & Nicholson, L. K. (2016). Neighboring phosphoSer-Pro motifs in the undefined domain of IRAK1 impart bivalent advantage for Pin1 binding. *The FEBS Journal, 283*(24), 4528-4548. doi:10.1111/febs.13943

Rottner, K., Behrendt, B., Small, J. V., & Wehland, J. (1999). VASP dynamics during lamellipodia protrusion. *Nat Cell Biol, 1*(5), 321-322. doi:10.1038/13040

Schaff, J., Fink, C. C., Slepchenko, B., Carson, J. H., & Loew, L. M. (1997). A general computational framework for modeling cellular structure and function. *Biophys J, 73*(3), 1135-1146. doi:10.1016/s0006-3495(97)78146-3

Smith, G. A., Theriot, J. A., & Portnoy, D. A. (1996). The tandem repeat domain in the Listeria monocytogenes ActA protein controls the rate of actin-based motility, the percentage of moving bacteria, and the localization of vasodilator-stimulated phosphoprotein and profilin. *J Cell Biol, 135*(3), 647-660.

Smith, M. A., Blankman, E., Deakin, N. O., Hoffman, L. M., Jensen, C. C., Turner, C. E., & Beckerle, M. C. (2013). LIM domains target actin regulators paxillin and zyxin to sites of stress fiber strain. *PLoS One, 8*(8), e69378. doi:10.1371/journal.pone.0069378 PONE-D-13-12623 [pii]

Smith, M. A., Blankman, E., Gardel, M. L., Luettjohann, L., Waterman, C. M., & Beckerle, M. C. (2010). A zyxin-mediated mechanism for actin stress fiber maintenance and repair. *Dev Cell, 19*(3), 365-376. doi:S1534-5807(10)00383-7 [pii] 10.1016/j.devcel.2010.08.008

Tokuo, H., & Ikebe, M. (2004). Myosin X transports Mena/VASP to the tip of filopodia. *Biochem Biophys Res Commun, 319*(1), 214-220. doi:10.1016/j.bbrc.2004.04.167 S0006291X04008484 [pii]

Tu, Y., Wu, S., Shi, X., Chen, K., & Wu, C. (2003). Migfilin and Mig-2 link focal adhesions to filamin and the actin cytoskeleton and function in cell shape modulation. *Cell, 113*(1), 37-47.

Vetter, I. R., Nowak, C., Nishimoto, T., Kuhlmann, J., & Wittinghofer, A. (1999). Structure of a Ran-binding domain complexed with Ran bound to a GTP analogue: implications for nuclear transport. *Nature, 398*(6722), 39-46. doi:10.1038/17969

Volkman, B. F., Prehoda, K. E., Scott, J. A., Peterson, F. C., & Lim, W. A. (2002). Structure of the N-WASP EVH1 domain-WIP complex: insight into the molecular basis of Wiskott-Aldrich Syndrome. *Cell, 111*(4), 565-576. doi:S0092867402010760 [pii]

Waudby, C. A., Ramos, A., Cabrita, L. D., & Christodoulou, J. (2016). Two-Dimensional NMR Lineshape Analysis. *Scientific Reports, 6*, 24826. doi:10.1038/srep24826
http://www.nature.com/articles/srep24826#supplementary-information

Zhang, Y., Tu, Y., Gkretsi, V., & Wu, C. (2006). Migfilin interacts with vasodilator-stimulated phosphoprotein (VASP) and regulates VASP localization to cell-matrix adhesions and migration. *J Biol Chem, 281*(18), 12397-12407. doi:10.1074/jbc.M512107200

Zimmermann, J., Labudde, D., Jarchau, T., Walter, U., Oschkinat, H., & Ball, L. J. (2002). Relaxation, Equilibrium Oligomerization, and Molecular Symmetry of the VASP (336-380) EVH2 Tetramer. *Biochemistry, 41*, 11143-11151.

CHAPTER 3

^{1}H, ^{13}C, and ^{15}N NMR assignments of cyclophilin LRT2 (OsCYP2) from rice [4].

Abstract

Cyclophilins are enzymes that catalyze the isomerization of a prolyl-peptide bond and are found in both prokaryotes and eukaryotes. LRT2 (also known as OsCYP2) is a cyclophilin in rice (*Oryza Sativa*), that has importance in lateral root development and stress tolerance. LRT2 is 172 amino acids long and has a molecular weight of 18.3kDa. Here, we report the backbone and sidechain resonance assignments of ^{1}H, ^{13}C, ^{15}N in LRT2 protein using several 2D and 3D heteronuclear NMR experiments at pH 6.7 and 298K. Our chemical shift data analysis predicts a secondary structure like the cytosolic wheat cyclophilin TaCypA-1 with 87.7% sequence identity. These assignments will be useful for further analysis in the NMR studies for function and structure of the enzyme.

Keywords NMR resonance assignments • TALOS-N prediction • Rice cyclophilin • Lateral root development • Protein chemical shift assignment

Biological context

Cyclophilins are a conserved class of peptidyl prolyl isomerases found in mammals, plants, insects, fungi and bacteria (Wang *et al.*, 2005). The primary function of Cyclophilins is to catalyze the isomerization of prolyl-peptide bonds, making this

[4] This chapter is a re-printed of the note published in Biomolecular NMR Assignments Springer Netherlands publisher, 2018, volume 12, Issue 1, pages 171-174, "^{1}H, ^{13}C, and ^{15}N NMR assignments of cyclophilin LRT2 (OsCYP2) from rice" by Lucila Andrea Acevedo, and Linda K. Nicholson.

class of enzymes important in fundamental processes such as protein folding, gene transcription, protein degradation, and cell signaling. The cis/trans isomerization of the X-Pro peptide bond has been studied as a molecular switch and timing device in diverse biological processes (Lu *et al.*, 2007), and the enzymes that regulate this switch can represent the rate-limiting step in these processes. Mammalian cyclophilins have been extensively studied, in particular Human Cyclophilin A which has been studied by NMR in order to determine the residues involved in its interaction with substrate and to investigate its mechanism of action (Eisenmesser *et al.*, 2002).

In rice (*Oryza Sativa*), there have been reported 27 Cyclophilin genes which encode 46 protein products (Kumari *et al.*, 2013). One of these protein products is the LRT2 protein. Expression of LRT2 has been induced by multiple abiotic stresses, and overexpression of it has been shown to enhance multiple stress tolerance in *E. Coli* and *S. cerevisiae*, and salinity stress tolerance in rice, making it a target protein for study of stress resistance mechanisms in plants (Kumari *et al.*, 2009; Ruan *et al.*, 2011). Also, LRT2 has recently been associated to the C2HC-type Zinc finger protein (OsZFP, Os01g0252900) by yeast two hybrid cDNA library screening, a protein that has an important regulatory role in lateral root development (Cui *et al.*, 2017). Importantly, LRT2 has been reported as the cyclophilin that affects lateral root development in rice, where LRT2 knock out or mutation shows defects on lateral root development (Kang *et al.*, 2013). In the same context, knock out of the auxin response (Aux/IAA) gene that codes for the transcriptional repressor protein OsIAA11 affects lateral root development (Zhu *et al.*, 2012). Auxin is a class of phytohormones that regulate essentially all developmental processes in plants through their action in feedback inhibition circuits

that control the expression of auxin-responsive genes. Notably, auxin is required for the E3 ubiquitin ligase $SCF^{TIR1/AFB}$ complex to bind specifically with the *cis* isomer of a highly conserved Trp-Pro degron motif in Aux/IAA proteins such as OsIAA11, thereby targeting these transcription repressor proteins for proteasomal degradation. In vitro interaction between LRT2 and OsIAA11 and LRT2 catalysis of the Trp-Pro peptide bond in the Aux/IAA degron motif of OsIAA11 has been reported (Jing *et al.*, 2015). This interaction is of importance in the field of plant biology, since LRT2 catalysis of cis/trans isomerization of OsIAA11 could accelerate ubiquitin-mediated proteasomal degradation of OsIAA11 via the cis conformation of the conserved Aux/IAA degron motif (Jing *et al.*, 2015). This degradation is crucial for transcription regulation since OsIAA11 is a repressor protein that regulates lateral root formation (Dinesh *et al.*, 2016). Therefore, if LRT2 is disrupted, OsIAA11 would not be degraded at the appropriate rate and could still repress gene expression in the absence of Auxin.

We report here the backbone and sidechain resonance assignments of LRT2 at room temperature in a 6.7 pH phosphate buffer. LRT2 represents a defined cis/trans switch and molecular timer that has been linked to a clear phenotype (Kang *et al.*, 2013), thus offering an opportunity to study the relationships between a specific isomerization rate and a developmental outcome in lateral roots.

Methods

Protein expression and purification

The cDNA for the LRT2 gene (Os02g0121300) was custom synthesized by Cyagen Biosciences (Santa Clara, CA). This gene was amplified by PCR using primers that introduced restriction enzyme digestion sites for NdeI at the 5' terminus and HindIII

at the 3' terminus to allow insertion of this gene into a PET28 vector with Kanamycin resistance, an N-terminal His_6-tag, and a TEV cleavage site. Expression of protein was carried out in M9 minimum media enriched with $^{15}NH_4Cl$ and ^{13}C-Glucose. Protein expression was induced by addition of 0.88mM IPTG when the culture reached 0.8 $O.D._{600}$. Expression proceeded over night at 17°C. Cells were spun down and recovered in 20ml lysis buffer (wash buffer (50mM NaH_2PO_4, 300mM NaCl, 20mM Imidazole, and 0.1mM TCEP pH=8.0), plus 100ul P.I. cocktail (Thermo scientific), 1mM TCEP, 2.5mM $MgCl_2$, 0.5mM $CaCl_2$), and frozen. Lysis of cells was carried out by addition of 0.02g lysozyme, 100ul Dnase, and 100ul Rnase. The solution was kept on ice for 30 minutes; further lysis was carried by 15 cycles of sonication with pulse on for 10 seconds and off for 15 seconds. Separation of soluble proteins was achieved by spinning down the solution at 15000rpm for 45 minutes at 4°C. Filtered supernatant was added to 2ml nickel beads pre-equilibrated in wash buffer. The binding was carried out for 45 mins, the column was washed with 50 ml of wash buffer and protein was eluted with ~10ml wash buffer + 300 mM Imidazole. A desalting column was used to exchange the eluent into TEV buffer (50mM $NaPO_4$, 100mM NaCl, 1mM TCEP, pH=8.0), followed by TEV cutting of His_6-Tag for 48 hours. 10mM imidazole and 50mM KCl were added to the solution, which was run again through the nickel column. The flow through of this process was run through a desalting column to exchange into "NMR" buffer (50mM KCl, 20mM KPO_4, 0.1mM TCEP, pH=6.67). This sample of $^{13}C/^{15}N$-labeled LRT2 was concentrated to 1.16mM in NMR buffer (plus 5mM NaN_3, 0.1%P.I. cocktail, 1mM TCEP, and 8% D_2O).

NMR spectroscopy

For backbone and side-chain assignments, a suite of 2D and 3D NMR experiments were acquired. The $^{13}C/^{15}N$-LRT2 sample was used to acquire 2D ^{15}N-^{1}H-HSQC and ^{13}C-^{1}H-HSQC spectra, and to acquire 3D HNCACB, HN(CO)CA, HNCA, (H)C(CO)NH, H(CCO)NH, HCCH-TOCSY, and HNCO spectra. All spectra were collected at 25^{o}C using a Varian Inova 600 MHz spectrometer with a (H, C, N) Z-axis gradient probe. Spectra were processed with nmrPipe (Delaglio *et al.*, 1995) and analyzed with Sparky (Goddard *et al.*).

Results and Discussion

For LRT2, chemical shift assignment of backbone and sidechain resonances were made for 163 of the 164 non-proline residues in the ^{15}N-^{1}H HSQC spectra (Figure 3.1). The only residue for which the main chain amide peak was not assigned was E88. Assignments were determined for 99% of C^{α}, C^{β} and C', for 93% of non-aromatic and non-carbonyl side-chain carbons, for 91% of non-aromatic side-chain hydrogens, and for 98% of H^{α}. The backbone and side chain resonance assignments were automatically assigned using PINE Server (http://pine.nmrfarm.wisc.edu/) followed by manual validation and correction. The chemical shift assignments of LRT2 have been deposited in the BioMagResBank (http://www.bmrb.wisc.edu) under accession number 27159.

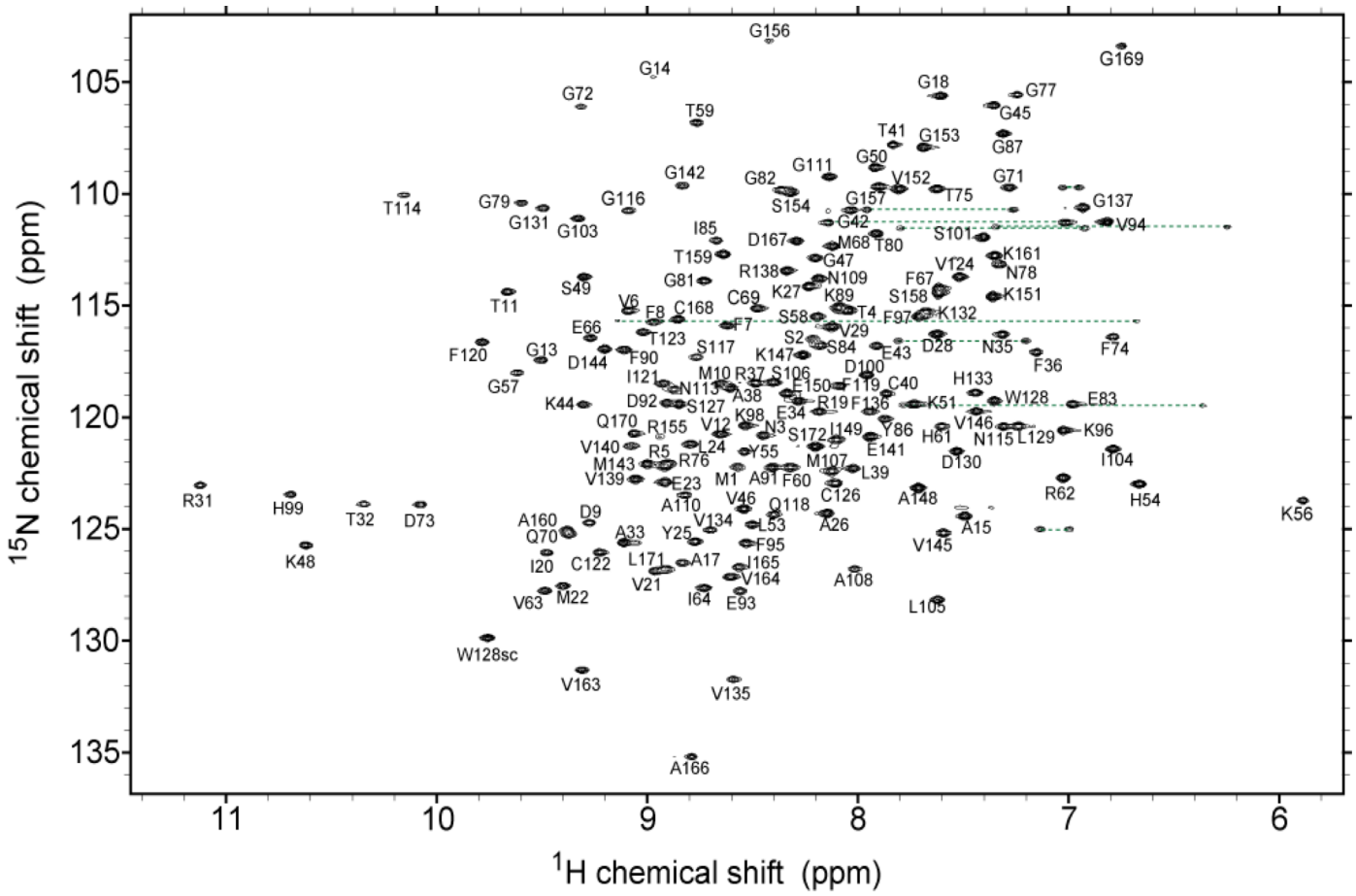

Figure 3.1 ^{15}N-^{1}H HSQC spectrum of 1.16mM ^{13}C,^{15}N labeled LRT2 recorded at 298K at 600MHz in 93%$H_2$0/7%$^{2}H_2O$, 20mM sodium phosphate buffer, pH 6.7, 50mM KCl, 5mM NaN3, 1mM TCEP. The cross peaks are labeled with single letter amino acid residue and number according to native sequence. Dotted lines indicate the side chain amides.

Our assigned LRT2 chemical shifts were used to predict the corresponding secondary structure using the TALOS-N Server (Shen *et al.*, 2013). LRT2 has 87.7% sequence identity to the cytosolic wheat cyclophilin TaCypA-1, for which its crystal structure has been solved (PDB entry 4HY7, Sekhon *et al.*, 2013). As expected, LRT2 chemical shift assignments predict a secondary structure similar to TaCypA-1 (Figure 2). In future work we will use the chemical shift assignments to study the complete thermodynamic cycle of the LRT2 enzyme acting on the OsIAA11 degron motif as well as on other Aux/IAA proteins of rice.

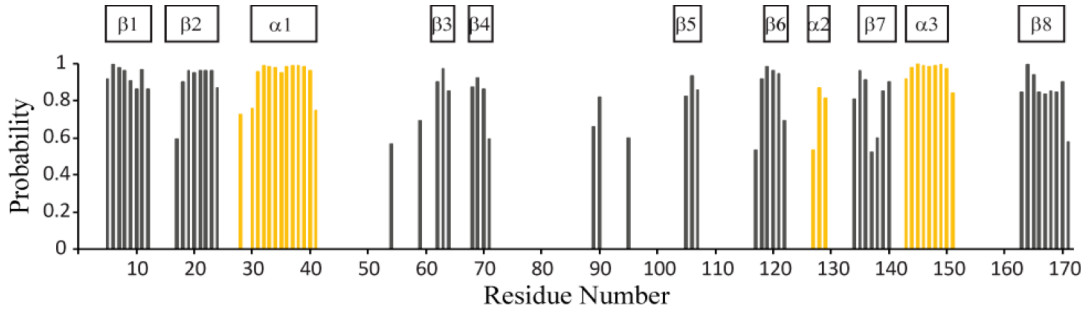

Figure 3.2 Probabilities for the secondary structure of LRT2 (yellow, a-helices; grey, b-strands) predicted from chemical shift with TALOS-N are plotted as a function of residue number. Probability values below 0.5 are not displayed. Position of secondary structure element of crystal structure of TaCypA-1 (PDB entry 4HY7 and 87.7% sequence identity to LRT2) are indicated on the top

Acknowledgments

This investigation was supported by the National Science Foundation (MCB-1615350) and through graduate student training grant support to LAA by the National Institutes of Health (2T32GM008267).

REFERENCES

Cui, P., Liu, H., Ruan, S., Ali, B., Gill, R. A., Ma, H., . . . Zhou, W. (2017). A zinc finger protein, interacted with cyclophilin, affects root development via IAA pathway in rice. *Journal of Integrative Plant Biology*, n/a-n/a. doi:10.1111/jipb.12531

Delaglio, F., Grzesiek, S., Vuister, G. W., Zhu, G., Pfeifer, J., & Bax, A. (1995). NMRPipe: A multidimensional spectral processing system based on UNIX pipes. *J Biomol NMR, 6*(3), 277-293. doi:10.1007/bf00197809

Dinesh, D. C., Villalobos, L. I., & Abel, S. (2016). Structural Biology of Nuclear Auxin Action. *Trends Plant Sci, 21*(4), 302-316. doi:10.1016/j.tplants.2015.10.019

Eisenmesser, E. Z., Bosco, D. A., Akke, M., & Kern, D. (2002). Enzyme Dynamics During Catalysis. *Science, 295*(5559), 1520-1523. doi:10.1126/science.1066176

Goddard, T. D., & Kneller, D. G. *SPARKY 3*. University of California, San Francisco.

Jing, H., Yang, X., Zhang, J., Liu, X., Zheng, H., Dong, G., . . . Zuo, J. (2015). Peptidyl-prolyl isomerization targets rice Aux/IAAs for proteasomal degradation during auxin signalling. *Nat Commun, 6*, 7395. doi:10.1038/ncomms8395

Kang, B., Zhang, Z., Wang, L., Zheng, L., Mao, W., Li, M., . . . Mo, X. (2013). OsCYP2, a chaperone involved in degradation of auxin-responsive proteins, plays crucial roles in rice lateral root initiation. *Plant J, 74*(1), 86-97. doi:10.1111/tpj.12106

Kumari, S., Roy, S., Singh, P., Singla-Pareek, S. L., & Pareek, A. (2013). Cyclophilins: proteins in search of function. *Plant Signal Behav, 8*(1), e22734. doi:10.4161/psb.22734

Kumari, S., Singh, P., Singla-Pareek, S. L., & Pareek, A. (2009). Heterologous expression of a salinity and developmentally regulated rice cyclophilin gene (OsCyp2) in E. coli and S. cerevisiae confers tolerance towards multiple abiotic stresses. *Mol Biotechnol, 42*(2), 195-204. doi:10.1007/s12033-009-9153-0

Lu, K. P., Finn, G., Lee, T. H., & Nicholson, L. K. (2007). Prolyl cis-trans isomerization as a molecular timer. *Nat Chem Biol, 3*(10), 619-629. doi:10.1038/nchembio.2007.35

Ruan, S.-L., Ma, H.-S., Wang, S.-H., Fu, Y.-P., Xin, Y., Liu, W.-Z., . . . Chen, H.-Z. (2011). Proteomic identification of OsCYP2, a rice cyclophilin that confers salt tolerance in rice (Oryza sativa L.) seedlings when overexpressed. *BMC Plant Biology, 11*, 34-34. doi:10.1186/1471-2229-11-34

Sekhon, S. S., Kaur, H., Dutta, T., Singh, K., Kumari, S., Kang, S., . . . Yoon, T. S. (2013). Structural and biochemical characterization of the cytosolic wheat cyclophilin TaCypA-1. *Acta Crystallogr D Biol Crystallogr, 69*(Pt 4), 555-563. doi:10.1107/s0907444912051529

Shen, Y., & Bax, A. (2013). Protein backbone and sidechain torsion angles predicted from NMR chemical shifts using artificial neural networks. *J Biomol NMR, 56*(3), 227-241. doi:10.1007/s10858-013-9741-y

Wang, P., & Heitman, J. (2005). The cyclophilins. *Genome Biology, 6*(7), 226-226. doi:10.1186/gb-2005-6-7-226

Zhu, Z. X., Liu, Y., Liu, S. J., Mao, C. Z., Wu, Y. R., & Wu, P. (2012). A gain-of-function mutation in OsIAA11 affects lateral root development in rice. *Mol Plant, 5*(1), 154-161. doi:10.1093/mp/ssr074

CHAPTER 4

Complete determination of the thermodynamic cycle between the cyclophilin LRT2 and its natural substrate OsIAA11[5].

Abstract

Protein-based molecular switches play essential roles in biological processes. While reversible phosphorylation and other covalent protein modifications are central to our understanding of signal transduction pathways, the non-covalent *cis-trans* isomerization of prolyl peptide bonds is an under-recognized yet potentially equally important class of bimodal switch utilized in biological pathways. The critical nature of the prolyl *cis-trans* switch is underscored by the presence from bacteria to humans of peptidyl prolyl isomerase enzymes such as cyclophilins that accelerate the intrinsically slow *cis-trans* exchange rate. A specific prolyl *cis-trans* switch in the transcription repressor protein OsIAA11, along with its associated cyclophilin LRT2, are known to be essential in a negative-feedback gene regulation circuit in rice that controls the initiation of lateral roots in response to the plant hormone auxin. Given their essential role in this auxin-responsive circuit, a quantitative characterization of the microscopic thermodynamic and kinetic parameters that define LRT2 catalysis of OsIAA11 is of great interest. Here we present NMR studies that determine and independently validate these parameters, providing important predictive power for understanding the impact of this reaction on the auxin-responsive circuit and the resulting lateral root phenotype in rice. These studies show that the observed

[5] This chapter is based on a manuscript to be submitted by Lucila Andrea Acevedo, Jeahoo Kwon, and Linda K. Nicholson.

isomerization rate is linearly dependent on LRT2 concentration but is independent of OsIAA11 concentration over a broad range, and that LRT2 is optimally tuned to maintain OsIAA11 at its equilibrium populations of *cis* and *trans* conformations to supply the slower downstream *cis*-specific proteasomal degradation pathway with maximal OsIAA11 substrate. Overall, these studies suggest that accelerating the LRT2-catalyzed isomerization would not impact circuit function, whereas decreasing this rate via LRT2 mutation could reveal the minimum isomerization rate for proper regulation of lateral root development.

Introduction

Peptidyl prolyl cis- trans isomerase (PPIase) enzymes are ubiquitous throughout essentially all biological systems, from bacteria to humans (Lu *et al*., 2007; Christoforides *et al.*, 2012; Davis *et al.*, 2010; Gothek *et al.*, 1999). These enzymes accelerate the rate of exchange between *cis* and *trans* isomers of X-Pro peptide bonds in target proteins. While the role of this class of enzymes was initially thought to be limited to protein folding, their functional involvements in a broad array of biological processes, including signal transduction, intracellular trafficking, gene transcription, cell cycle regulation, refolding of aggregated proteins, and regulation of reactive oxygen species by scavenging systems, are now convincingly demonstrated (Gothek *et al.*, 1999; G Fischer *et al.*, 2003; Lu *et al.*, 2007; Hanes, 2015; Perrucci *et al.*, 2015). Notably, a key way that a PPIase can regulate a biological pathway is to function as a molecular timer (Lu *et al.*, 2007). For plant cyclophilins, essential functions in the plant

cell have been determined for stress survival and for the initiation of lateral root development (Kumari *et al.*, 2012).

The *cis-trans* equilibrium of a prolyl peptide bond can operate as a binary molecular switch, since the structurally distinct *cis* and *trans* states can in principle have different binding partners (Figure 4.1B). For the amino acid Pro, the largely ignored backbone torsion angle ω can be either 0° (*cis*), or 180° (*trans*, as it is for the other 19 common amino acids in proteins) (Figure 4.1A). Proline is unique in its ability to adopt the *cis* isomer due to its closed ring sidechain structure that brings the *cis* and *trans* isomers of the peptide bond much closer in free energy (Williamson, 1994). For Pro in free peptides in aqueous solution, the *cis* isomer can exist at populations up to nearly 50%, while the remaining 19 amino acids are almost exclusively in *trans* (G Fischer et al., 2003). Because the transition energy barrier between *cis* and *trans* states is large (Figure 4.1A), in the absence of PPIases the isomerization of the peptidyl prolyl bond is relatively slow, $\sim 10^{-3}$ s^{-1} (Reimer *et al.*, 1998). Upon addition of PPIases this isomerization rate can increase by up to ~5 orders of magnitude (Hamelberg et al., 2009), bringing the exchange kinetics into the micro-to-millisecond regime that is typical for many types of cellular signaling events (Papin et al., 2005).

Auxin is a class of phytohormones that regulates essentially all developmental processes in plants (Normanly *et al.*, 2010). A major mechanism by which auxin acts is through feedback inhibition circuits that control the expression of auxin-responsive genes that are involved in specific developmental pathways (Del Pozo *et al.*, 2014; Enders *et al.*, 2015; Hagen *et al.*, 2002; Hayashi, 2012) (Figure 4.1C). The LRT2/OsIAA11 enzyme/substrate pair play an essential role in the auxin-responsive

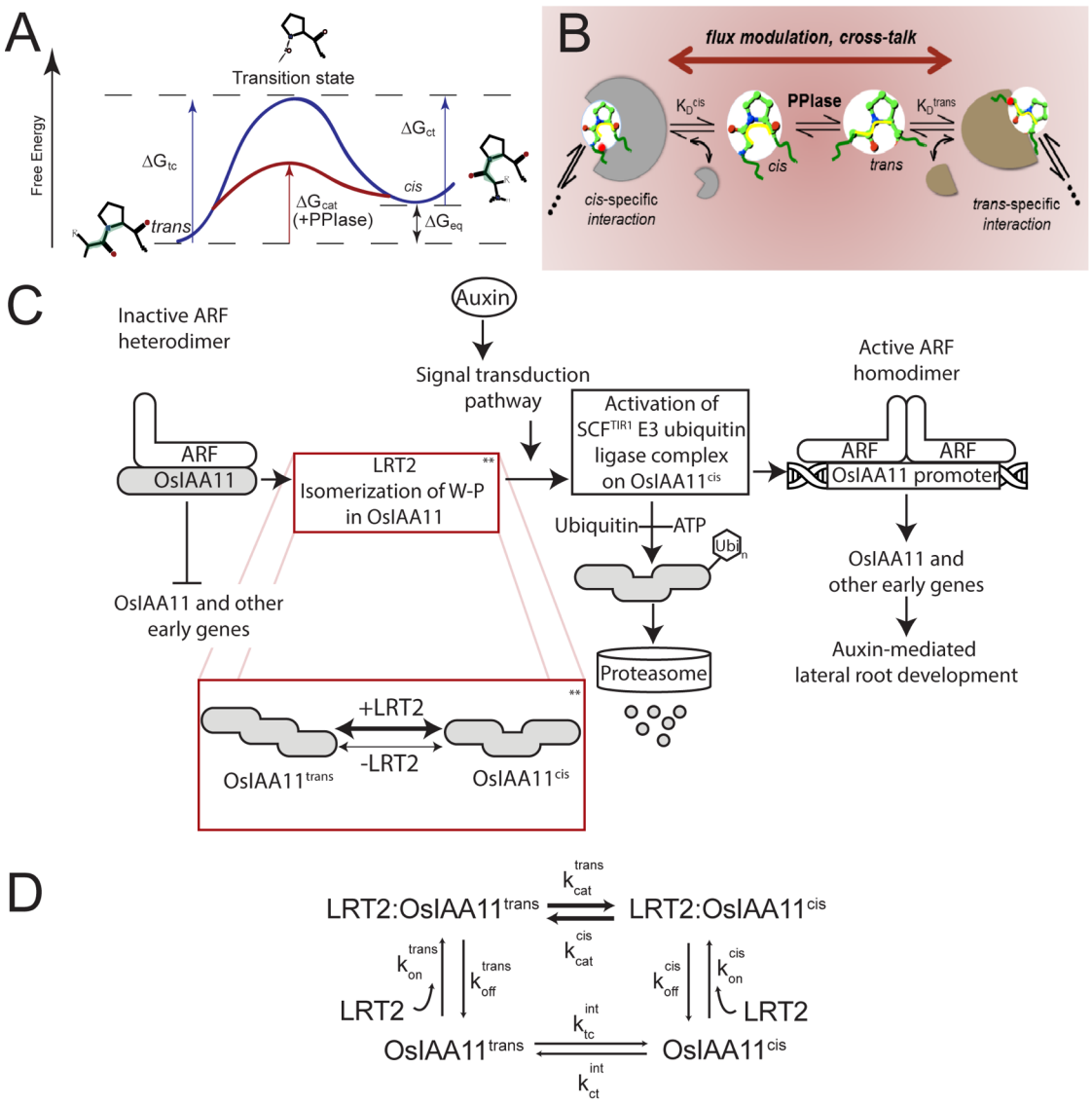

Figure 4.1 The prolyl *cis-trans* equilibrium as a bimodal switch. A. Energy landscape of uncatalyzed (blue) and catalyzed (red) *cis-trans* isomerization, where the activation barrier is lowered via catalysis by a PPIase enzyme such as LRT2. **B.** Illustration of how *cis-trans* isomerization of an X-Pro motif in a given protein can connect between otherwise isolated pathways, with kinetics governed by a PPIase enzyme. **C.** Schematic diagram of the auxin circuit. **D.** The four-state model for Lineshape fitting of ^{15}N-OsIAA11. This model describes four states: the *cis* and *trans* isomers of OsIAA11 ^{104}W-P^{105} bond in the free state, and each of the *cis* and *trans* isomers bound to LRT2.

circuit that controls the initiation of lateral roots in rice (Jing *et al.*, 2015; Su *et al.*, 2015). The repression of lateral root initiation genes is achieved through binding of OsIAA11 to an activating ARF transcription activator on the targeted promoter (Figure 4.1C). In the presence of auxin, OsIAA11 binds to auxin and the TIR1 component of the SCF^{TIR1} E3 ubiquitin ligase complex, inducing its release from ARF (Dharmasiri *et al.*, 2003; Kepinski *et al.*, 2005; Tan *et al.*, 2007). OsIAA11 is subsequently ubiquitinated and irreversibly degraded via the proteasome (Ramos *et al.*, 2001). The release of OsIAA11 from ARF activates transcription of the OsIAA-targeted auxin-responsive genes, including the gene encoding OsIAA11. Hence, as OsIAA11 is degraded, expression of its gene is activated, which leads again to repression as new OsIAA11 accumulates and binds to ARF on the promoter (Liscum *et al.*, 2002; Gray *et al.*, 2001; Mockaitis *et al.*, 2008; Reed, 2001; Tiwari *et al.*, 2001), thereby generating a classic negative feedback circuit (Figure 4.1C). The *cis*-specific interaction of OsIAA11 with TIR1, together with the essential role of LRT2 (Kang *et al.*, 2013; Zheng *et al.*, 2013), places this *cis- trans* molecular switch at a critical regulatory point in the auxin circuit (Figure 4.1C). This system offers an important opportunity for quantitative studies of a specific cis-trans molecular switch in a well-defined biological system characterized by a classic negative feedback circuit (Liscum *et al.*, 2002; Gray *et al.*, 2001; Mockaitis *et al.*, 2008; Reed, 2001; Tiwari *et al.*, 2001).

Here, we have applied Nuclear Magnetic Resonance (NMR) to quantitatively determine the microscopic thermodynamic and kinetic parameters of the four-state LRT2 reaction cycle acting on the OsIAA11 degron motif (Figure 4.1D). Isomerase activity assays are commonly used to define isomerization rates. However, this type of

assay uses specific peptides such as chymotrypsin to evaluate the enzyme activity (G. Fischer et al., 2003). Previous research has established that isomerization studies depend on the substrate sequence and that NMR can be used for the study of "natural" substrates for cyclophilin (Holliday et al., 2015). And as it has been discussed in previous works, the chymotrypsin assay only measures k_{cat}/K_m for the *cis/trans* isomerization (Bosco *et al.*, 2010). Conversely, NMR provides direct observation of *cis* and *trans* populations due to the slow timescale of interconversion which gives rise to distinct peaks, and has been widely used for the determination of isomerization in PPIases (Holliday et al., 2015; Greenwood et al., 2011). The detailed analysis of line shapes in NMR titration is a well-established method to extract information of mechanism, thermodynamics, and kinetics in protein-protein or protein-ligand interactions. Recently, multidimensional line shape analysis to determine mechanism of interaction has been used (Acevedo et al., 2017; Rennie et al., 2017; Shinya et al., 2017). Here, we used multidimensional lineshape analysis to determine the microscopic rates in the interaction of LRT2 with OsIAA11. Moreover, we demonstrate that flanking regions do not significantly alter LRT2 activity on the core degron motif. The resulting catalytic cycle parameters provide important predictive power for understanding this reaction at cellular concentrations, and for gaining critical insights regarding the utilization of an isomerase/substrate pair as a timing device in a developmental process.

Experimental

Plasmids, protein expression and purification

LRT2 was purified as previously described (Acevedo *et al.*, 2018), with the difference of using LB media for expression of unlabeled protein, and using M9

enriched only with $^{15}NH_4Cl$ for ^{15}N labeled protein. All LRT2 NMR samples were in 50mM KCl, 100mM KPO_4, 1mM TCEP, 0.1%P.I. cocktail, 5mM NaN_3, and 8% D2O, pH=6.67.

OsIAA11$^{72\text{-}125}$ gene was purchased from Genscript with a 3CPro recognition cleavage site at the N-terminal end. PCR was performed to introduce the recognition cutting sites of BamHI and HindIII. The PCR product was digested and followed by ligation into a PET28 vector with His6tag, TEV cleavage site and SUMO fusion protein at the N-terminus. The mutants of OsIAA11$^{72\text{-}125}$ (Figure 4.5) where purchased in a PET28 a(+) vector with the SUMO sequence, a 3CPro recognition cleavage site and same sequence as OsIAA11$^{72\text{-}125}$ except for point mutations. OsIAA11$^{72\text{-}125}$-1XP means that the four proline that can be binding to the cyclophilin are mutated to Alanine except for the $_{104}WP_{105}$ proline (e.g. OsIAA11$^{72\text{-}125}$ P89A, P91A, P94A, P97A). OsIAA11$^{72\text{-}125}$-2XP means that there are two X-P substrates for LRT2 (e.g. OsIAA11$^{72\text{-}125}$ P89A, P91A, P94A). OsIAA11$^{72\text{-}125}$-3XP means that there are three XP binding partners for LRT2 (e.g. OsIAA11$^{72\text{-}125}$ P89A, P91A). OsIAA11$^{72\text{-}125}$-4XP has all but the further XP possible (e.g. OsIAA11$^{72\text{-}125}$ P89A). Expression and purification was again carried like LRT2, with the exception of using 3CPro for cutting of His-SUMO tag for 48 hours.

The OsIAA11$^{98\text{-}109}$ peptide with acetyl and amide blocking groups on the N- and C-termini, respectively, was synthesized and purified by Tufts Core Facility.

NMR experiments

NMR experiments were performed at 25^{o}C on a Varian Inova 600 MHz spectrometer with a (H, C, N) Z-axiz gradient probe.

For lineshape analysis titration experiments, ^{15}N- OsIAA11$^{72\text{-}125}$ was held at 0.26mM concentration, while unlabeled LRT2 concentrations were 0, 0.002, 0.011, 0.020, 0.039, 0.110, 0.200, 0.390, and 0.800 mM. At each titration point, an ^{15}N-^{1}H fast HSQC spectrum (Mulder *et al.*, 1999) was taken with a spectral width of 2.0kHz (8 kHz) in t1 (t2), and a total of 512 (2048) complex data points. A total of 64 scans were taken for each titration point, for a total time of 11 hours per spectrum. Spectra were processed with nmrPipe (Delaglio *et al.*, 1995). Free induction decays were processed with an exponential window function, a zero filled with 8192 points in the proton dimension and 2048 as well as a linear prediction prior to Fourier transformation.

[^{15}N] LRT2 HSQC titration experiments were performed with OsIAA11$^{72\text{-}125}$ protein to measure K_D^{App}. The sample with the highest concentration of unlabeled ligand was produced first, and then subsequent dilution samples with a stock solution of [^{15}N] LRT2 was produced to have same [^{15}N]-label LRT2 protein concentration. The concentration of [^{15}N] LRT2 was held at 0.235mM. The concentrations of OsIAA11$^{72\text{-}125}$ were 0, 0.04, 0.09, 0.17, 0.33, 0.71, 1.50, and 2.79 mM. The concentrations of the proteins were determined by UV absorbance based on the theoretical extinction coefficient of 10,220 cm^{-1}M^{-1} and 5,500 cm^{-1}M^{-1} at 280 nm for LRT2 and OsIAA11$^{72\text{-}125}$ respectively. At each titration point, an ^{15}N-^{1}H fast HSQC spectrum (Mulder *et al.*, 1999) was taken with a spectral width of 2.4kHz (8 kHz) in t1 (t2), and a total of 512 (2048) complex data points. The number of scans were 16, 64, 20, 26, 24, 20, 64, 16 respectively for each titration point. Spectra were processed and analyzed with nmrPipe (Delaglio *et al.*, 1995), Sparky (Goddard *et al.*,), and TITAN (Waudby *et al.*, 2016). Free induction decays were processed with an exponential window function, a zero

filled as well as a linear prediction prior to Fourier transformation. ^{15}N-LRT2 assignments have been previously reported (Acevedo *et al.*, 2018)

For rate measurements, 0.8mM of ^{15}N- OsIAA11$^{72-125}$ WT and its mutants with and without 16μM of LRT2 was prepared. The rate of interconversion between the *cis* and *trans* isomers was measured by taking a series of ZZ-exchange (Montelione *et al.*, 1989; Farrow *et al.*, 1994) spectra with varying mixing time. The rate measurements were taken with mixing times of 0.011, 0.11, 0.22, 0.44, 0.55, 0.67, 0.89 and 1.00 s. Spectra width were 2.4kHz in the Nitrogen dimension and 8kHz in the proton dimension, and 512 (2048) complex data points. A total of 48 scans per FID were acquired. Spectra were processed and analyzed with nmrPipe (Delaglio *et al.*, 1995), Sparky (Goddard *et al.*,). Free induction decays were apodized using a shifted sine bell function, a zero filled as well as a linear prediction were used prior to Fourier transformation. Additionally, the LRT2-catalyzed W-P isomerization rate of the shorter degron peptide, OsIAA11$^{98-109}$ ($_{98}$KAQVVGWPPVRS$_{109}$), was measured by Rotating frame Overhauser Effect SpectroscopY (ROESY) (Bax *et al.*, 1985). A stock solution was prepared into same buffer conditions of LRT2 (50mM KCl, 100mM KPO_4, 1mM TCEP, 0.1%P.I. cocktail, 5mM NaN_3, and 8% D2O, pH=6.67). For the ROESY set of experiments, LRT2 concentration was 120μM and OsIAA11$^{98-109}$ concentration was 1.84mM. ROESY experiments were run with mixing times of 30, 50, 70, 90, 110, and 130 ms. Each ROESY spectrum was taken with a spectral window of 8.4kHz in both dimensions, and a total of 512 (4096) complex points in t1 (t2). A total of 16 scans were acquired per FID. Spectra were processed with nmrPipe (Delaglio *et al.*, 1995), nmrdraw (Delaglio *et al.*, 1995) and Sparky (Goddard *et al.*,). Free induction decays

were apodized using a shifted sine bell function, where zero filled was applied prior to Fourier transformation.

Data fitting

Two dimensional lineshape analysis was performed using TITAN software (Waudby *et al.*, 2016). For ^{15}N-OsIAA11$^{72\text{-}125}$ titrated with LRT2, data was fit to the built-in four state model, which considers the free and bound states of the *cis* and *trans* isomer. Fitted parameters include the on-enzyme equilibrium (K_{eq}^{bound}), the on-enzyme catalysis rate (k_{ex}^{cat}), the apparent affinity (K_D^{App}), the chemical shift of the bound state for each isomer, and the linewidths of the bound state of each isomer ($R_{2,0}^{bound}$). Constrained parameters include the equilibrium constant in the free state (K_{eq}^{free}), which was measure by 1D spectroscopy (Appendix 4.1), the intrinsic exchange rate (k_{ex}^{int}), the chemical shift of the free state for each isomer, the linewidth of the free state ($R_{2,0}^{free}$) and the reverse binding rates (k_{off}^{cis}, k_{off}^{trans}). The chemical shift of the free state, and $R_{2,0}^{free}$ were fit for ^{15}N-OsIAA11$^{72\text{-}125}$ with 0mM LRT2 and values obtained from this spectrum were used throughout the lineshape analysis. The intrinsic exchange rate (k_{ex}^{int}) was kept to 0.0008 s^{-1} based on rate constants previously reported for a W-P peptide bond (Reimer *et al.*, 1998). The reverse binding rates were not deemed to be reliable extractable parameters, they were constrained assuming a diffusion limit on rate of $\geq 10^7$ M^{-1} s^{-1}. Other parameters were calculated based on the following equations:

$$K_D^{cis} = K_D^{App} \frac{\left(1+k_{eq}^{bound}\right)}{\left(1+k_{eq}^{free}\right)} \quad \text{Eq. 1}$$

$$K_D^{trans} = K_D^{App} \frac{\left(k_{eq}^{free}\right)}{\left(k_{eq}^{bound}\right)} \frac{\left(1+k_{eq}^{bound}\right)}{\left(1+k_{eq}^{free}\right)} \quad \text{Eq.2}$$

To confirm the apparent affinity, ^{15}N-LRT2 titrated with OsIAA11$^{72\text{-}125}$ data was fit using a built-in two state model in TITAN to determined K_D^{App}, as well as bound chemical shifts. For all TITAN fittings a bootstrap error with 100 replicas was carried to calculate uncertainties in the fitted values.

ZZ- exchange and ROESY peak heights for auto-peaks and cross-peaks corresponding to the indole proton in W104 were obtained by using Sparky processing software (Goddard *et al.*,). Peak intensities were fit as described elsewhere (Greenwood *et al.*, 2011; Nechama *et al.*, 2018).

Results

Determination of the Microscopic Thermodynamic and Kinetic Parameters for LRT2 Catalysis of OsIAA11 Degron Motif

Given the essential function of the LRT2:OsIAA11 interaction in the auxin circuit and in the initiation of later root development in rice plants, it is important to obtain a quantitative characterization of this timing device. To quantify the thermodynamic and kinetic parameters that govern LRT2 catalysis of the WP peptide bond in the degron motif of OsIAA11, we applied NMR titration spectroscopy and lineshape analysis (Greenwood *et al.*, 2011; Waudby *et al.*, 2016). From the perspective of OsIAA11, this reaction can be modeled as a four-state equilibrium, with an equilibrium constant and forward and reverse rate constants for each of the four connecting steps (Figure 4.1D). The free *trans* and *cis* states of OsIAA11 are maintained at their equilibrium populations determined by their relative energies, and the bound populations are determined by the binding affinities of the *trans* and *cis* OsIAA11 isomers to LRT2. Exchange between these four states occurs at rates determined by the

rate constants and concentrations of the system components. The thermodynamic and rate constants provide a complete characterization of the catalytic reaction, providing predictive power for calculating the expected overall exchange rate between free *trans* and *cis* for any concentrations of LRT2 and OsIAA11.

To measure the microscopic reaction parameters, the concentration of ^{15}N-OsIAA11$^{72\text{-}125}$ was kept constant and a reverse-titration with unlabeled LRT2 was performed to generate a series of two-dimensional (2D) ^{1}H-^{15}N-HSQC spectra that were subjected to lineshape analysis. To reduce the number of fitted parameters in the four-state model, required parameters associated with free ^{15}N-OsIAA11$^{72\text{-}125}$ were determined independently of the titration. Peak volumes corresponding to the well-resolved W104 indole H_N in *cis* and *trans* states in a one-dimensional NMR spectrum of apo ^{15}N-OsIAA11$^{72\text{-}125}$ (Appendix Figure 4.1) were used to quantify the equilibrium constant K_{eq}^{free}. The resulting value, K_{eq}^{free} = 1.113, reflects nearly equal *cis* (0.46) and *trans* (0.54) fractional populations, similar to previously reported values for W-P peptide bonds (Reimer *et al.*, 1998). Moreover, based on the ~0.2 ppm separation of the distinct *cis* and *trans* peaks in the ^{1}H dimension, the intrinsic exchange rate must be much slower than 0.008 s^{-1} (i.e., $k_{ex}^{int} = k_{ct}^{int} + k_{tc}^{int} << 0.008$ s^{-1}). Since this regime of k_{ex}^{int} is too slow to influence lineshapes, k_{ex}^{int} was set to 0.0008 s^{-1} for the purpose of simulation, which is consistent with the intrinsic rate previously reported for a W-P peptide bond (Reimer *et al.*, 1998). The determined K_{eq}^{free} and k_{tc}^{int} values are independent of LRT2 and were held constant throughout the titration simulation. Additionally, the chemical shifts and R_2 values for the free state of individual peaks

were determined through fitting the apo 2D ^{1}H-^{15}N-HSQC spectrum of ^{15}N-OsIAA11$^{72-125}$ using TITAN (Waudby *et al.*, 2016) (Table 4.1).

The backbone N-H of Gly103 and the indole NH of W104 each give rise to well-resolved *trans* and *cis* peaks in the 2D ^{1}H-^{15}N-HSQC spectrum of ^{15}N-OsIAA11$^{72-125}$ (Figure 4.2A), providing two independent views of the isomerization reaction. As the concentration of unlabeled LRT2 was changed, changes in position and lineshape of these peaks were observed (Figure 4.2B,C and Appendix Figure 4.2). These changes were simulated and fit using TITAN to determine the microscopic parameters for the four state model (Waudby *et al.*, 2016). Notably, residuals of the fits were found to be insensitive to the dissociation rate constants k_{off}^{cis} and k_{off}^{trans} when these values were > 1000 s^{-1}, and to increase (corresponding to worsening fit) when these rates were reduced below 1000 s^{-1}, indicating that these rates were too fast to influence lineshapes (Table 4.2). Thus, these parameters were constrained at values consistent with diffusion-limited on-rates (Table 4.1) as previously described (Greenwood *et al.*, 2011). Applying a bootstrap error analysis and simultaneously fitting the G103 and W104 sets of peaks using TITAN, the lineshape analysis yielded optimized K_{eq}^{bound}, K_D^{App} and k_{ex}^{cat} values (Table 4.1) as well as the chemical shifts and R_2 values for the bound state of individual peaks (Table 4.1). The binding affinities (K_D^{cis}= K_D^{trans} = 1.55 mM) were obtained using Eqs. 1 and 2, and are consistent with the weak affinity characteristic of other PPIases (Greenwood *et al.*, 2011). The binding and equilibrium constants indicate that the LRT2:OsIAA11 reaction is strikingly balanced from a thermodynamic perspective, with nearly equal affinities of *cis* and *trans* isomers, and with both on-enzyme and free equilibrium constants near 1. Also notable is the on-enzyme exchange rate of ~95 Hz,

which is relatively slow in comparison with values reported for other isomerase:substrate reactions that have been examined at the same level of detail (Labeikovsky *et al.*, 2007; Greenwood *et al.*, 2011; Holliday *et al.*, 2015).

Table 4.1 Summary of fitted and constrained parameters

Fit Parameters	**On-enzyme trans/cis**		**K_D^{App} (mM)**		**On-enzyme k_{ex} (s^{-1})**	
	1.119±0.110		1.55±0.19		94.72±8.49	
Constrained Parameters	**Free trans/cis[a]**		**Uncatalyzed k_{ex} (s^{-1})[b]**		**k_{off}^{cis} (s^{-1})[c]**	**k_{off}^{trans} (s^{-1})[c]**
	1.113		0.0008		17000	15000
Nucleus-Specific Parameters	**Residue**	**Isomer**	**Nuclei**	**State**	**ω (p.p.m.)**	**R_2 (Hz)**
	G103	*cis*	^{1}H	Free	8.518±0.002	33.617±1.625
				Bound	8.471±0.002	22.071±6.395
			^{15}N	Free	113.083±0.003	18.422±1.522
				Bound	112.874±0.021	20.841±8.552
		trans	^{1}H	Free	8.292±0.001	31.241±1.501
				Bound	8.314±0.002	21.300±5.406
			^{15}N	Free	112.655±0.002	14.996±1.243
				Bound	113.135±0.020	22.361±6.289
	W104	*cis*	^{1}Hε	Free	10.277±0.001	12.252±0.442
				Bound	10.265±0.001	21.941±4.708
			^{15}N Hε	Free	129.961±0.001	10.659±0.491
				Bound	129.849±0.009	22.130±4.432
		trans	^{1}Hε	Free	10.088±0.001	11.325±0.386
				Bound	10.072±0.001	23.152±4.978
			^{15}N Hε	Free	129.155±0.001	7.909±0.377
				Bound	129.031±0.008	22.027±4.455

[a] Determined from peak volume (Supplemental Figure 4.1)

[b] Based on rate constants previously reported for a W-P peptide bond (Reimer *et al.*, 1998)

[c] Assuming a diffusion-limited on-rate of $\geq 10^7 M^{-1}s^{-1}$

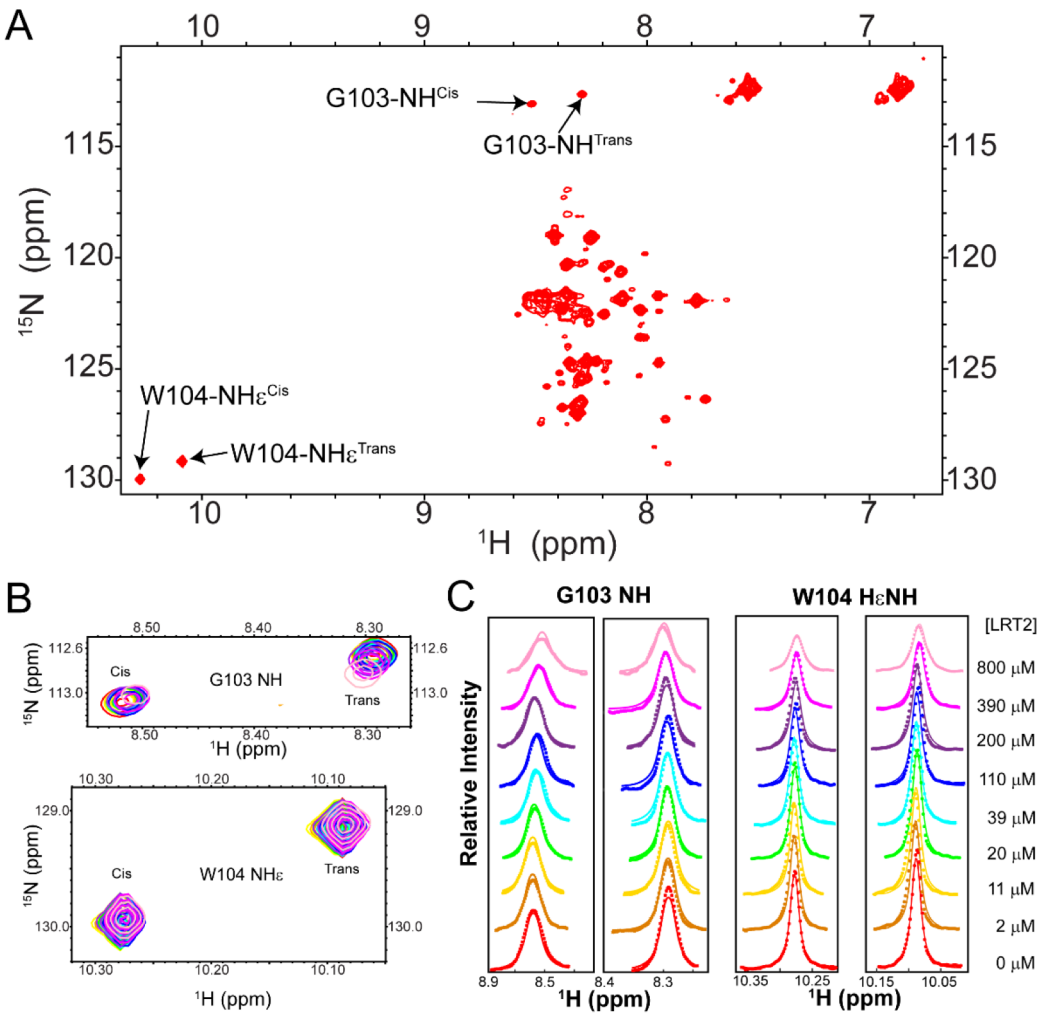

Figure 4.2 NMR lineshape fitting of ^{15}N-OsIAA11$^{72\text{-}125}$ titration data. A. ^{15}N-^{1}H-HSQC of OsIAA11$^{72\text{-}125}$, where G103NH is well resolved, as well as the indole proton for W104 both cis and trans isomers. **B.** Overlay of ^{15}N- ^{1}H-HSQC spectra of 0.26mM ^{15}N-labeled OsIAA11$^{72\text{-}125}$ expanded for G103HN and W104 indole NH with varying amounts of unlabeled LRT2, from 0 mM (red) to 800µM (pink). **C.** Lineshape simulations using the microscopic kinetic rates found by lineshape analysis with TITAN (K_{eq}^{free}=1.113, K_{eq}^{bound}=1.119, k_{ex}^{bound}=k_{cat}^{cis}+k_{cat}^{trans} =94.7s^{-1}, K_D^{app}=1.55mM). $R_{2,0}^{free}$, $R_{2,0}^{bound}$, and bound chemical shift were allowed to fit in this simulation where the scalar coupling values were set at 6.5Hz for the G103HN and 3Hz for the Indole HN in W104. For simplicity only the signal in the proton dimension is shown here, 2D lineshape analysis simulation with TITAN in Appendix 4.2.

Table 4.2 K_{eq}^{bound} and K_{ex}^{bound} calculated with different values of K_{off}^{cis} and K_{off}^{trans}

Constrained parameters		Fit Parameters		Residual (TITAN)
K_{off}^{cis}	K_{off}^{trans}	K_{eq}^{bound}	K_{ex}^{bound}	
17000[a]	15000 [a]	1.119±0.110 [a]	94.72±8.49 [a]	3.8141 x10^6
170	150	1.119±0.108	90.930±7.817	3.9267 x10^6
1700	1500	1.131±0.109	95.105±9.292	3.8153 x10^6
170000	150000	1.136±0.116	93.420±7.221	3.8133 x10^6

[a] Values used and reported in Table 4.1.

Independent measurements validate the fitted microscopic thermodynamic and kinetic parameters

Independent validation of the fitted parameters obtained from lineshape analysis is important, since TITAN provides neither a mechanism for discriminating between models nor a rigorous approach for evaluating the accuracy of the fitted parameters. The ^{15}N-ZZ-exchange and ROESY NMR experiments provide independent measures of the overall catalyzed isomerization exchange rate, k_{ex}^{obs} (Figure 4.3A and Figure 4.7A, respectively), for specific enzyme and substrate concentrations. The reversible Michaelis-Menten equation expresses this NMR-observed exchange rate in terms of the microscopic constants and the concentrations of enzyme and substrate (Greenwood *et al.*, 2011):

$$k_{ex}^{obs} = \left(\frac{k_{cat}^{trans}}{K_D^{trans}} + \frac{k_{cat}^{cis}}{K_D^{cis}}\right) \frac{[E]^{total}}{1 + \frac{[trans]^{free}}{K_D^{trans}} + \frac{[cis]^{free}}{K_D^{cis}}} \qquad \text{Eq. 3}$$

where $[E]^{total}$ is the total enzyme concentration, while $[trans]^{free}$ and $[cis]^{free}$ are the concentrations of the indicated isomer in the free state. Using Eq. 3 and the fitted parameters obtained from lineshape analysis, k_{ex}^{obs} can be predicted for a given sample condition, and compared with the NMR-measured exchange rate for that sample.

To evaluate the validity of the model and the fitted parameters, k_{ex}^{obs} was measured using the 2D ^{1}H-^{15}N heteronuclear (ZZ) exchange experiment. The indole N-H of Trp104 in the *cis* and *trans* states show distinct exchange cross peaks for a sample containing 0.8 mM ^{15}N-OsIAA11 and 16 μM LRT2, whereas these cross peaks are absent when no LRT2 is present (Figure 4.4A). Acquisition of a series of spectra with different mixing times and quantitative analysis of the auto- and cross-peak intensities of the well resolved W^{104} indole NH as a function of mixing time allowed determination of the overall exchange rate (Figure 4.4B,C), as described elsewhere (Greenwood *et al.*,

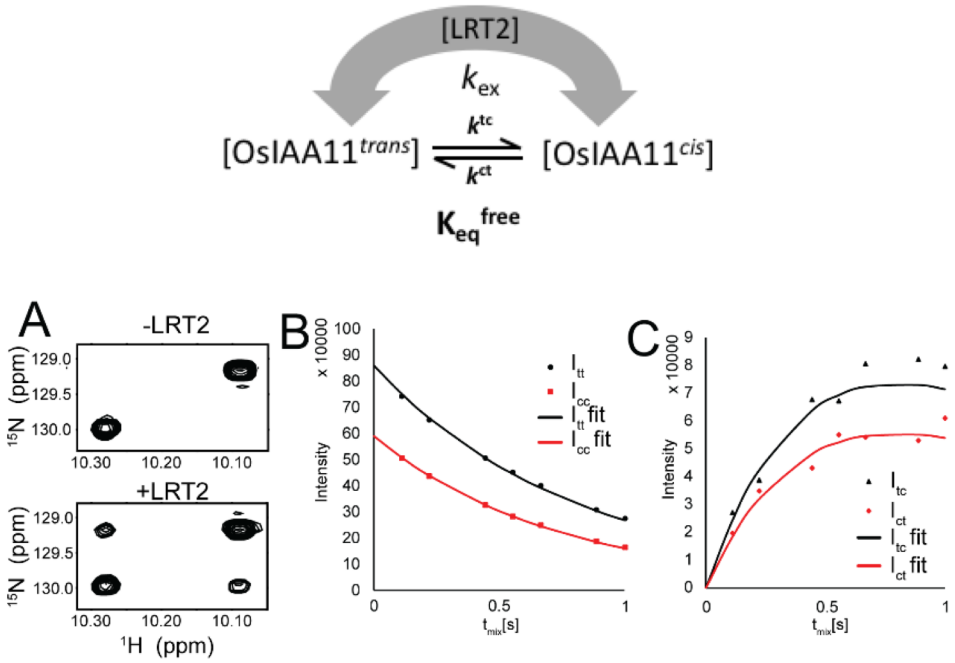

Figure 4.3 ZZ-exchange experiments in ^{15}N-OsIAA11$^{72-125}$ in the presence of LRT2. A. ZZ-exchange spectra with mixing time of 0.55s for the indole HN in W104 without LRT2 (top) and with 16μM LRT2 (bottom) show isomerization. **B.** Intensity of auto-peaks for indole HN in W104 in the presence of 16μM LRT2 as function of mixing time, t_{mix}. **C.** Intensity of cross-peaks for indole HN in W104 in the presence of 16μM LRT2 as function of mixing time, t_{mix}.

2011). The resulting value, k_{ex}^{obs} = 0.62 s^{-2}, agrees extremely well with the value predicted by Eq. 3 for these conditions, k_{ex}^{obs} = 0.64s^{-1}. This demonstrates that the four-state catalytic model and the fitted parameters summarized in Table 4.1 are able to accurately predict the experimentally observed exchange rate for a specific sample condition.

For further validation, K_D^{App} was experimentally measured from the ^{15}N-LRT2 perspective. Of the 164 non-proline backbone peaks in the ^{15}N-LRT2 ^{1}H-^{15}N-HSQC spectrum, 20 have a significant composite chemical shift perturbation when 2.79mM of OsIAA11$^{72\text{-}125}$ is added, and trajectories that can be tracked throughout the titration (Figure 4.4A). Significant change corresponds to a composite chemical shift perturbation that is one standard deviation larger than the average across the protein ($\overline{\Delta\omega}$ = 0.026ppm with standard deviation σ=0.030ppm). The LRT2 amino acid sequence is 87.7% identical to a cytosolic wheat cyclophilin, TaCypA-1, which is the closest LRT2 homolog for which a structure has been solved (Protein Data Bank ID 4hy7.1 Sekhon *et al.*, 2013). Using 4hy7.1 as a template, a high quality (QMEAN=0.95, GMQE=0.95) LRT2 homology model was constructed (Figure 4.4B). Alignment of this homology model with the structure of Human Cyclophilin A (CypA) shows a conserved structure (Figure 4.4C). Based on this alignment, all residues selected to determine the binding affinity are located in or near the well-conserved binding region of CypA (Figure 4.4B,C). Some of these selected peaks broaden considerably upon addition of OsIAA11$^{72\text{-}125}$ (e.g., G72, N109, W128sc), likely due to intermediate exchange associated with binding and/or isomerization kinetics. The 20 selected residues were fit simultaneously using the one bound state

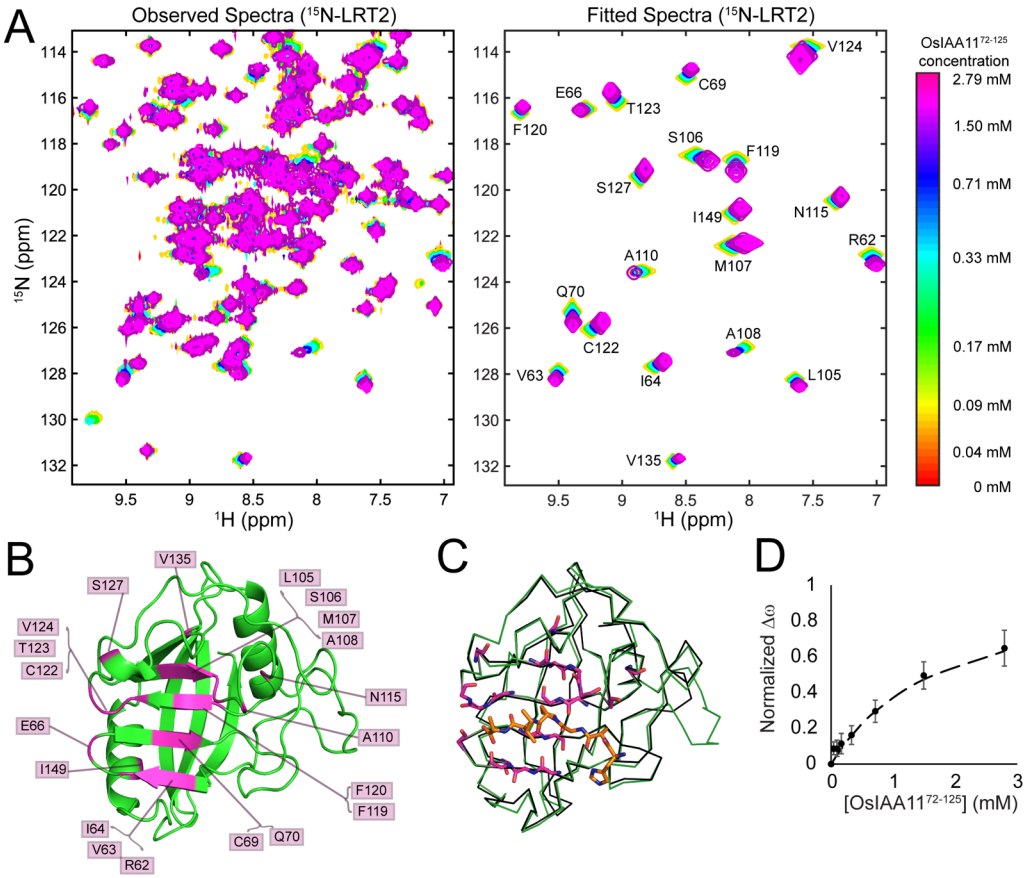

Figure 4.4 ^{15}N-labeled LRT2 titration with unlabeled OsIAA11$^{72-125}$. A. Chemical shift perturbation of ^{15}N-labeled LRT2 upon titration with unlabeled OsIAA11$^{72-125}$. Overlay of region where residues with a significant chemical shift perturbation is observed, experimental spectra on left and fitted by TITAN on right. **B.** Residues selected to determine the binding affinity are shown in magenta mapped on the homology model for LRT2. **C.** Structural alignment of LRT2 homology model (green) and crystal structure of Human Cyclophilin (black) bound to HAGPIA peptide (orange sticks) (PDB=1AWR). Residues selected for determining the affinity to OsIAA11$^{72-125}$ are shown (magenta sticks). **D.** Binding curve for K_D=1.54mM (dash line), and experimental data points corresponding to the average of normalized chemical shift change for the 20 residues used to determine the affinity (dots). **E.** Sequence alignment of LRT2, TaCypA and Human Cyclophilin A. Residues used to determine affinity are colored magenta.

model in TITAN. A bootstrap error analysis was carried out for 100 runs, yielding a K_D^{App}=1.54±0.06mM and k_{off}=8850±2350s^{-1}. These values agree fully with those derived above from lineshape analysis of ^{15}N-OsIAA11 titrated with unlabeled LRT2 (K_D^{App}= 1.55 mM, k_{off}^{cis} and k_{off}^{trans} > 1000 s^{-1}), providing further validation of the fitted parameters of the four-state model (Table 4.1). Notably, although OsIAA11$^{72\text{-}125}$ has five X-Pro peptide bonds that could serve as substrates for LRT2 (Figure 4.5A), the complete agreement between the K_D^{App} values determined from the LRT2 and OsIAA11 perspectives suggests that the additional X-P peptide bonds do not significantly interfere with LRT2 catalysis of the W-P motif in OsIAA11.

LRT2-catalyzed isomerization of OsIAA11 degron motif is not altered by upstream X-P motifs

Previous studies of LRT2 catalysis of the OsIAA11 degron motif have utilized a 12-residue peptide corresponding to OsIAA11 residues 98 – 109 (OsIAA11$^{98\,-\,109}$, Figure 4.5A; Jing et al., 2015). However, flanking regions outside this degron motif have been reported to be important for setting the degradation rate and for recognition by the E3 ligase (Moss *et al.*, 2015; Winkler *et al.*, 2017). These flanking regions are conserved in phylogenetically distant members of Arabidopsis, including rice. As noted above, upstream of the degron motif in OsIAA11 there are four additional X-P motifs (Figure 4.5A). To investigate potential influence of these other X-P motifs on the LRT2-catalyzed isomerization rate of the degron motif, Pro-to-Ala mutagenesis was used to generate constructs with between one and five X-P motifs (Figure 4.5A). For example, OsIAA11$^{72\text{-}125}$-1XP has only W^{104}-P^{105} present, while OsIAA11$^{72\text{-}125}$-2XP

retains W^{104}-P^{105} and includes the nearest X-P motif, A^{96}-P^{97}, with the other X-P sites mutated to X-A, and so on (Figure 4.5A). Application of the ^{15}Nzz-exchange experiment to each ^{15}N-OsIAA11 mutant (0.8 mM) in the presence of catalytic concentration of LRT2 (16μM) shows that LRT2-catalyzed isomerization occurs (Figure 4.5B), whereas in the absence of LRT2, cross peaks are not detected (data not shown). The isomerization rate of the W^{104}-P^{105} peptide bond, k_{ex}^{obs}, was measured for each mutant in the presence of LRT2 using the W^{104} indole N-H peaks as described above. The intensity signal for the auto peaks (I_{tt}, I_{cc}) and cross peaks (I_{tc}, I_{ct}) were fit

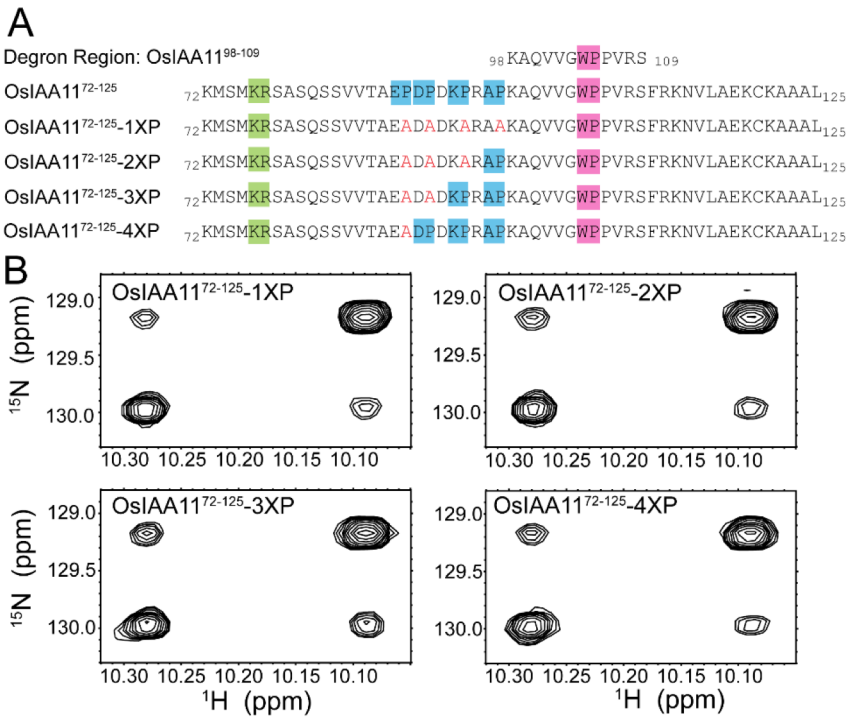

Figure 4.5. Flanking X-P peptide bonds do not affect the isomerization of LRT2. **A.** Sequence alignment for OsIAA11 mutants to determine if flanking X-P (blue boxes) affect isomerization in ^{104}W-P^{105} peptide bond (magenta box). KR (green box) has been previously shown as an important flanking region for degradation rates of Aux/IAA proteins. **B.** ZZ-exchange spectra with mixing time of 0.55s for the indole HN in W104 with 16μM LRT2 shows similar isomerization for all the mutants.

to the two state solution of the Block-McConnell equations (Cavanagh *et al.*, 2010; Farrow *et al.*, 1994) to determine the isomerization rate (Data not shown). Upon global fitting the exchange value $k_{ex}^{obs} = k_{cis \rightarrow trans} + k_{trans \rightarrow cis}$ was obtained for each mutant (Table 4.3). The resulting k_{ex}^{obs} values are all highly similar to WT (ranging from 0.78 to 1.24 times WT), indicating that the additional X-P motifs do not alter significantly LRT2 catalysis of the W-P peptide bond in the degron motif of OsIAA11.

Peptide OsIAA11$^{98\text{-}109}$ accurately represents OsIAA11 as an LRT2 substrate

Table 4.3 Isomerization rates of LRT2 acting on OsIAA11$^{72\text{-}125}$ WT and mutants

OsIAA11$^{72\text{-}125}$ construct	Isomerization rate k_{ex} [s^{-1}]
WT	0.620±0.013
1XP	0.487±0.011
2XP	0.678±0.012
3XP	0.767±0.013
4XP	0.582±0.011

The insensitivity of k_{ex}^{obs} to the additional X-P motifs upstream of the W^{104}-P^{105} peptide bond raises the question of whether the microscopic thermodynamic and kinetic parameters determined for LRT2:W^{104}-P^{105} reaction using the longer OsIAA11$^{78\text{-}125}$ construct might accurately predict LRT2 binding and isomerization of the previously reported 12-residue degron peptide *OsIAA11$^{98\text{-}109}$* (Jing *et al.*, 2015). To address this question, the OsIAA11$^{98\text{-}109}$ peptide (blocked on each end) was employed, K_D^{App} was measured using ^{15}N-6xHis-LRT2 titrated with *OsIAA11$^{98\text{-}109}$* (Figure 4.6), and k_{ex}^{obs} was measured using the 2D homonuclear ROESY experiment using the well-resolved indole H_N peaks of Trp104 for a sample containing 1.84 mM OsIAA11$^{98\text{-}109}$ and 120 μM LRT2

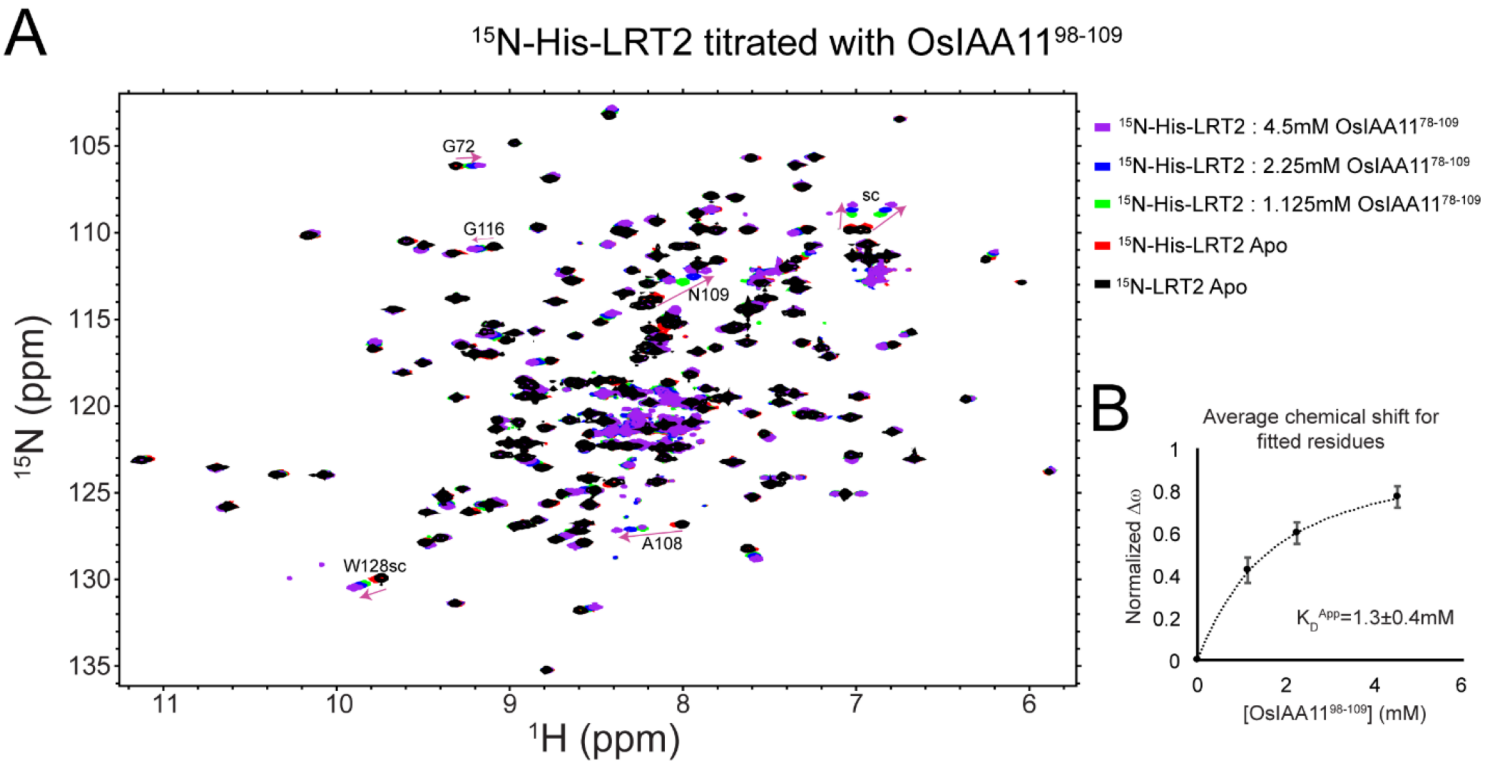

Figure 4.6 Dissociation affinity determination for LRT2:OsIAA11$^{78-109}$. A. Overlay of ^{15}N-^{1}H HSQC spectra of ^{15}N-His-LRT2 (0.55 mM) with varied degron peptide concentrations (shown) and ^{15}N-LRT2 apo (black). **B.** Binding curve for K_D^{App}=1.3 ± 0.4 mM (dash line), average of normalized chemical shift change for the 7 residues used to determine the affinity (dots). Buffer conditions were 50mM KCl, 100mM KPO_4, 1mM TCEP, 0.1%P.I. cocktail, 5mM NaN_3, 8% D_2O, pH=6.5. *The expression, purification, NMR acquisition and analysis of this titration was performed by co-author in the paper to be submit Jeahoo Kwon. The author of this dissertation create the figure.*

(Figure 4.7). The resulting K_D^{App} value (1.3 ± 0.4mM, Figure 4.6) is within the experimental error of the corresponding value determined for OsIAA11$^{72\text{-}125}$ (1.54 ± 0.06mM), demonstrating that the core degron sequence represents the complete LRT2 binding epitope. Moreover, the measured k_{ex}^{obs} value of 3.6 s^{-1} (Figure 4.7) is in excellent agreement with the predicted value of 3.4 s^{-1} (from Eq.3 using the fitted constants in Table 4.1). The previously published k_{ex}^{obs} value of 0.95 s^{-1} measured by ROESY for a sample containing 50μM LRT2 and 2 mM OsIAA11$^{98\text{-}109}$ is also reasonably predicted as 1.3 s^{-1}, even though the sample buffer conditions were not identical to those used here (Jing *et al.*, 2015). Together, these independent measurements demonstrate that the microscopic thermodynamic and kinetic parameters determined here provide broad predictive power, and that the 12-residue degron peptide accurately represents the LRT2 substrate in the longer OsIAA11 domain II sequence.

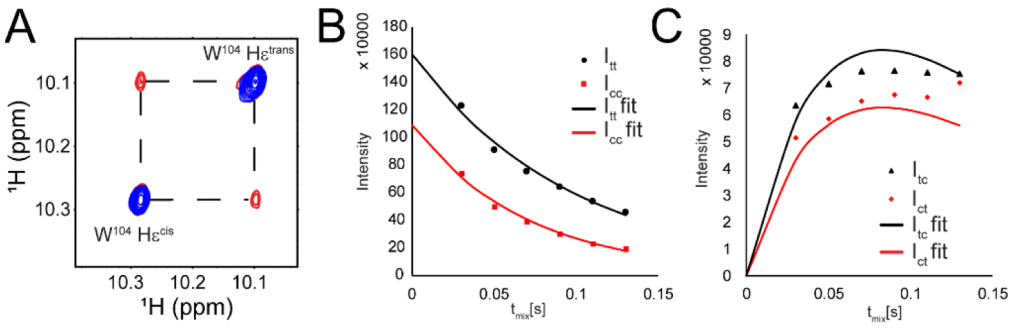

Figure 4.7 ROESY set experiments show isomerization for degron peptide OsIAA11$^{98\text{-}109}$ A. Rotating frame Overhause Effect Spectroscopy spectra with mixing time of 0.55s for the indole HN in W104 overlay without LRT2 (blue) and with 120μM LRT2 (red) show isomerization. **B.** Intensity of auto-peaks for indole HN in W104 in the presence of 120μM LRT2 as function of mixing time, t_{mix}. **C.** Intensity of cross-peaks for indole HN in W104 in the presence of 120μM LRT2 as function of mixing time, t_{mix}.

DISCUSSION

The quantitative characterization of the catalytic reaction cycle for a given isomerase/substrate pair is a first step toward understanding the impact of this timing device in living cells and on phenotypes in whole organisms. Here, we have determined the microscopic dissociation and equilibrium constants and kinetic rates for catalyzed isomerization of the degron motif in the transcription repressor OsIAA11 by the rice cyclophilin LRT2. The recent identification of LRT2 as a key regulator of OsIAA11 degradation in rice places this isomerase/substrate switch at the center of a well-characterized molecular circuit that is directly linked to the lateral root phenotype in rice (Jing *et al.*, 2015; Kang *et al.*, 2013; Su *et al.*, 2015). The microscopic parameters describing the LRT2/OsIAA11 catalytic reaction reported here provide essential predictive power and open avenues for integrating knowledge across the levels of molecular interaction, cellular dynamics, and organism development.

Our determination of the microscopic equilibrium and rate constants that describe the full LRT2 reaction cycle for the OsIAA11 substrate allow prediction of the LRT2-catalyzed isomerization of OsIAA11 in the cell. While the NMR titration lineshape analysis studies reported here were necessarily performed at protein concentrations that far exceed the nanomolar to micromolar protein concentrations that can be reasonably expected in cells (Beck *et al.*, 2011), our demonstration of the accurate prediction of independent measurements of k_{ex}^{obs} at different sample conditions indicates that the determined parameters are quite robust. Using these parameters and Eq. 3, the dependence of k_{ex}^{obs} on the concentrations of OsIAA11 and LRT2 can be visualized (Figure 4.8). As displayed in the 3D plot, since the cellular OsIAA11

concentration is far below the K_D value of 1.55 mM, k_{ex}^{obs} is insensitive to the cellular concentration of OsIaa11 but is linearly dependent on the concentration of LRT2 (Eq. 3). Based on the abundance of cyclophilins in human cells (Beck *et al.*, 2011) and reported LRT2 mRNA levels in rice (Kawahara *et al.*, 2013), a reasonable estimate of LRT2 concentration is 1 - 10 μM. The OsIAA11 concentration must necessarily vary between levels sufficiently high to shut down the transcription of its target genes, and sufficiently low to turn them on (Middleton *et al.*, 2010; Vernoux *et al.*, 2011; Farcot *et al.*, 2015). Thus, our NMR lineshape analysis predicts that the LRT2-catalyzed isomerization of OsIAA11 is an invariable step in the auxin circuit that maintains a constant k_{ex}^{obs} rate for a given LRT2 concentration and for the wide range of OsIAA11 concentrations encountered during the initiation of lateral root development.

The reaction parameters determined here reflect a highly balanced enzyme, with *cis-trans* equilibrium constants close to unity in both free (K_{eq}^{free}) and bound (K_{eq}^{bound}) forms. The on-enzyme equilibrium constant K_{eq}^{bound} has important implications for the catalytic effectiveness in the cell (Burbaum *et al.*, 1989). An enzyme with $K_{eq}^{bound} = 1$ is optimized for the case where the ratio of the steady-state cellular concentrations of substrate and product, [S]/[P], is equal to their ratio at equilibrium, $[S]_{eq}/[P]_{eq}$. This happens when the next step in the pathway that depletes the product is much slower than the conversion of substrate to product. In the case of LRT2 and the auxin circuit, considering $OsIAA11_{trans}$ as the substrate and $OsIAA11_{cis}$ as the product specifically recognized by the SCF^{TIR1} E3 ubiquitin ligase, the next reaction is the ubiquitin-mediated proteasomal degradation of OsIAA11. The half-life

of OsIAA11 has been approximated as 20 min (Moss *et al.*, 2015), which corresponds to a rate of ~0.0006 s^{-1}. This suggests that, indeed, this slow degradation would allow LRT2 to maintain the steady state $OsIAA11_{trans}$ and $OsIAA11_{cis}$ concentrations at equilibrium, corresponding to optimized catalytic effectiveness.

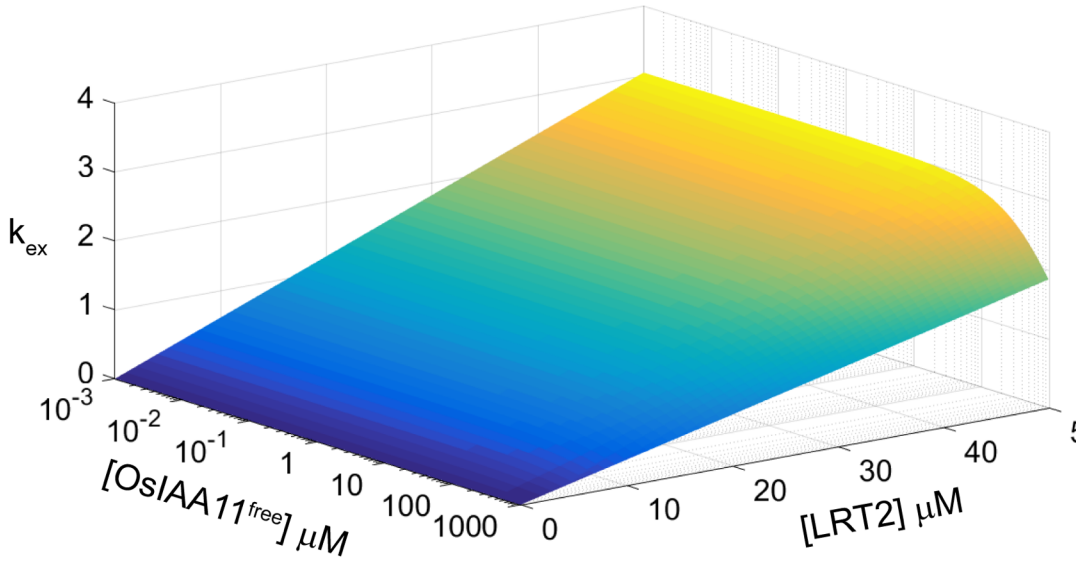

Figure 4.8 Exchange rate as function of free OsIAA11 and LRT2 at cellular concentrations. The microscopic thermodynamic and kinetic parameters determined by NMR lineshape analysis predict an exchange rate dependent linearly to the LRT2 concentration, and invariant to OsIAA11 concentration for concentration lower than the dissociation constant order (<1mM).

The studies presented here reveal that the level of LRT2 governs the isomerization rate for a broad range of OsIAA11 concentrations, and that LRT2 is optimized for its role in supplying $OsIAA11_{cis}$ to the proteasomal degradation pathway. Moreover, these results suggest that accelerating the isomerization reaction even further would not impact the auxin circuit, since the wild type LRT2 reaction is much faster than the downstream degradation process that it feeds. Rather, tuning the LRT2 reaction

to slower rates would be necessary for altering the circuit dynamics. Therefore, further studies of LRT2 mutants with diminished activities would be of particular interest for investigating the relationship between isomerization rate, auxin circuit dynamics, and phenotypic changes in lateral root development.

REFERENCES

Acevedo, L. A., Greenwood, A. I., & Nicholson, L. K. (2017). A Noncanonical Binding Site in the EVH1 Domain of Vasodilator-Stimulated Phosphoprotein Regulates Its Interactions with the Proline Rich Region of Zyxin. *Biochemistry*. doi:10.1021/acs.biochem.7b00618

Acevedo, L. A., & Nicholson, L. K. (2018). 1H, 13C and 15N NMR assignments of cyclophilin LRT2 (OsCYP2) from rice. *Biomolecular NMR Assignments*. doi:10.1007/s12104-018-9803-x

Bax, A., & Davis, D. G. (1985). Practical aspects of two-dimensional transverse NOE spectroscopy. *Journal of Magnetic Resonance (1969), 63*(1), 207-213. doi:https://doi.org/10.1016/0022-2364(85)90171-4

Beck, M., Schmidt A Fau - Malmstroem, J., Malmstroem J Fau - Claassen, M., Claassen M Fau - Ori, A., Ori A Fau - Szymborska, A., Szymborska A Fau - Herzog, F., . . . Aebersold, R. (2011). The quantitative proteome of a human cell line. (1744-4292 (Electronic)).

Bosco, D. A., Eisenmesser Ez Fau - Clarkson, M. W., Clarkson Mw Fau - Wolf-Watz, M., Wolf-Watz M Fau - Labeikovsky, W., Labeikovsky W Fau - Millet, O., Millet O Fau - Kern, D., & Kern, D. (2010). Dissecting the microscopic steps of the cyclophilin A enzymatic cycle on the biological HIV-1 capsid substrate by NMR. *Journal of Molecular Biology, 403*(1089-8638 (Electronic)), 723-738.

Burbaum, J. J., Raines, R. T., Albery, W. J., & Knowles, J. R. (1989). Evolutionary optimization of the catalytic effectiveness of an enzyme. *Biochemistry, 28*(24), 9293-9305. doi:10.1021/bi00450a009

Cavanagh, J., Fairbrother, W. J., Palmer, A. G., Skelton, N. J., & Rance, M. (2010). *Protein NMR Spectroscopy: Principles and Practice*: Elsevier Science.

Christoforides, E., Dimou, M., Katinakis, P., Bethanis, K., & Karpusas, M. (2012). Structure of a bacterial cytoplasmic cyclophilin A in complex with a tetrapeptide. *Acta Crystallographica Section F: Structural Biology and Crystallization Communications, 68*(Pt 3), 259-264. doi:10.1107/S1744309112000188

Davis, T. L., Walker, J. R., Campagna-Slater, V., Finerty, P. J., Jr., Paramanathan, R., Bernstein, G., . . . Dhe-Paganon, S. (2010). Structural and Biochemical Characterization of the Human Cyclophilin Family of Peptidyl-Prolyl Isomerases. *PLOS Biology, 8*(7), e1000439. doi:10.1371/journal.pbio.1000439

Del Pozo, J. C., & Manzano, C. (2014). Auxin and the ubiquitin pathway. Two players-one target: the cell cycle in action. *J Exp Bot, 65*(10), 2617-2632. doi:10.1093/jxb/ert363

Delaglio, F., Grzesiek, S., Vuister, G. W., Zhu, G., Pfeifer, J., & Bax, A. (1995). NMRPipe: A multidimensional spectral processing system based on UNIX pipes. *J Biomol NMR, 6*(3), 277-293. doi:10.1007/bf00197809

Dharmasiri, N., Dharmasiri, S., Jones, A. M., & Estelle, M. (2003). Auxin Action in a Cell-Free System. *Current Biology, 13*(16), 1418-1422. doi:https://doi.org/10.1016/S0960-9822(03)00536-0

Enders, T. A., & Strader, L. C. (2015). Auxin activity: Past, present, and future. *Am J Bot, 102*(2), 180-196. doi:10.3732/ajb.1400285

Farcot, E., Lavedrine, C., & Vernoux, T. (2015). A Modular Analysis of the Auxin Signalling Network. *PLoS One, 10*(3), e0122231. doi:10.1371/journal.pone.0122231

Farrow, N. A., Zhang, O., Forman-Kay, J. D., & Kay, L. E. (1994). A heteronuclear correlation experiment for simultaneous determination of 15N longitudinal decay and chemical exchange rates of systems in slow equilibrium. *J Biomol NMR, 4*(5), 727-734.

Fischer, G., & Aumuller, T. (2003). Regulation of peptide bond cis/trans isomerization by enzyme catalysis and its implication in physiological processes *Rev Physiol Biochem Pharmacol* (pp. 105-150). Germany: Springer.

Fischer, G., & Aumuller, T. (2003). Regulation of peptide bond cis/trans isomerization by enzyme catalysis and its implication in physiological processes. *Rev Physiol Biochem Pharmacol, 148*, 105-150. doi:10.1007/s10254-003-0011-3

Goddard, T. D., & Kneller, D. G. *SPARKY 3*. University of California, San Francisco.

Gothek, S. F., & Marahiel, M. A. (1999). Peptidyl-prolyl cis-trans isomerases, a superfamily of ubiquitous folding catalysts. *Cellular and Molecular Life Sciences, 55*(3), 423-436.

Gray, W. M., Kepinski, S., Rouse, D., Leyser, O., & Estelle, M. (2001). Auxin regulates SCFTIR1-dependent degradation of AUX/IAA proteins. *Nature, 414*, 271. doi:10.1038/35104500

Greenwood, A. I., Rogals, M. J., De, S., Lu, K. P., Kovrigin, E. L., & Nicholson, L. K. (2011). Complete determination of the Pin1 catalytic domain thermodynamic cycle by NMR lineshape analysis. *J Biomol NMR, 51*(1-2), 21-34. doi:10.1007/s10858-011-9538-9

Hagen, G., & Guilfoyle, T. (2002). Auxin-responsive gene expression: genes, promoters and regulatory factors. *Plant Molecular Biology, 49*(3), 373-385. doi:10.1023/A:1015207114117

Hamelberg, D., & McCammon, J. A. (2009). Mechanistic Insight into the Role of Transition-State Stabilization in Cyclophylin A. *Journal of the American Chemical Society, 131*(1), 147-152.

Hanes, S. D. (2015). Prolyl isomerases in gene transcription. *Biochim Biophys Acta, 1850*(10), 2017-2034. doi:10.1016/j.bbagen.2014.10.028

Hayashi, K. (2012). The interaction and integration of auxin signaling components. *Plant Cell Physiol, 53*(6), 965-975. doi:10.1093/pcp/pcs035

Holliday, M. J., Armstrong, G. S., & Eisenmesser, E. Z. (2015). Determination of the Full Catalytic Cycle among Multiple Cyclophilin Family Members and Limitations on the Application of CPMG-RD in Reversible Catalytic Systems. *Biochemistry, 54*(38), 5815-5827. doi:10.1021/acs.biochem.5b00746

Jing, H., Yang, X., Zhang, J., Liu, X., Zheng, H., Dong, G., . . . Zuo, J. (2015). Peptidyl-prolyl isomerization targets rice Aux/IAAs for proteasomal degradation during auxin signalling. *Nat Commun, 6*, 7395. doi:10.1038/ncomms8395

Kang, B., Zhang, Z., Wang, L., Zheng, L., Mao, W., Li, M., . . . Mo, X. (2013). OsCYP2, a chaperone involved in degradation of auxin-responsive proteins, plays crucial roles in rice lateral root initiation. *Plant J, 74*(1), 86-97. doi:10.1111/tpj.12106

Kawahara, Y., de la Bastide, M., Hamilton, J. P., Kanamori, H., McCombie, W. R., Ouyang, S., . . . Matsumoto, T. (2013). Improvement of the Oryza sativa Nipponbare reference genome using next generation sequence and optical map data. *Rice, 6*(1), 4. doi:10.1186/1939-8433-6-4

Kepinski, S., & Leyser, O. (2005). The Arabidopsis F-box protein TIR1 is an auxin receptor. *Nature, 435*, 446. doi:10.1038/nature03542

Kumari, S., Roy, S., Singh, P., Singla-Pareek, S., & Pareek, A. (2012). Cyclophilins: Proteins in search of function. *Plant Signaling and Behaviour, 8*(1), 25-30.

Labeikovsky, W., Eisenmesser, E. Z., Bosco, D. A., & Kern, D. (2007). Structure and Dynamics of Pin1 During Catalysis by NMR. *Journal of Molecular Biology, 367*(5), 1370-1381. doi:https://doi.org/10.1016/j.jmb.2007.01.049

Liscum, E., & Reed, J. W. (2002). Genetics of Aux/IAA and ARF action in plant growth and development. *Plant Molecular Biology, 49*(3), 387-400. doi:10.1023/A:1015255030047

Lu, K. P., Finn, G., Lee, T. H., & Nicholson, L. K. (2007). Prolyl cis-trans isomerization as a molecular timer. *Nat Chem Biol, 3*(10), 619-629. doi:10.1038/nchembio.2007.35

Middleton, A. M., King Jr Fau - Bennett, M. J., Bennett Mj Fau - Owen, M. R., & Owen, M. R. (2010). Mathematical modelling of the Aux/IAA negative feedback loop. (1522-9602 (Electronic)).

Mockaitis, K., & Estelle, M. (2008). Auxin receptors and plant development: a new signaling paradigm. *Annu Rev Cell Dev Biol, 24*, 55-80. doi:10.1146/annurev.cellbio.23.090506.123214

Montelione, G. T., & Wagner, G. (1989). 2D Chemical exchange NMR spectroscopy by proton-detected heteronuclear correlation. *J Am Chem Soc, 111*(8), 3096-3098. doi:10.1021/ja00190a072

Moss, B. L., Mao, H., Guseman, J. M., Hinds, T. R., Hellmuth, A., Kovenock, M., . . . Nemhauser, J. L. (2015). Rate Motifs Tune Auxin/Indole-3-Acetic Acid Degradation Dynamics. *Plant Physiol, 169*(1), 803-813. doi:10.1104/pp.15.00587

Mulder, F. A., Schipper D Fau - Bott, R., Bott R Fau - Boelens, R., & Boelens, R. (1999). Altered flexibility in the substrate-binding site of related native and engineered high-alkaline Bacillus subtilisins. (0022-2836 (Print)).

Nechama, M., Kwon, J., Wei, S., Kyi, A. T., Welner, R. S., Ben-Dov, I. Z., . . . Lu, K. P. (2018). The IL-33-PIN1-IRAK-M axis is critical for type 2 immunity in IL-33-induced allergic airway inflammation. *Nat Commun, 9*(1), 1603. doi:10.1038/s41467-018-03886-6

Normanly, J., Slovin, J. P., & Cohen, J. D. (2010). Auxin Biosynthesis and Metabolism. In P. J. Davies (Ed.), *Plant Hormones: Biosynthesis, Signal Transduction, Action!* (pp. 36-62). Dordrecht: Springer Netherlands.

Papin, J. A., Hunter, T., Palsson, B. O., & Subramaniam, S. (2005). Reconstruction of cellular signalling networks and analysis of their properties. *Nat Rev Mol Cell Biol, 6*(2), 99-111. doi:nrm1570 [pii] 10.1038/nrm1570

Perrucci, G. L., Gowran, A., Zanobini, M., Capogrossi, M. C., Pompilio, G., & Nigro, P. (2015). Peptidyl-prolyl isomerases: a full cast of critical actors in cardiovascular diseases. (1755-3245 (Electronic)).

Ramos, J. A., Zenser, N., Leyser, O., & Callis, J. (2001). Rapid Degradation of Auxin/Indoleacetic Acid Proteins Requires Conserved Amino Acids of Domain II and Is Proteasome Dependent. *The Plant Cell, 13*(10), 2349-2360. doi:10.1105/tpc.010244

Reed, J. W. (2001). Roles and activities of Aux/IAA proteins in Arabidopsis. *Trends Plant Sci, 6*(9), 420-425.

Reimer, U., Scherer, G., Drewello, M., Kruber, S., Schutkowski, M., & Fischer, G. (1998). Side-chain effects on peptidyl-prolyl cis/trans isomerisation. *J Mol Biol, 279*(2), 449-460. doi:S0022-2836(98)91770-3 [pii] 10.1006/jmbi.1998.1770

Rennie, M. L., Doolan, A. M., Raston, C. L., & Crowley, P. B. (2017). Protein Dimerization on a Phosphonated Calix[6]arene Disc. *Angewandte Chemie, 129*(20), 5609-5613. doi:10.1002/ange.201701500

Sekhon, S. S., Kaur, H., Dutta, T., Singh, K., Kumari, S., Kang, S., . . . Yoon, T.-S. (2013). Structural and biochemical characterization of the cytosolic wheat

cyclophilin TaCypA-1. *Acta Crystallographica Section D, 69*(4), 555-563. doi:doi:10.1107/S0907444912051529

Shinya, S., Ghinet, M. G., Brzezinski, R., Furuita, K., Kojima, C., Shah, S., . . . Fukamizo, T. (2017). NMR line shape analysis of a multi-state ligand binding mechanism in chitosanase. *J Biomol NMR, 67*(4), 309-319. doi:10.1007/s10858-017-0109-6

Su, S.-H., Gray, W. M., & Masson, P. H. (2015). Auxin: Shape matters. *Nature Plants, 1*, 15097. doi:10.1038/nplants.2015.97

Tan, X., Calderon-Villalobos, L. I., Sharon, M., Zheng, C., Robinson, C. V., Estelle, M., & Zheng, N. (2007). Mechanism of auxin perception by the TIR1 ubiquitin ligase. *Nature, 446*(7136), 640-645. doi:10.1038/nature05731

Tiwari, S. B., Wang, X.-J., Hagen, G., & Guilfoyle, T. J. (2001). AUX/IAA Proteins Are Active Repressors, and Their Stability and Activity Are Modulated by Auxin. *The Plant Cell, 13*(12), 2809-2822. doi:10.1105/tpc.010289

Vernoux, T., Brunoud, G., Farcot, E., Morin, V., Van den Daele, H., Legrand, J., . . . Traas, J. (2011). The auxin signalling network translates dynamic input into robust patterning at the shoot apex. *Molecular Systems Biology, 7*(1).

Waudby, C. A., Ramos, A., Cabrita, L. D., & Christodoulou, J. (2016). Two-Dimensional NMR Lineshape Analysis. *Scientific Reports, 6*, 24826. doi:10.1038/srep24826 http://www.nature.com/articles/srep24826#supplementary-information

Williamson, M. P. (1994). The structure and function of proline-rich regions in proteins. *Biochem J, 297 (Pt 2)*, 249-260.

Winkler, M., Niemeyer, M., Hellmuth, A., Janitza, P., Christ, G., Samodelov, S. L., . . . Calderón Villalobos, L. I. A. (2017). Variation in auxin sensing guides AUX/IAA transcriptional repressor ubiquitylation and destruction. *8*, 15706. doi:10.1038/ncomms15706

Zheng, H., Li, S., Ren, B., Zhang, J., Ichii, M., Taketa, S., . . . Wang, H. (2013). LATERAL ROOTLESS2, a cyclophilin protein, regulates lateral root initiation

and auxin signaling pathway in rice. *Mol Plant, 6*(5), 1719-1721. doi:10.1093/mp/sst052

Zhu, Z. X., Liu, Y., Liu, S. J., Mao, C. Z., Wu, Y. R., & Wu, P. (2012). A gain-of-function mutation in OsIAA11 affects lateral root development in rice. *Mol Plant, 5*(1), 154-161. doi:10.1093/mp/ssr074

CHAPTER 5

Effects of Mutation on LRT2 Catalysis of the Natural Substrate OsIAA11

Abstract

Peptidyl Prolyl Isomerases (PPIases) have gained recognition as enzymes that may potentially regulate biological processes. PPIases regulate the interconversion between *cis* and *trans* isomers of peptide bonds between any residue and a following proline. In rice, LRT2 (a PPIase) has been found to be crucial in lateral root initiation. This PPIase is classified as a cyclophilin, and has shown *in vitro* isomerization of its natural substrate, OsIAA11. OsIAA11 belongs to the well conserved Aux/IAA repressor proteins. Aux/IAA proteins get targeted to ubiquitin proteasomal degradation only in the *cis* isomer of the W-P peptide bond. The ability to modify the rate of how fast the interconversion between *cis* and *trans* isomers occurs is an important tool to understand and model the regulation in biological processes. In this chapter, we present results of the design and characterization of the thermal stability and isomerization rates for different mutants of LRT2 acting on the ^{104}W-P^{105} peptide bond of OsIAA11. We found that some of the designed mutants abolished significantly isomerization (R62A, W128A, and H133Q). We also found mutants that reduce more moderately the catalysis of the isomerization (P125K, and V124A/P125K/C127T/S127E). Additionally, we tested two homologs of LRT2, human Cyclophilin A (hCypA) and E. Coli Peptidyl-Prolyl Isomerase B (PPIB), to determine their catalytic activity acting on the ^{104}W-P^{105} peptide bond of OsIAA11. These homologs have been tested before with many other substrates and have demostrated faster isomerization rates than the ones measured in

this chapter. We also found that the catalysis of the ^{104}W-P^{105} peptide bond in OsIAA11 by these homologs is very similar to LRT2, and then we hypothesize that the substrate determines a low rate limiting isomerization.

Introduction

Peptidyl-prolyl isomerases (PPIases) have emerged as key regulators of many biological processes (Fischer *et al.*, 2004). PPIases are known for being enzymes that catalyze the interconversion between the *cis* and *trans* isomers of a peptide bond of any amino acid followed by a proline residue. PPIases are ubiquitously expressed in prokaryotes and eukaryotes (Galat *et al.*, 1998). There are three subfamilies within this family of proteins: Cyclophilins, FK506-Binding Proteins, and parvulins (Schiene *et al.*, 2000). Functions of these enzymes include cell signaling (Sarkar *et al.*, 2007), aid for protein folding (Fischer *et al.*, 1985; Gething *et al.*, 1992; Lorenz *et al.*, 2008), gene transcription (Nelson *et al.*, 2006; Thapar, 2015;Hanes, 2015), and neurodegeneration (Lu *et al.*, 1999). In plants, cyclophilins have been shown to have essential functions necessary for stress survival (Kumari *et al.*, 2013).

Recently, a cyclophilin in rice, LRT2, has gained attention due to its significance in lateral root development (Jing *et al.*, 2015; Zheng *et al.*, 2013; Ruan *et al.*, 2011; Cui *et al.*, 2017). Lateral root formation associated with LRT2 has been primarily linked to development dependent on the auxin circuit. The auxin circuit refers to the dynamic regulation of early genes in plants that depend on the phytohormone Auxin (Kutschera *et al.*, 2016). In short, when low concentrations of auxin are present, the Aux/IAA repressor proteins interact with the Auxin responsive factor (ARF) (Dinesh *et al.*, 2016). This protein-protein interaction inhibits the expression of early genes in plants,

including the own expression of the Aux/IAA protein (Liscum *et al.*, 2002). When the concentration of Auxin increases, Auxin acts like a binding factor between the SFC^{TIR1} complex, an E3 ubiquitin ligase, and the conserved degron motif GWPPV in Aux/IAA repressor proteins (Calderon Villalobos *et al.*, 2012). Curiously, the crystal structure of this bound complex shows that the peptide bond between W-P is in a *cis* isomer (Tan *et al.*, 2007). This isomer specific selection sparked interest in studying the relevance of a PPIase in regulation of this circuit. In the case of lateral root development in rice, the PPIase responsible for this regulation is the cyclophilin LRT2 (Jing *et al.*, 2015; Zheng *et al.*, 2013). Since LRT2 feeds the degradation pathway with the correct OsIAA11 isomer to be recognized by SCF^{TIR1}, we hypothesized that different isomerization rates of LRT2 acting on the W-P peptide bond will affect the rate of degradation of OsIAA11 and therefore Auxin response in the plant root development.

Cyclophilins have been previously studied to measure the catalytic activity (Fischer *et al.*, 1985). However, this has been done mostly in substrates that are not necessary biologically relevant such as proteolysis release of 4-nitroaniline assay (Lin *et al.*, 1983; Garcia-Echeverria *et al.*, 1992). In the case of more biologically relevant substrates, Nuclear Magnetic Resonance (NMR) has been used to understand catalytic cycles where cyclophilins are present (Holliday *et al.*, 2015). NMR can measure the dynamics of exchanges between different isomers. Experiments such as CPMG (Bosco *et al.*, 2010), ZZ-Exchange (Greenwood *et al.*, 2014; Schlegel *et al.*, 2009; Chapter 4), or ROESY (Greenwood *et al.*, 2011; Jing *et al.*, 2015; Zhou *et al.*, 2009; Chapter 4) have been used to identify and characterize PPIases substrates interactions. We have hypothesized that the isomerization rate of the prolyl *cis-trans* molecular switch in

OsIAA11 is a determining factor in Auxin circuit dynamics and sets the timing of lateral root development. In order to evaluate this hypothesis, we need to be able to regulate the isomerization rates, which is proposed to be achieved through mutagenesis in LRT2.

In this mutation study we test mutants as well as homolog proteins to LRT2 to determine whether isomerization rates are affected. In this chapter, we summarize the thermostable studies of mutants proposed to change isomerization and test their effect in the indole proton of the ^{104}W in the degron motif of OsIAA11$^{98-109}$ by ROESY. A subset of mutants was further tested by ZZ-exchange experiments by observing the indole proton of the ^{104}W in the ^{15}N-OsIAA11$^{72-125}$. These mutants showed reduced isomerization rates. Additionally, we tested two homologs of LRT2 and confirmed comparable isomerization on the W-P peptide of OsIAA11. We conclude that isomerization is highly dependent in the substrate and whether a specific cyclophilin is present but not necessarily a specific characteristic of LRT2 isomerization effect.

Experimental

Plasmids, protein expression and purification.

The plasmid for LRT2 has been described previously (Acevedo *et al.*, 2018). Mutations in the LRT2 sequence were achieved either by site direct mutagenesis Polymerase Chain Reaction (PCR) or overlap extension method PCR (Heckman *et al.*, 2007). For H61Q, R62A, Q118A, W128A, H133Q, QuickChange II Site-Directed Mutagenesis (Agilent) was performed following manufacturer's instructions. For G72A, F120A, P125K, and V124A/P125K/C126T/S127E mutants the overlap extension method was used. This method consists of creating two initial PCR products followed by a final PCR. One of the initial PCR products was created with a nested

forward primer (LRT2-NdeI-FW) and the reverse primer with the wanted mutation, the other initial PCR product was created with a forward primer with the mutation and a reverse nested primer (LRT2-HindIII-Rev). Using both PCR products as DNA template and both nested primers, a long final PCR product that contains all the entire LRT2 gene with the wanted mutation was then restricted enzyme digested with NdeI (New England Biolabs) and HindIII (New England Biolabs) according to manufacturer's instructions. Ligation with T4 DNA Ligase (New England Biolabs) of the final PCR product to the original Pet28 vector was achieved following manufacturer's instructions. Primers sequences can be found in Appendix Table 5.1.

LRT2 wild type (WT) and its mutants were purified as previously described (Chapter 3 and 4). Protein was concentrated with 10000 MWC centrifugal concentrator to either 5μM in a simplified buffer for thermal shift assays (50mM KCl, 100mM KPO_4, 1mM TCEP, pH=6.67) for thermostability test or to higher concentration for NMR experiments. The protein concentration was determined by UV absorption at 280nm, using the theoretical extinction coefficient of 10220 $cm^{-1}M^{-1}$ for all mutants but W128A LRT2 which has a theoretical extinction coefficient of 4720 $cm^{-1}M^{-1}$.

Human Cyclophilin A (hCypA) plasmid (a gift from C. Kalodimos, Rutgers University, Piscataway, NJ) has been described previously (Greenwood *et al.*, 2014). The Petidyl-prolyl isomerase B (PPIB) from E. Coli (Uniprot entry P23869) was purchased in pet28a (+) kanamycin resistance vector with N-terminus His tag and TEV recognition cleavage site from GenScript (Piscataway, NJ). Expression and purification was carried out as described in Chapter 3, and 4, with the exception that hCypA does not have a cleavage site. Therefore, for hCypA purification, after Ni-NTA affinity

column purification, protein was loaded into a desalting column for exchange into the simplified NMR buffer (50mM KCl, 100mM KPO_4, 1mM TCEP, pH=6.67). PPIB from E. Coli was purified the same way as LRT2 WT and its mutants, which included TEV cleavage. PPIB concentration was measured by UV absorption at 280nm using a theoretical extinction coefficient of 10095 $cm^{-1}M^{-1}$.

^{15}N-OsIAA11$^{72-125}$ was purified as described in Chapter 4. For NMR experiments, 5mM NaN3, 0.1%P.I. cocktail and, 3mM TCEP were added to the final protein product in simplified NMR buffer and protein was concentrated to a final concentration of 800μM of ^{15}N-OsIAA11$^{72-125}$ and 16μM of enzyme (P125K LRT2, W128A LRT2, V124A/P125K/C126T/S127E LRT2, hCypA, or PPIB from E. Coli).

OsIAA11$^{98-109}$ was purchased from Tufts University Core Facility and a stock solution was prepared into NMR Buffer (50mM KCl, 100mM KPO_4, 3mM TCEP, 5mM NaN_3, 0.1% P.I. cocktail pH=6.67). Samples with and without enzyme were prepared. All samples had a 1.84mM concentration of OsIAA11$^{98-109}$, and samples with enzyme had a 120μM concentration of LRT2 mutants (R62A, P125K, W128A, H133Q, or V124A/P125K/C126T/S127E).

Thermal shift assay

Five repeats for each mutant and a no protein control were prepared by mixing 45μl of 5uM protein (or buffer) and 5μl of 200X Sypro Orange (Fischer). The thermal cycle was set up according to the Protein Thermal Shift Studies User Guide (Thermal Invitrogen), and the thermal shift assay was carried in a 96 well plate in an Aplied Biosystems ViiA 7 (Thermofisher). The average of the five repeats signal was taken and the fluorescence of the no protein control was subtracted from each average.

Additionally, signal for each sample was normalized to the maximum signal for that sample to allow comparison between all mutants.

NMR experiments.

The buffer used for all NMR samples was 50mM KCl, 100mM KPO_4, 5mM TCEP, 0.1% PI cocktail, 5mM NaN_3, 8% ^2H_2O, pH=6.67. ^1H-^1H ROESY and ^1H-^{15}N ZZ exchange experiments were taken and analyzed following the same description as in Chapter 4.

Results

Mutant design and thermostability test gives a subset of atractive LRT2 modifications.

The mutants tested in this Chapter are based on the conservation of LRT2 sequence with hCypA. In Chapter 4, we reported the homology model built with the crystal structure of TaCypA-1 from wheat (PDB:4hy7.1, Sekhon *et al.*, 2013). The homology model structure aligned with the hCypA structure shows a very conserved structure (Figure 5.1 A). Importantly, the residues that were studied by Zydowsky et al (1992) are well conserved. Therefore, we decided to design mutations proposed in that study with the intention of creating a library of mutants that exhibit a lower isomerization activity. In LRT2 sequence mumbering, these mutants are H61Q, R62A, Q118A, F120A, W128A, and H133Q. Additionally, since LRT2 G72A mutant in rice has been shown to have a reduction in lateral root development (Kang *et al.*, 2013), we decided to study this mutant as well.

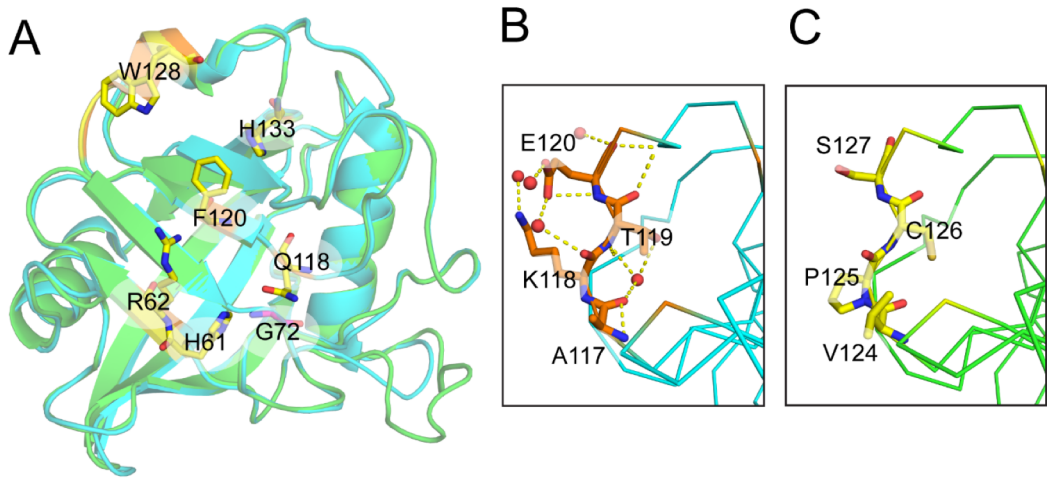

D

```
LRT2        MSNTRVFFDMTVGGAPAGRIVMELYAKDVPRTAENFRALCTGEKGVGKSGKPLHYKGSTF    60
TaCypA      MANPRVFFDMTVGGAPAGRIVMELYKDAVPRTVENFRALCTGEKGVGKSGKPLHYKGSAF    60
hCypA       MVNPTVFFDIAVDGEPLGRVSFELFADKVPKTAENFRALSTGEKGFG-------YKGSCF    53
PPIB        ---------MVTFHTNHGDIVIKTFDDKAPETVKNFLDYCREG----------FYNNTIF    41

LRT2        HRVIPEFMCQGGDFTRGNGTGGESIYGEKFADEVFKFKHDSPGILSMA-NAGPNTNGSQF    119
TaCypA      HRVIPDFMCQGGDFTRGNGTGGESIYGEKFADEKFVHKHTKPGILSMA-NAGPNTNGSQF    119
hCypA       HRIIPGFMCQGGDFTRHNGTGGKSIYGEKFEDENFILKHTGPGILSMA-NAGPNTNGSQF    112
PPIB        HRVINGFMIQGGGFEPGMKQKATK---EPIKNEANNGLKNTRGTLAMARTQAPHSATAQF    98

LRT2        FICTVPCSWLDG--------KHVVFGRVVEGMDVVKAIEKVGSRGGSTAKPVV----IAD    167
TaCypA      FICTVPCNWLDG--------KHVVFGEVVEGMDVVKNIEKVGSRSGTCSKQVV----IAD    167
hCypA       FICTAKTEWLDG--------KHVVFGKVKEGMNIVEAMERFGSRNGKTSKKIT----IAD    160
PPIB        FINVVDNDFLNFSGESLQGWGYCVFAEVVDGMDVVDKIKGVATGRSGMHQDVPKEDVIIE    158

LRT2        CGQLS-   172
TaCypA      CGQL--   171
hCypA       CGQLE-   165
PPIB        SVTVSE   164
```

Figure 5.1 Mutagenesis of LRT2 residues. A. The structure of the homology model of LRT2 (green) aligned with the crystal structure of human Cyclophilin A (cyan, PDB:1awr.1) shows the conserved catalytic residues H61, R62, Q118, F120, W128 and H133 in LRT2 notation. **B.** Neighbor residues of W121 in hCypA which are not conserved in LRT2. **C.** Neighbor residues of W128 in the homology model of LRT2. **D.** Sequence alignment between LRT2; TaCypA, used to build the homology model; human Cyclophilin A; and Peptidyl-prolyl isomerase from E. Coli, used as test of isomerization later.

In order to obtain a set of mutants that does not necessary abolish enzyimatic activity, we paid attention to the sequence alignment of LRT2 and hCypA (Figure 5.1 D). We saw that in general sequence surrounding the residues in the catalytic binding site are well conserved. However, a region near to the W128(LRT2) or W121(hCypA) caught our attention (Figure 5.1 B and C) since this residue is important for binding and the preceding sequence is different between hCypA and LRT2. We decided to study mutantions within this loop, and the P125K and V124A/P125K/C126T/S127E LRT2 mutants were formulated.

Having expressed and purified WT and mutants of LRT2, we decided to test the thermal stability to ensure that isomerization rates are due to characteristics of binding and not due to instability of protein. For this, the Thermofluor test was run by using a Polymerase Chain Reaction instrument as a fluorometer. In short, solutions of proteins

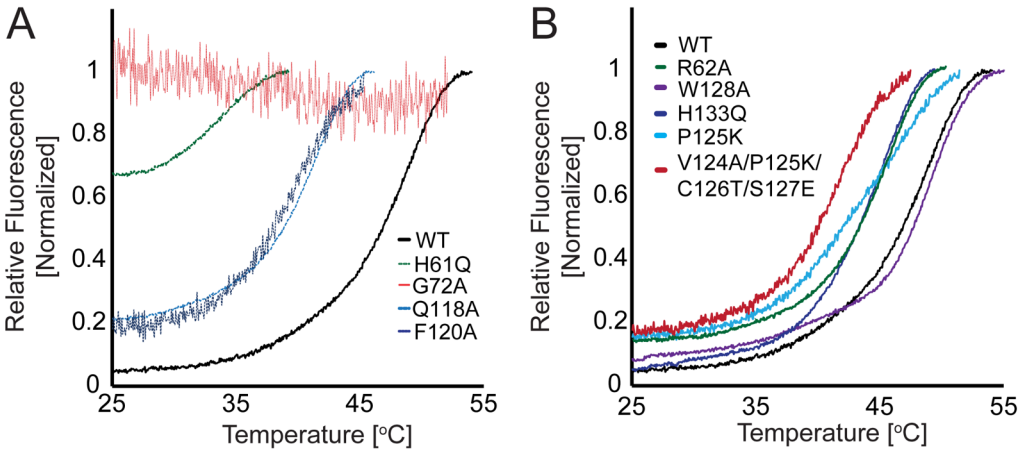

Figure 5.2 Thermofluor test of LRT2 mutants. A. G72A LRT2 mutant shows a completely unfolded profile even at room temperature, while H61Q, Q118A, F120A show larger shift to lower melting temperature (T_m) in the thermal curve, thus these mutants were not considered for further NMR experiments. **B.** All remaining mutants show a smaller thermal shift compared to WT LRT2 (black), including the W128A LRT2 mutant that interestingly has a slight thermal shift to higher T_m indicating a more stable protein (purple).

with Sypro Orange were prepared and temperature was changed while fluorescence intensity was recorded (Figure 5.2). Sypro Orange binds to hydrophobic patches in the protein; this reaction emits a fluorescence signal that can be measured. As temperature rises, the protein unfolds which results in available hydrophobic regions, and then the fluorescent signal increases displays a sigmoidal curve profile. The melting temperature is defined as the inflection point in the curve (Huynh *et al.*, 2015). Melting temperature values for WT and mutants of LRT2 were determined (Table 5.1). Importantly, G72A is unfolded in the buffer conditions that we selected for NMR, suggesting that this mutation results also in a constitutively unfolded protein in the plant.

Table 5.1 Melting temperature of LRT2 mutants measured by Thermofluor assay

LRT2	Melting Temperature (C^o)
WT	48.78 ±0.54
H61Q	34.98±1.18
R62A	45.86±0.33
G72A	NA
Q118A	41.75±0.59
F120A	40.28±2.21
P125K	46.46±2.77
W128A	49.03±0.17
V124A/P125K/C126T/S127E	41.13±1.10
H133Q	45.20±0.55

Except for H61Q LRT2 mutant, all the other mutants tested have similar melting temperature (less than 20% difference between them, Table 5.1). We selected all mutants that were within 10% of the melting temperature compared to WT for future NMR experiments. Additionally, we also selected the V124A/P125K/C126T/S127E

LRT2 which was measured to be 16% less stable than WT by comparing the melting temperature. This mutant corresponds to residues that differs to hCypA.

I*somerization rates of OsIAA11 in the presence of LRT2 mutants*.

In a similar manner as in Chapter 4, we measured isomerization by Rotating frame Overhauser Effect Spectroscopy (ROESY) at different mixing times of the degron peptide OsIAA11$^{98\text{-}109}$. The presence of exchange peaks in the ^{1}H-^{1}H ROESY spectrum corresponding to the indole proton of ^{104}WHε^{cis} and ^{104}WHε^{trans} auto peaks, which provides clear evidence of isomerization was observed for only two of the mutants (P125K and V124A/P125K/C126T/S127E, Figure 5.3A). We collected ^{1}H-^{1}H ROESY spectra for the apo as well as in the presence of mutants as function of mixing time, which allows us to determine the observed exchange rates (Figure 5.3B, Table 5.2). The P125K and V124A/P125K/C126T/S127E mutants have a slight change compared to WT isomerization rates at same conditions determined in Chapter 4. However, for the R62, W128A, H133Q LRT2 mutants the isomerization is significantly reduced (Table 5.2). As we determined in Chapter 4, there is no significant difference between the smaller sequence of OsIAA11$^{98\text{-}109}$, and the longer substrate OsIAA11$^{72\text{-}125}$. We decided to test ZZ-exchange experiment in ^{15}N-OsIAA11$^{72\text{-}125}$ which would allow us to determine whether the ROESY shows the same systematic isomerization reduction at different concentration conditions for W128A, P125K and V124A/P125K/C126T/S127E LRT2 mutants. The build up of exchange peaks in the ^{1}H-^{15}N ZZ exchange experiment for P125K and V124A/P125K/C126T/S127E LRT2 is again observed (Figure 5.4B and D) and no exchange peaks in the presence of W128A LRT2. We collected a set of ^{1}H-^{15}N ZZ exchange spectra as function of mixing time in

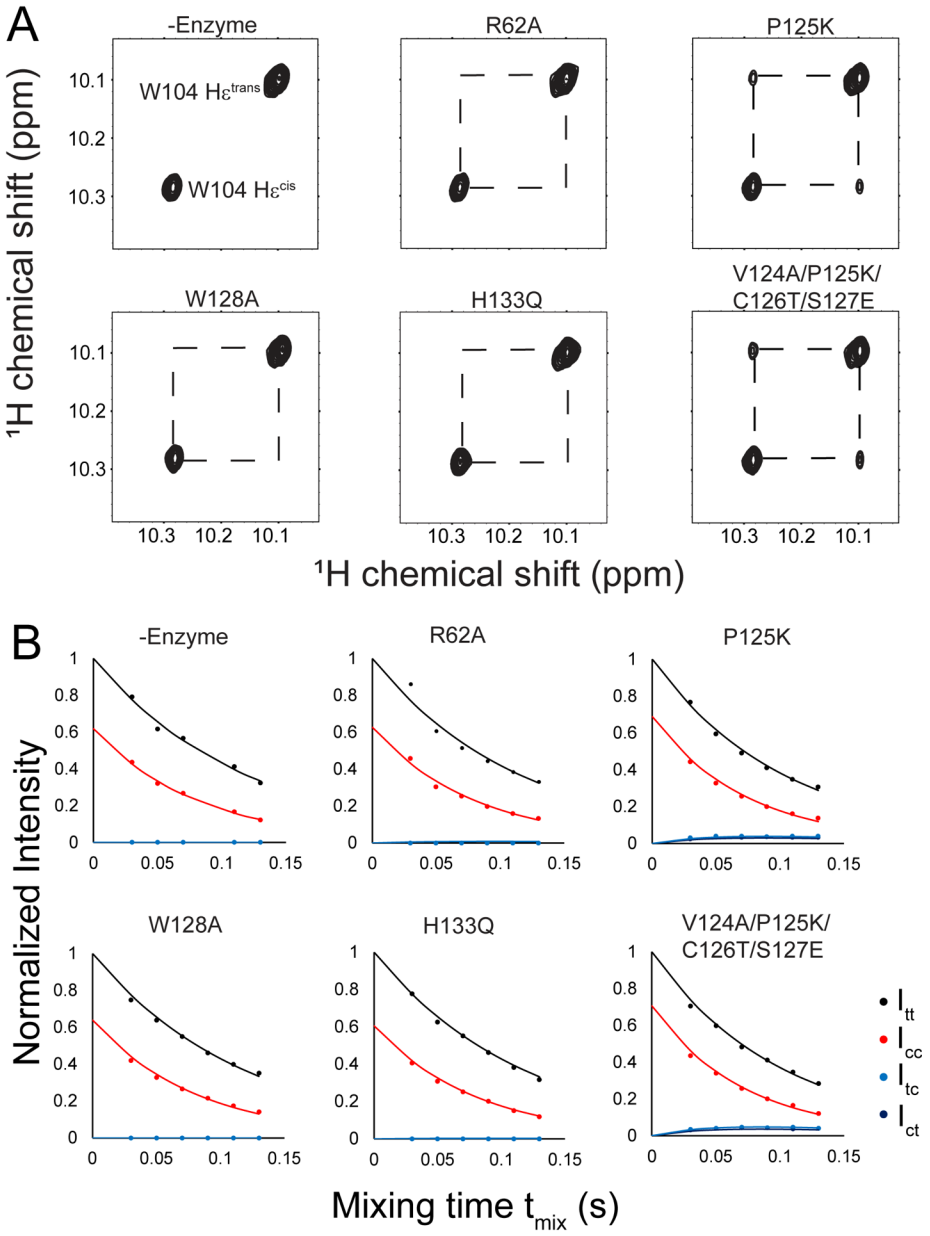

Figure 5.3 Effects of mutants in the catalysis of W-P isomerization measured by ROESY. (A) The ^{1}H-^{1}H ROESY spectrum of OsIAA11$^{98\text{-}109}$ (mixing time of 120 ms) shows that the *cis* and *trans* isomers of ^{104}W-P^{105} interconversion is observed only in the presence of P125K LRT2 and V124A/P125K/C126T/S127E LRT2 mutants. This interconversion is observed by the apparance of cross-peaks. **(B)** Normalized intensity as function of mixing time for the auto and exchange peaks of ^{104}WHε without LRT2 or in the presence of 120μM of LRT2 mutants.

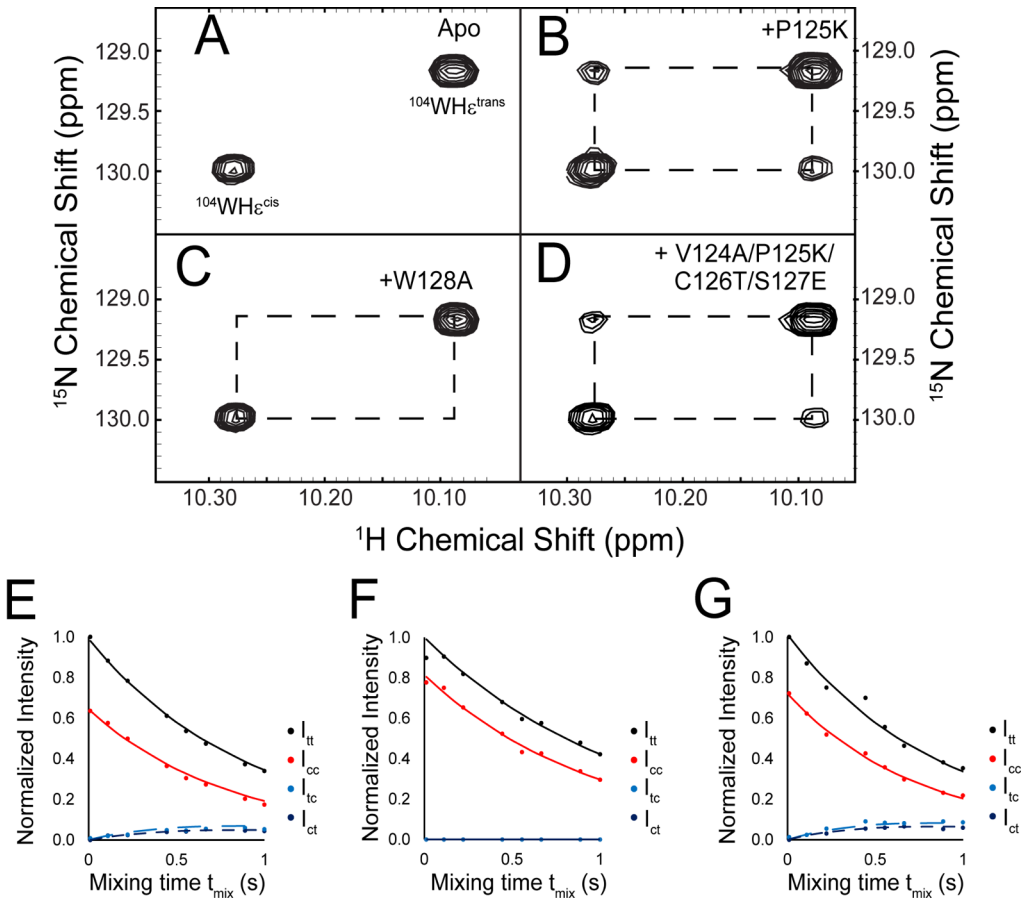

Figure 5.4 Effects of Mutations on LRT2 catalysis of ^{104}W-P^{105} isomerization measured by ZZ-exchange experiments. (A-D) Expanded region of 2D ^{1}H-^{15}N ZZ-exchange spectra for 800μM ^{15}N-OsIAA11$^{72-125}$ without enzyme (A) and in the presence of mutants of LRT2 (B-D) using a mixing time of 0.55s (A-D). Exchange peaks between the ^{104}WHε^{cis} and ^{104}WHε^{trans} auto peaks are observed for the mutants (B) P125K and (D) V124/P125K/C126T/S127E. (C) Exchange peaks are not observed in the presence of W128A LRT2. **(E-G)** Fitting (lines) of intensity peaks (dots) for auto peaks and exchange peaks in the presence of LRT2 mutants. (E) Fitting of ^{104}WHε auto-peaks and exchange peaks intensities in the presence of catalytic amount of P125K LRT2 gives a *cis/trans* isomerization rate k_{ex}=0.46±0.01s^{-1}. (F) The auto-peaks intensity decay is well fit for ^{104}WHε in the presence of W128A and *cis/trans* isomerization rate k_{ex}=0.00±0.01s^{-1}. (G) The auto peaks and exchange peaks intensities for the indole proton of ^{104}W in the cis and trans conformation in the presence of V124/P125K/C126T/S127E LRT2 has a fitting with isomerization rate k_{ex}=0.55±0.01s^{-1}

Table 5.2 Isomerization rates for different mutants of LRT2 determined by ^{1}H-^{1}H ROESY and ^{1}H-^{15}N ZZ exchange experiments.

Mutant	k_{ex} measure by ROESY (s^{-1})	k_{ex} measured by Nzz (s^{-1})
WT	3.63±0.08[a]	0.62±0.01[a]
R62A	0.52±0.16	-
P125K	2.58±0.06	0.46±0.01
W128A	0.00±0.06	0.00±0.01
H133Q	0.09±0.01	-
V124A/P125K/C126T/S127E	3.27±0.12	0.55±0.01

[a]Data reported in Chapter 4

the presence of LRT2 mutants to determined isomerization rates (Figure 5.4 F-G, Table 5.2).

Homologs of LRT2 do not have a higher isomerization rate for the W-P peptide bond in OsIAA11.

Additionally, we performed NMR isomerization rate studies with LRT2 homologs: hCypA and the Peptidy-Prolyl Isomerase B (PPIB) from E. Coli. We decided to test the PPIB of E. Coli because it has been reported to have a higher catalytic activity in the Succinyl-Ala-Ala-Pro-Phe-NH-Mec peptide substrate assay than other PPIases; $k_{cat}/K_m=6.74\times10^{7}M^{-1}s^{-1}$ (Compton *et al.*, 1992) compared to 4.4×10^{6} $M^{-1}s^{-1}$ for Human Cyclophilin A (Janowski *et al.*, 1997). Surprisingly, these enzymes have very similar exchange peaks as LRT2 (Figure 5.5A-B compared to Figure 4.3A). We decided to run a set of ZZ-exchange experiments changing the mixing time to determine the observed isomerization rate (Figure 5.5C-D). We measured an isomerizasion rate of $0.69\pm0.02s^{-1}$ for Human Cyclophilin A and a isomerization rate of $0.37\pm0.01s^{-1}$ in the case of PPIB E.Coli. Remarkably, at least hCypA has a very similar isomerization rate compared to LRT2. This is an interesting result that shows that the isomerization rate likely has a maximum rate tuned by the substrate and not by the enzyme.

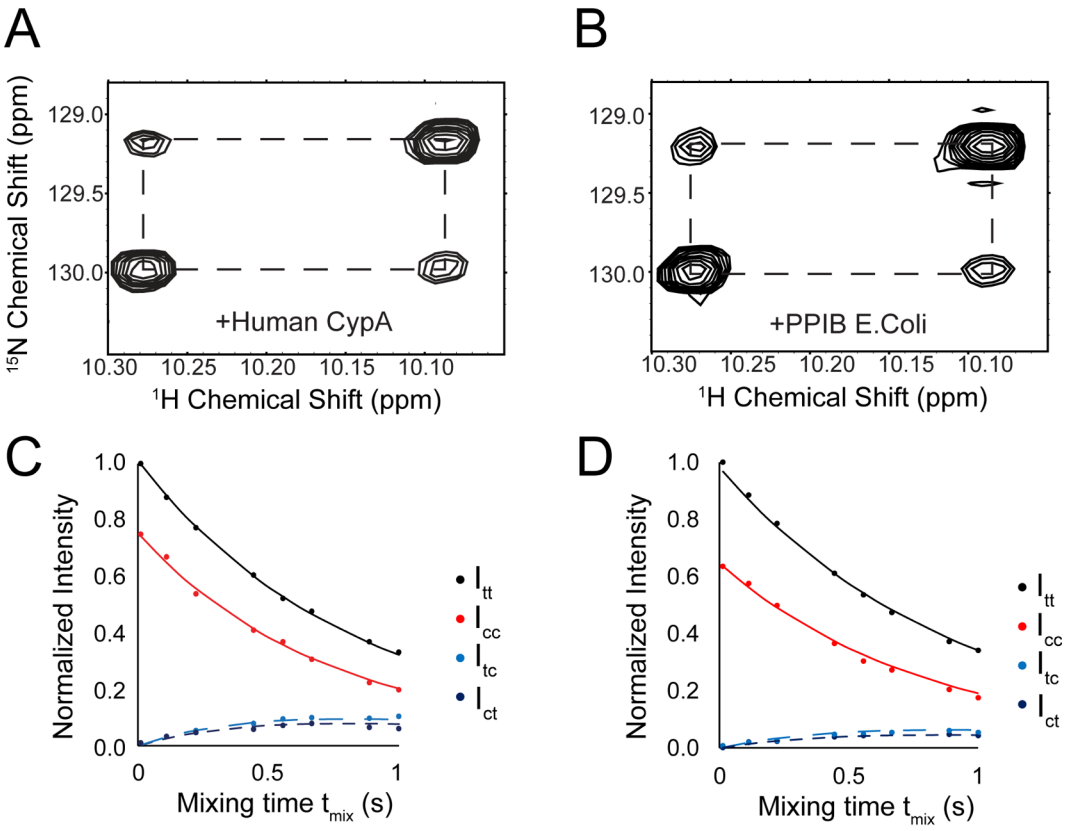

Figure 5.5 Homolog cyclophilins have isomerization effects on the W-P measured by ZZ-exchange. (A-B) Expansion of 2D 1H-15N heteronuclear ZZ exchange NMR spectra for 840μM of ^{15}N-OsIAA11$^{72\text{-}125}$ with 16 μM of hCypA (A) or with 16μM of PPIB from E. Coli (B) using a mixing time of 0.55s (A-B). Exchange peaks between the ^{104}WHε^{cis} and ^{104}WHε^{trans} auto peaks are observed for both cyclophilins. **(C)** Fitting of ^{104}WHε auto-peaks and exchange peaks intensities in the presence of catalytic amount of hCypA gives a *cis/trans* isomerization rate k_{ex}=0.69±0.02s^{-1}. **(D)** The auto peaks and exchange peaks intensities for the indole proton of ^{104}W in the *cis* and *trans* conformation in the presence of PPIB from E. Coli has a fitting with isomerization rate k_{ex}=0.37±0.01s^{-1}

Discussion

An initial objective of this study was to identify mutants in LRT2 that could tune the isomerization step in the Auxin circuit. We proposed several mutants of LRT2, tested their stability by thermal denaturation, and tested their catalytic activity by NMR. Additionally, we considered two homologs of LRT2 acting on the W-P peptide bond of the degron motif of OsIAA11.

One of the mutants proposed in this study was the G72A LRT2. G72A mutant of LRT2 had a qualitatively reported lower isomerization than LRT2 WT (Jing *et al.*, 2015). As mentioned before, G72A mutant is defective in Auxin response and lack of lateral roots (Kang *et al.*, 2013). Interestingly, another mutation in the conserved glycine residue in moss (G72D or dgt-$176^{G\text{-}D}$ as name in Lavy *et al.*, 2012) shows a strong phenotype with no gametophores development (Lavy *et al.*, 2012). These mutation effects could be explained by the instability of the protein upon mutation, as demonstrated by our thermostability test. Nonetheless, in WT LRT2, G72 reports a chemical shift perturbation upon binding to $OsIAA11^{79\text{-}109}$ (Figure 4.6). As Jing et al pointed out, this residue is near the catalytic domain (Figure 5.6 A and B). G72 is a highly conserved residue, and interestingly the reported structure shows dihedral angles only allowed for glycine residues (Figure 5.6D), which could explain why any change in the dihedral angles through mutagenesis results in unfolded protein.

Here, we performed an initial isomerization testing for mutants in LRT2 that could tune the isomerization reaction. This study has identified at least three worthy mutants (W128A, P125K, V124/P125K/C126T/S127E) to further study as mutants with different isomerization rates. A limitation of this study is related with the analysis of

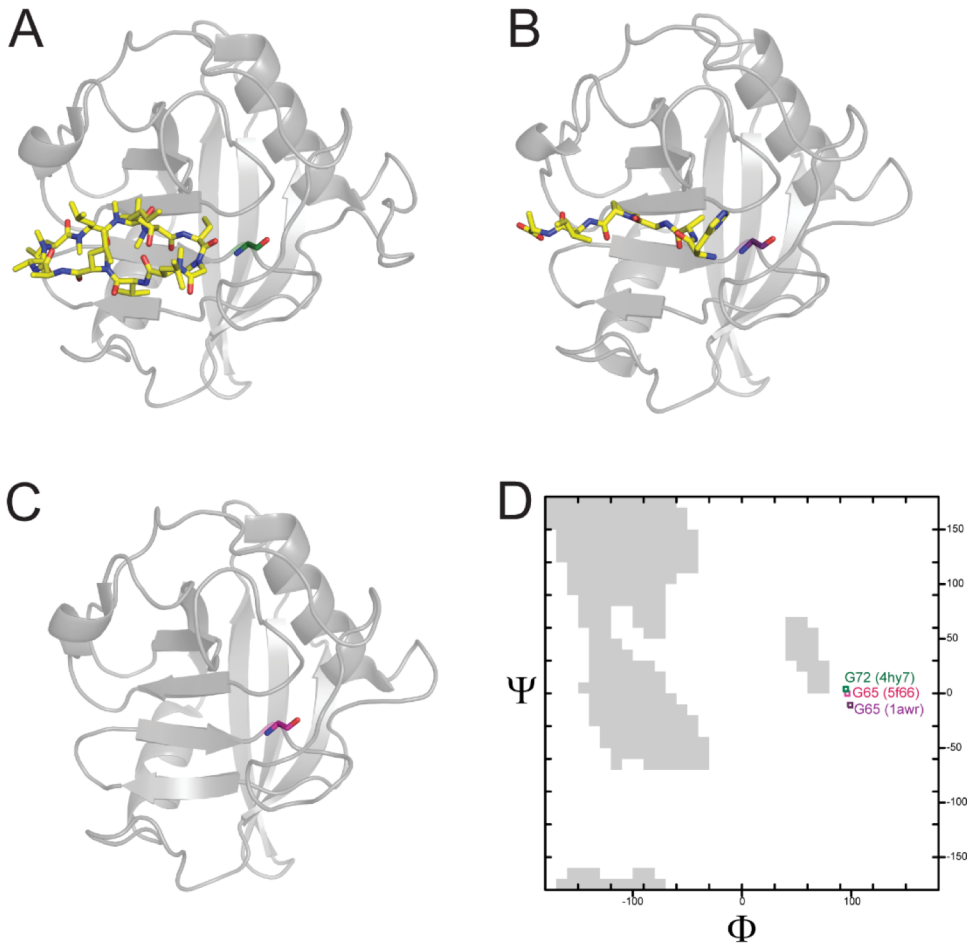

Figure 5.6 Structure analysis of G72. A. Crystal structure of cytosolic wheat cyclophilin TaCypA-1 bound to Cyclosporin A (PDB: 4hy7). **B.** Crystal structure of Human Cyclophilin A bound to HAGPIA peptide (PDB: 1awr). **C.** Crystal structure of Human Cyclophilin A in Apo state (PDB: 5f66) **D.** Ramachandran plot indicates the dihedral restriction values for the conserved glycine (green, purple and pink dot indicates for TaCypA:Cyclosporin A, hCypA:HAGPIA and hCypA respectively), Classical allowed values are in gray.

whether the lower isomerization rates are due to reduction in the on-enzyme isomerization rate or in the binding affinity to the degron motif. A natural progression of this work will be to study the complete thermodynamic and kinetic cycle through lineshape analysis, in a similar manner as in Chapter 4 for WT LRT2. Prior studies have noted the importance of dissecting the characteristics of the catalytic event for hCypA acting on a natural substrate and concluded that a clear quantitative analysis is needed (Bosco *et al.*, 2010). In their analysis, several mutants were identified as mutants where the rate limiting step was either the dissociation of the substrate or the CypA-catalyzed rate. In future investigations, it might be possible to use some of the mutants Bosco *et al* studied. For instance, F113W CypA reports an overall observed isomerization rate twice as fast as WT CypA but with a lower affinity, while H126A CypA has a similar binding affinity but lower overall observed isomerization rate compared to WT. These additional mutants together with a further examination of the complete thermodynamic cycle of the mutants tested in this chapter could address the implications of mutagenesis in the Auxin circuit when studied *in vivo*.

One of the issues that emerges from our isomerization studies with homologs of LRT2 is the fact that these homologs have a comparable isomerization rate. An implication of this is the possibility that the substrate (OsIAA11) is what limits the catalytic cycle. This finding, while preliminary, suggests that any cyclophilin present in the cell could have a similar enzymatic activity to control the equilibrium between *cis* and *trans* isomer of $_{104}$W-P$_{105}$ peptide bond. This fact poses intriguing questions regarding the importance and uniqueness of LRT2 in lateral root development when other cyclophilins could easily control the equilibrium between *cis* and *trans* isomers.

Curiously, in immunoprecipitation of OsTIR1-Myc, His-OsIAA11 and plant extract, LRT2 was detected by immunoblotting (Jing *et al.*, 2015). It will be important to determine whether LRT2 has a meaningful role in the interaction between OsIAA11 and TIR1 other than regulation of *cis*/*trans* equilibrium of $_{104}$W-P$_{105}$ peptide bond. And then selecting mutants that change only either the catalytic or binding properties for further studies in plants will help to understand in more detail the role of LRT2 in regulation of lateral root development. This is an important issue for future research.

In reviewing the literature, only two substrates where the W-P peptide bond has been studied were found. The first case was studied by a previous doctoral student in our lab. The undefined domain of IRAK1 binds only in the *trans* isomer of the $_{168}$W-P$_{169}$ peptide bond to the EVH1 domain of the actin polymerize VASP. CypA catalyzes this *cis*/*trans* isomerization with an observed k_{ex}=1.61s^{-1} when 8μM of CypA is added to 0.8mM of ^{15}N-IRAK1-UD (Greenwood *et al.*, 2014). Recently, PPIF, a mitochondrial cyclophilin, was reported to catalyze the isomerization of the $_{624}$W-P$_{625}$ peptide bond in the TransActivation domain (TAD) of the regulator in the mammalian circadian clock BMAL1. Upon addition of 100μM PPIF into 0.4mM of BMAL1 TAD, a ~300-fold increase in isomerization rate compared to the uncatalyzed isomerization was observed, which represents a k_{ex} of approximately 2.68s^{-1} (Gustafson *et al.*, 2017). Both examples measured the observed isomerization at different concentration and buffer conditions that those discussed in this chapter. Nevertheless, neither of these isomerization rates have been as fast as reported for G-P peptide bonds. For instance, when 73μM of CypA was added to 0.87mM of the N-terminal domain of the human immunodeficiency virus type 1 capsid (CA^{N}), an observed isomerization rate was 6.5s^{-1} (Bosco *et al.*, 2010). This

is almost 10-fold compared to what we measured ($0.69s^{-1}$) where we used just a fifth of the enzyme concentration (16μM). A possible explanation for this might be due to the affinity of the substrate, which is reported to be an apparent tight affinity of K_D=13±11μM (Bosco *et al.*, 2010). While for our substrate, based on the similar isomerization rate for LRT2, we will expect it to be similar to the affinity measured for LRT2 in Chapter 4 (K_D=1.5mM).

An important aspect to keep in mind is that aromatic residues, such as Trp, help to stabilize the *cis* isomer by favorable interactions between the aromatic ring and the proline ring (Wu *et al.*, 1998). This translates in an increase of *cis* population in the equilibrium state. In our case the *cis* isomer of the $_{104}$W-P$_{105}$ in OsIAA11 represents 45% of the population, while for the case of the $_{89}$G-P$_{90}$ in CA^N the *cis* isomer was just 15% of the population (Bosco *et al.*, 2010). It is important to study whether the group preceding the proline has a systematic effect in the on enzyme equilibrium constant.

Several possible catalytic mechanisms have been proposed for the *cis/trans* isomerization by PPIases (Fanghanel *et al.*, 2004). One of the possible mechanism is the rotation of the N-terminal part of the peptide bond, which was proposed upon X-ray comparison of HIV-1 capsid mutants (Howard *et al.*, 2003). More recently, this mechanism has been supported by further NMR, molecular dynamic simulations, and density functional theory calculations (Camilloni *et al.*, 2014). These studies are limited to the case of an isomerization of G-P peptide bond. Remarkably, the crystal structure of bound *trans* $_{89}$G-P$_{90}$ in CA^N would not have space for a side chain (Gamble *et al.*, 1996), substitution of Gly 89 to Ala weakens the binding from K_D~20μM to ~500μM (Yoo *et al.*, 1997), which aligns with the high K_D that we measured in Chapter 4 for

LRT2. On the other hand, there have been studies that support a C-terminal rotation mechanism. For instance, in solution NMR dynamics of CypA acting on a four residue peptide substrate, with a Phe-Pro peptide bond, the data were interpreted as the Phe to have the side chain towards the solvent for both *cis* and *trans* isomer and then the proline is the element that rotates (Eisenmesser *et al.*, 2002). They also measured a relatively weak affinity between CypA and their test substrate (K_D=1.18mM). It is natural to ask whether the difference of the interpretation in the mechanism of action is due to the substrate used to study, and then a generalization of the mechanism of action of PPIases is not feasible, since perhaps the PPIase molds to the substrate.

In conclusion, we found stable mutants that reduce the isomerization rates in the $_{104}$W-P$_{105}$ peptide bond of OsIAA11. We also explored a substitution of Gly 72 in LRT2 found by random mutagenesis (Kang *et al.*, 2013) and an analysis of homolog structures determined dihedral angles only allowed to Glycine at this position. Additionally, we explored the isomerization activity in homolog cyclophilins, and found that, as a preliminary conclusion, any typical cyclophilin could act on the $_{104}$W-P$_{105}$ peptide bond with similar effectiveness. It will be important to explore the specific mechanism of action for a W-P peptide bond to understand better the regulation of this *cis/trans* isomerization.

REFERENCES

Acevedo, L. A., & Nicholson, L. K. (2018). 1H, 13C and 15N NMR assignments of cyclophilin LRT2 (OsCYP2) from rice. *Biomolecular NMR Assignments*. doi:10.1007/s12104-018-9803-x

Bosco, D. A., Eisenmesser Ez Fau - Clarkson, M. W., Clarkson Mw Fau - Wolf-Watz, M., Wolf-Watz M Fau - Labeikovsky, W., Labeikovsky W Fau - Millet, O., Millet O Fau - Kern, D., & Kern, D. (2010). Dissecting the microscopic steps of the cyclophilin A enzymatic cycle on the biological HIV-1 capsid substrate by NMR. *Journal of Molecular Biology, 403*(1089-8638 (Electronic)), 723-738.

Calderon Villalobos, L. I., Lee S Fau - De Oliveira, C., De Oliveira C Fau - Ivetac, A., Ivetac A Fau - Brandt, W., Brandt W Fau - Armitage, L., Armitage L Fau - Sheard, L. B., . . . Estelle, M. (2012). A combinatorial TIR1/AFB-Aux/IAA co-receptor system for differential sensing of auxin. (1552-4469 (Electronic)).

Camilloni, C., Sahakyan, A. B., Holliday, M. J., Isern, N. G., Zhang, F., Eisenmesser, E. Z., & Vendruscolo, M. (2014). Cyclophilin A catalyzes proline isomerization by an electrostatic handle mechanism. *Proceedings of the National Academy of Sciences, 111*(28), 10203-10208. doi:10.1073/pnas.1404220111

Compton, L. A., Davis, J., Macdonald, J. R., & BÄChinger, H. P. (1992). Structural and functional characterization of Escherichia coli peptidyl-prolyl cis-trans isomerases. *European Journal of Biochemistry, 206*(3), 927-934. doi:10.1111/j.1432-1033.1992.tb17002.x

Cui, P., Liu, H., Ruan, S., Ali, B., Gill, R. A., Ma, H., . . . Zhou, W. (2017). A zinc finger protein, interacted with cyclophilin, affects root development via IAA pathway in rice. *Journal of Integrative Plant Biology*, n/a-n/a. doi:10.1111/jipb.12531

Dinesh, D. C., Villalobos, L. I., & Abel, S. (2016). Structural Biology of Nuclear Auxin Action. *Trends Plant Sci, 21*(4), 302-316. doi:10.1016/j.tplants.2015.10.019

Eisenmesser, E. Z., Bosco, D. A., Akke, M., & Kern, D. (2002). Enzyme Dynamics During Catalysis. *Science, 295*(5559), 1520-1523. doi:10.1126/science.1066176

Fanghanel, J., & Fischer, G. (2004). Insights into the catalytic mechanism of peptidyl prolyl cis/trans isomerases. *Front Biosci, 9*, 3453-3478.

Fischer, G., & Aumüller, T. (2004). Regulation of peptide bond cis/trans isomerization by enzyme catalysis and its implication in physiological processes *Rev Physiol Biochem Pharmacol* (pp. 105-150). Berlin, Heidelberg: Springer Berlin Heidelberg.

Fischer, G., & Bang, H. (1985). The refolding of urea-denatured ribonuclease A is catalyzed by peptidyl-prolyl cis-trans isomerase. *Biochim Biophys Acta, 828*(1), 39-42.

Galat, A., & Riviére, S. (1998). *Peptidyl-prolyl Cis/trans Isomerases*: Oxford University Press.

Gamble, T. R., Vajdos, F. F., Yoo, S., Worthylake, D. K., Houseweart, M., Sundquist, W. I., & Hill, C. P. (1996). Crystal structure of human cyclophilin A bound to the amino-terminal domain of HIV-1 capsid. *Cell, 87*(7), 1285-1294.

Garcia-Echeverria, C., & Rich, D. H. (1992). New intramolecularly quenched fluorogenic peptide substrates for the study of the kinetic specificity of papain. *FEBS Letters, 297*(1), 100-102. doi:https://doi.org/10.1016/0014-5793(92)80336-F

Gething, M.-J., & Sambrook, J. (1992). Protein folding in the cell. *Nature, 355*(6355), 33-45.

Greenwood, A. I., Kwon, J., & Nicholson, L. K. (2014). Isomerase-Catalyzed Binding of Interleukin-1 Receptor-Associated Kinase 1 to the EVH1 Domain of Vasodilator-Stimulated Phosphoprotein. *Biochemistry, 53*(22), 3593-3607. doi:10.1021/bi500031e

Greenwood, A. I., Rogals, M. J., De, S., Lu, K. P., Kovrigin, E. L., & Nicholson, L. K. (2011). Complete determination of the Pin1 catalytic domain thermodynamic cycle by NMR lineshape analysis. *J Biomol NMR, 51*(1-2), 21-34. doi:10.1007/s10858-011-9538-9

Gustafson, C. L., Parsley, N. C., Asimgil, H., Lee, H.-W., Ahlbach, C., Michael, A. K., . . . Partch, C. L. (2017). A Slow Conformational Switch in the BMAL1 Transactivation Domain Modulates Circadian Rhythms. *Mol Cell, 66*(4), 447-457.e447. doi:https://doi.org/10.1016/j.molcel.2017.04.011

Hanes, S. D. (2015). Prolyl isomerases in gene transcription. *Biochim Biophys Acta, 1850*(10), 2017-2034. doi:10.1016/j.bbagen.2014.10.028

Heckman, K. L., & Pease, L. R. (2007). Gene splicing and mutagenesis by PCR-driven overlap extension. *Nature Protocols, 2*, 924. doi:10.1038/nprot.2007.132

Holliday, M. J., Armstrong, G. S., & Eisenmesser, E. Z. (2015). Determination of the Full Catalytic Cycle among Multiple Cyclophilin Family Members and Limitations on the Application of CPMG-RD in Reversible Catalytic Systems. *Biochemistry, 54*(38), 5815-5827. doi:10.1021/acs.biochem.5b00746

Howard, B. R., Vajdos, F. F., Li, S., Sundquist, W. I., & Hill, C. P. (2003). Structural insights into the catalytic mechanism of cyclophilin A. *Nat Struct Biol, 10*, 475. doi:10.1038/nsb927

Huynh, K., & Partch, C. L. (2015). Current Protocols in Protein Science: Analysis of protein stability and ligand interactions by thermal shift assay. *Current protocols in protein science / editorial board, John E. Coligan ... [et al.], 79*, 28.29.21-28.29.14. doi:10.1002/0471140864.ps2809s79

Janowski, B., Wöllner, S., Schutkowski, M., & Fischer, G. (1997). A Protease-Free Assay for Peptidyl Prolylcis/transIsomerases Using Standard Peptide Substrates. *Analytical Biochemistry, 252*(2), 299-307. doi:https://doi.org/10.1006/abio.1997.2330

Jing, H., Yang, X., Zhang, J., Liu, X., Zheng, H., Dong, G., . . . Zuo, J. (2015). Peptidyl-prolyl isomerization targets rice Aux/IAAs for proteasomal degradation during auxin signalling. *Nat Commun, 6*, 7395. doi:10.1038/ncomms8395

Kang, B., Zhang, Z., Wang, L., Zheng, L., Mao, W., Li, M., . . . Mo, X. (2013). OsCYP2, a chaperone involved in degradation of auxin-responsive proteins, plays crucial roles in rice lateral root initiation. *Plant J, 74*(1), 86-97. doi:10.1111/tpj.12106

Kumari, S., Roy, S., Singh, P., Singla-Pareek, S. L., & Pareek, A. (2013). Cyclophilins: proteins in search of function. *Plant Signal Behav, 8*(1), e22734. doi:10.4161/psb.22734

Kutschera, U., & Niklas, K. J. (2016). The evolution of the plant genome-to-morphology auxin circuit. *Theory in Biosciences, 135*(3), 175-186. doi:10.1007/s12064-016-0231-0

Lavy, M., Prigge, M. J., Tigyi, K., & Estelle, M. (2012). The cyclophilin DIAGEOTROPICA has a conserved role in auxin signaling. *Development, 139*(6), 1115-1124. doi:10.1242/dev.074831

Lin, L. N., & Brandts, J. F. (1983). Isomerization of proline-93 during the unfolding and refolding of ribonuclease A. *Biochemistry, 22*(3), 559-563.

Liscum, E., & Reed, J. W. (2002). Genetics of Aux/IAA and ARF action in plant growth and development. *Plant Molecular Biology, 49*(3), 387-400. doi:10.1023/A:1015255030047

Lorenz, T., & Reinstein, J. (2008). The influence of proline isomerization and off-pathway intermediates on the folding mechanism of eukaryotic UMP/CMP Kinase. *J Mol Biol, 381*(2), 443-455. doi:10.1016/j.jmb.2008.06.001

Lu, P. J., Wulf, G., Zhou, X. Z., Davies, P., & Lu, K. P. (1999). The prolyl isomerase Pin1 restores the function of Alzheimer-associated phosphorylated tau protein. *Nature, 399*(0028-0836 (Print)), 784-788. doi:10.1038/21650

Nelson, C. J., Santos-Rosa, H., & Kouzarides, T. (2006). Proline Isomerization of Histone H3 Regulates Lysine Methylation and Gene Expression. *Cell, 126*(5), 905-916. doi:https://doi.org/10.1016/j.cell.2006.07.026

Ruan, S.-L., Ma, H.-S., Wang, S.-H., Fu, Y.-P., Xin, Y., Liu, W.-Z., . . . Chen, H.-Z. (2011). Proteomic identification of OsCYP2, a rice cyclophilin that confers salt tolerance in rice (Oryza sativa L.) seedlings when overexpressed. *BMC Plant Biology, 11*, 34-34. doi:10.1186/1471-2229-11-34

Sarkar, P., Reichman, C., Saleh, T., Birge, R. B., & Kalodimos, C. G. (2007). Proline cis-trans Isomerization Controls Autoinhibition of a Signaling Protein. *Mol Cell, 25*(3), 413-426. doi:https://doi.org/10.1016/j.molcel.2007.01.004

Schiene, C., & Fischer, G. (2000). Enzymes that catalyse the restructuring of proteins. *Current Opinion in Structural Biology, 10*(1), 40-45. doi:https://doi.org/10.1016/S0959-440X(99)00046-9

Schlegel, J., Redzic, J. S., Porter, C. C., Yurchenko, V., Bukrinsky, M., Labeikovsky, W., . . . Eisenmesser, E. Z. (2009). Solution characterization of the extracellular region of CD147 and its interaction with its enzyme ligand cyclophilin A. *J Mol Biol, 391*(3), 518-535. doi:10.1016/j.jmb.2009.05.080

Sekhon, S. S., Kaur, H., Dutta, T., Singh, K., Kumari, S., Kang, S., . . . Yoon, T. S. (2013). Structural and biochemical characterization of the cytosolic wheat cyclophilin TaCypA-1. *Acta Crystallogr D Biol Crystallogr, 69*(Pt 4), 555-563. doi:10.1107/s0907444912051529

Tan, X., Calderon-Villalobos, L. I., Sharon, M., Zheng, C., Robinson, C. V., Estelle, M., & Zheng, N. (2007). Mechanism of auxin perception by the TIR1 ubiquitin ligase. *Nature, 446*(7136), 640-645. doi:10.1038/nature05731

Thapar, R. (2015). Roles of Prolyl Isomerases in RNA-Mediated Gene Expression. *Biomolecules, 5*(2), 974-999. doi:10.3390/biom5020974

Wu, W. J., & Raleigh, D. P. (1998). Local control of peptide conformation: stabilization of cis proline peptide bonds by aromatic proline interactions. *Biopolymers, 45*(5), 381-394. doi:10.1002/(SICI)1097-0282(19980415)45:5<381::AID-BIP6>3.0.CO;2-H

Yoo, S., Myszka, D. G., Yeh, C., McMurray, M., Hill, C. P., & Sundquist, W. I. (1997). Molecular recognition in the HIV-1 capsid/cyclophilin A complex. *J Mol Biol, 269*(5), 780-795.

Zheng, H., Li, S., Ren, B., Zhang, J., Ichii, M., Taketa, S., . . . Wang, H. (2013). LATERAL ROOTLESS2, a cyclophilin protein, regulates lateral root initiation and auxin signaling pathway in rice. *Mol Plant, 6*(5), 1719-1721. doi:10.1093/mp/sst052

Zhou, W., Yang, Q., Low, C. B., Karthik, B. C., Wang, Y., Ryo, A., . . . Liou, Y. C. (2009). Pin1 catalyzes conformational changes of Thr-187 in p27Kip1 and mediates its stability through a polyubiquitination process. *J Biol Chem, 284*(36), 23980-23988. doi:10.1074/jbc.M109.022814

CHAPTER 6

CONCLUSIONS AND FUTURE DIRECTION

In this work, we presented two very different examples of protein-protein interaction. The first related to the mechanism of binding when multiple binding sites are presented. This protein-protein interaction is important in actin regulation in mammalian cells. The second related to an enzyme acting on a substrate and determined not only the equilibrium constants but also the kinetic rates associated with the catalytic cycle. This protein-protein interaction is important in lateral root development in rice. The versatility of the examples we had, shows once again the versatility of NMR as a tool to elucidate protein-protein interactions.

Remarkably, it was surprising to find a secondary binding site in the EVH1 domain of VASP that interacts with the proline rich region of Zyxin (Chapter 2). Even more striking was to observe that this secondary binding site favors an orientation that imparts a bivalent EVH1:Zyxin binding mode, a binding state that was captured by the EVH1-Zyxin$^{82\text{-}124}$ chimera protein. Through a phosphomimetic mutation, we could answer a question opened by the work of Maruoka *et al.*, 2012. In their work, a phosphorylation of a tyrosine far from the canonical binding site in EVH1 seems to regulate Zyxin binding. Noteworthy, when we tested binding of EVH1 and Zyxin upon a phosphomimetic mutation Y39E, we observed a complete lack of binding at the novel secondary site. Indeed, we concluded that the preference to a bivalent interaction was no longer observed. This study has broader implications in the context given by another study (Zimmermann *et al.*, 2002). They proposed a possibility of VASP functioning as a crosslinker between several protein partners and we proposed that based on our NMR studies multiple molecules could bind individually to each EVH1 domain in a tetramer VASP, and this is regulated by phosphorylation in Tyrosine 39.

Chapter 2 proposes a mechanistic model where phosphorylation of the Tyr39 in the EVH1 domains could regulate VASP binding to an individual binding partner with multiple EVH1 binding motifs, or the possibility of binding to multiple binding partners by bivalent interactions to each EVH1 domain when unphosphorylated (Figure 2.7). This implicates that VASP could function as a crosslinker between multiple proteins in the cell. In future directions, this model could be easily studied by Small Angle X-ray Scattering (SAXS). SAXS is a valuable technique that can give information on the overall shape and degree of disorder of proteins and complexes. A VASP:Zyxin complex would probably have a "broccoli" like shape since multiple Zyxin will bind to the VASP tetramer, while a VASP Y39E: Zyxin complex will have a cylindrical shape since one molecule of Zyxin will pull together the EVH1 domains in VASP based on our model.

We reported the secondary binding site observed for EVH1:Zyxin interaction. Interestingly, EVH1 has been studied by NMR previously and this novel binding site is not reported except for work done by a previous grad student in our lab (Greenwood, 2014). However, the chemical shift perturbation by the individual peptides is very weak compared to when full length proline rich region is titrated. Therefore, it is likely that the chemical shift perturbation has been unnoticed. There are several binding partners for EVH1 that contain poly-proline motifs such as ActA (Machner *et al.*, 2001), Lamellipodin (Krause *et al.*, 2004), Lipoma Prefered Partner (Petit *et al.*, 2000), Vinculin (Harbeck *et al.*, 2000), and Migfilin (Zhang *et al.*, 2006). To our current knowledge, none of these other binding partners have been tested as full-length binding to EVH1 by NMR. It would be interesting to test whether any of these binding partners interacts with EVH1 in a similar mechanism as Zyxin.

In this dissertation. we also discussed the enzyme LRT2 acting on their natural substrate OsIAA11. These two proteins have important roles in lateral root initiation (Z.

X. Zhu *et al.*, 2012; Kang *et al.*, 2013). In Chapter 3, we first reported the backbone and sidechain resonance assignments of ^{1}H, ^{13}C, ^{15}N in LRT2. These assignments have been used to confirm the binding site of LRT2 in Chapter 4.

LRT2 is classified as a Peptidyl Prolyl *Cis/trans* Isomerase (PPIase). PPIases have emerged as key regulators of many biological processes (Fischer *et al.*, 2004). They are particularly important when one or both isomers have distinct isomer-specific binding partners. This isomer-specific binding could deplete the amount of the specific isomer and disrupt the balance of the equilibrium in the cell. This leads to the requirement for PPIases, which can combat the imbalance through rapid restoration of equilibrium, as well as maintain the flow to the isomer-specific binding event. In the case of plants, a *cis* specific binding was reported for binding between the conserved degron domain of Aux/IAA repressor proteins and its cognate E3 ligase (Tan *et al.*, 2007). Thus, a PPIase is important to maintain the equilibrium population of Aux/IAA when auxin abruptly activates the degradation pathway.

In Chapter 4, we characterized the isomerization of the $^{104}W\text{-}P^{105}$ peptide bond of OsIAA11 catalyzed by LRT2. We applied NMR lineshape analysis to determine the thermodynamic and kinetic parameters for LRT2 acting on domain II of OsIAA11. We found that this interaction has a weak affinity (K_D^{app}=1.5mM), the binding affinity is almost equal to *cis* as to *trans* and, the equilibrium constant is conserved during bound states with value almost equal to one. Curiously, the on-enzyme rate constants for conversion between cis and trans states are relatively slow (k_{ex}=94.75s^{-1}) compared to other PPIases acting on other substrates (Greenwood *et al.*, 2011; Bosco *et al.*, 2010). We confirmed these fitted values by additionally performing NMR exchange spectroscopy and through our determination of the apparent affinity from the perspective of LRT2. In Chapter 4, we also tested whether additional X-P motifs in OsIAA11 domain II could alter the isomerization rate of LRT2 acting on the $^{104}W\text{-}P^{105}$

peptide bond. Interestingly, we found that the additional motifs did not affect the isomerization rate. Indeed, we could predict the isomerization rate for a 12-residue peptide representing the degron motif by using the thermodynamic and kinetic parameters found by lineshape analysis for the longer substrate. The findings of this research provide insights for the effectiveness of LRT2 to keep the flow of the *cis* isomer of the ^{104}W-P^{105} peptide bond. For other Aux/IAA proteins, the half-life has been reported to be on the order of a few minutes (Abel *et al.*, 1994; Gray *et al.*, 2001). If isomerization rates of the PPIase acting on those Aux/IAA are like the ones found on the OsIAA11:LRT2 case, we could conclude that the rate limiting step for the Auxin dependent system is probably related to the ubiquitination and/or degradation and not necessarily in the isomerization. However, it is important to notice that if the degradation process abruptly depletes the *cis* isomer, LRT2 will effectively maintain equilibrium.

LRT2 mutants that either introduce an early stop codon or do a single mutation of G72A reduced the lateral root development in rice (Kang *et al.*, 2013). In Chapter 5, we found that the G72A mutant was highly unstable. A logical explanation for this is that the dihedral angles at this residue in the canonical cyclophilin structure are allowed only for glycine. Remarkably, we measured isomerization rates for several other mutants that reduce the isomerization rates acting on the ^{104}W-P^{105} peptide bond. We recognized, that a complete analysis to determine all the thermodynamic and kinetic parameters will be necessary to completely understand how a mutation in the enzyme can affect isomerization rates. Additionally, we tested two homologs of LRT2 and found that the isomerization rates are comparable to the values found in Chapter 4. This finding is consistent with the conclusion drawn in the previous paragraph, namely that isomerization by LRT2 is not necessarily the rate limiting step in the auxin circuit, since other cyclophilins could act with very similar effectiveness.

PPIases are conserved across species and their *in vivo* function has recently been characterized as molecular regulator of the *cis/trans* isomerization (Lu *et al.*, 2007; Hanes, 2015). However, quantitative characterization of the impact of specific *cis/trans* isomerization rates on biological process in living cells and on phenotypes in the whole organism are still unknown. The main goal of the study described from Chapter 3 to 5 was to determine one such *cis/trans* isomerization rate and, to try to manipulate it through mutagenesis. Previous knowledge about the Auxin circuit combined with our determination of the rates provides a quantitative description of the role of specific *cis/trans* isomerization rates that can act like a timer device in gene expression with a well-defined phenotype. For this, it will be also essential to determine other rates in the circuit, for instance the degradation of OsIAA11, the binding of OsIAA11 to Auxin Responsive Factor, as well as the rate of expression of OsIAA11. In the Nicholson lab, there is current work being done to pursue this information. Once all the details are known, we could introduce the mutants of LRT2 in the rice plant and determine the importance of the isomerization rate in the whole circuit by monitoring OsIAA11 tagged with a fluorescent protein by confocal microscopy in individual cells and, by analyzing whole phenotype of plants.

OsIAA11 was found to be important in lateral root development when mutation of Proline 106 to Leucine in OsIAA11 showed a remarkable reduction of lateral root number (Zhu *et al.*, 2012). Dependence further from the W-P motif for binding to LRT2 has not been studied yet. Looking at the structure determined for the TIR1-Auxin-IAA7 degron motif complex (Tan *et al.*, 2007), the second Proline in the degron motif (P106) could perhaps have a pi interaction with the tryptophan ring (Figure 6.1) and whether this interaction is present in the free peptide could be interested for the Auxin circuit regulation. This hypothesis could be measured by NMR in a similar manner as has been

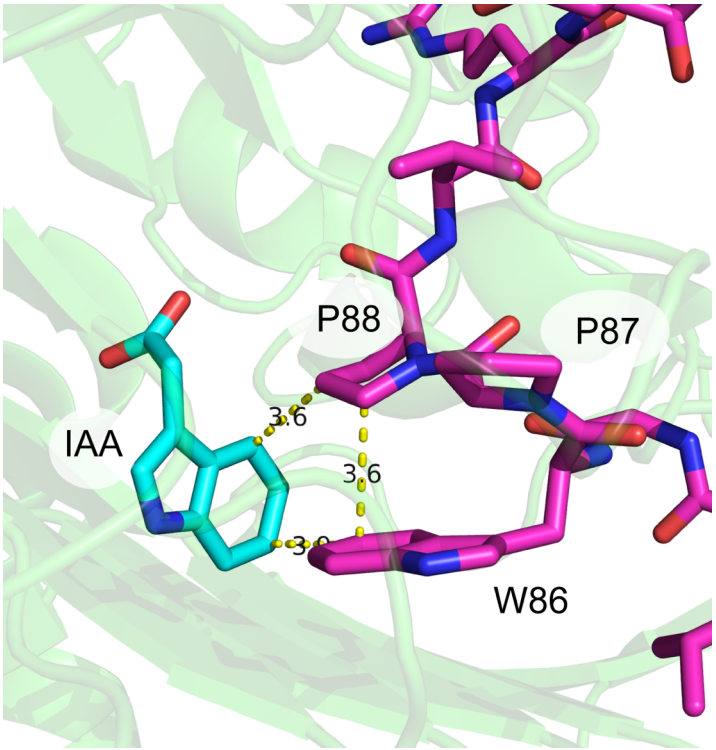

Figure 6.1 Structure of TIR1 bound to Auxin and IAA7 degron motif. A close-up view of the auxin (cyan) binding to TIR1 (green, cartoon) and the IAA7 degron motif (Magenta) shows a possible interaction between W86, P88, and Auxin (PDB:2P1Q). Distance measured between the P88-C^{δ} to Auxin-$C^{\varepsilon 3}$ is 3.6Å, the distance between P88-C^{δ} and W86-$C^{\zeta 3}$ is also 3.6Å, and the distance between W86-$C^{\zeta 3}$ and the Auxin $C^{\eta 2}$ is 3.9Å. With these distances, the W86, P88 and the Auxin molecule could have Van Der Waals interactions that stabilize the structure to fit in the binding pocket of the cognate E3 ligase.

measured for peptides containing PP-X residues and where it was shown that when X is an aromatic amino-acid a CH-pi interaction is observed (Ganguly *et al.*, 2012). If this interaction is observed for OsIAA11 free in solution, it could indicate that the isomerization by LRT2 maintains the highest possible supply of the perfect substrate to fit into the E3 ligase as high as possible. As mentioned before, an aromatic residue stabilizes the *cis* isomer of the X-P peptide bond. It will be interesting to see whether a Tryptophan residue can stabilize both the X-P peptide bond in the *cis* isomer and the structure of the following proline in the X-PP case.

As it was explained in Chapter 1, the auxin circuit is a well-established mechanism of gene regulation in plants. In general, we could expect that a peptidyl prolyl isomerase pairs with an Aux/IAA to regulate a specific gene expression. A possible example further from the work presented here could be the flowering in Arabidopsis. An inhibitor of peptidyl prolyl isomerases, specifically of parvulins, shows that binding between IAA7 and TIR1 is reduced in the presence of the inhibitor, Juglone (Dharmasiri *et al.*, 2003). This was observed before the crystal structure of the TIR1 complex and the IAA7 degron motif was determined (Tan *et al.*, 2007), and thereby before knowing the importance of a peptidyl prolyl isomerase in the auxin circuit. Curiously, IAA7 negatively regulates the time of flowering under short-day light conditions in Arabidopsis (Mai *et al.*, 2011). Interestingly, another hormone is known to regulate this timing, the Gibberellins (Langridge, 1957). The overlap between auxin and gibberellins mechanism has been previously reported (Fu *et al.*, 2003; Frigerio *et al.*, 2006). Further molecular studies into how PPIases could regulate this overlap are needed.

In the Nicholson lab Pin1, another Peptidyl Prolyl isomerase, has been widely studied with important roles in Alzheimer's disease and Asthma (Pastorino *et al.*, 2006; Rogals *et al.*, 2016; Fisher *et al.*, 2017; Nechama *et al.*, 2018). Pin1 has an added level

of regulation because of the requirement that its substrates must be phosphorylated (Hsu *et al.*, 2001; Pastorino *et al.*, 2006). Curiously, an Arabidopsis PIN1-type parvulin 1, Pin1AT, controls flowering time by *cis/trans* isomerization of Ser/Thr-Pro motifs in MAD-box transition factors (Wang *et al.*, 2010). Additionally, the over-expression of PvPin1, the bamboo homolog of Pin1, delays flowering time in transgenic Arabidopsis and rice (Zheng *et al.*, 2017). Pin1 like proteins in plants only have the PPIase domain, compared to human and yeast homologs that also contained a WW domain (Yao *et al.*, 2001). To our knowledge, a Pin1 homolog for rice has not been cloned or defined a function. It will be expected that the mechanism of Pin1 like proteins will be different from the auxin circuit due to the additional regulation of Ser/Thr-Pro. A greater focus on Pin1 like proteins could produce interesting findings that reveal additional importance of PPIases in plants.

REFERENCES

Abel, S., Oeller, P. W., & Theologis, A. (1994). Early auxin-induced genes encode short-lived nuclear proteins. *Proceedings of the National Academy of Sciences, 91*(1), 326.

Bosco, D. A., Eisenmesser Ez Fau - Clarkson, M. W., Clarkson Mw Fau - Wolf-Watz, M., Wolf-Watz M Fau - Labeikovsky, W., Labeikovsky W Fau - Millet, O., Millet O Fau - Kern, D., & Kern, D. (2010). Dissecting the microscopic steps of the cyclophilin A enzymatic cycle on the biological HIV-1 capsid substrate by NMR. *Journal of Molecular Biology, 403*(1089-8638 (Electronic)), 723-738.

Dharmasiri, N., Dharmasiri, S., Jones, A. M., & Estelle, M. (2003). Auxin Action in a Cell-Free System. *Current Biology, 13*(16), 1418-1422. doi:https://doi.org/10.1016/S0960-9822(03)00536-0

Fischer, G., & Aumüller, T. (2004). Regulation of peptide bond cis/trans isomerization by enzyme catalysis and its implication in physiological processes *Rev Physiol Biochem Pharmacol* (pp. 105-150). Berlin, Heidelberg: Springer Berlin Heidelberg.

Fisher, C. L., Resnick, R. J., De, S., Acevedo, L. A., Lu, K. P., Schroeder, F. C., & Nicholson, L. K. (2017). Cyclic cis-Locked Phospho-Dipeptides Reduce Entry of AbetaPP into Amyloidogenic Processing Pathway. *J Alzheimers Dis, 55*(1), 391-410. doi:10.3233/jad-160051

Frigerio, M., Alabadí, D., Pérez-Gómez, J., García-Cárcel, L., Phillips, A. L., Hedden, P., & Blázquez, M. A. (2006). Transcriptional Regulation of Gibberellin Metabolism Genes by Auxin Signaling in Arabidopsis. *Plant Physiol, 142*(2), 553.

Fu, X., & Harberd, N. P. (2003). Auxin promotes Arabidopsis root growth by modulating gibberellin response. (0028-0836 (Print)).

Ganguly, H. K., Majumder, B., Chattopadhyay, S., Chakrabarti, P., & Basu, G. (2012). Direct Evidence for CH···π Interaction Mediated Stabilization of Pro-cisPro Bond in Peptides with Pro-Pro-Aromatic motifs. *J Am Chem Soc, 134*(10), 4661-4669. doi:10.1021/ja209334v

Gray, W. M., Kepinski, S., Rouse, D., Leyser, O., & Estelle, M. (2001). Auxin regulates SCFTIR1-dependent degradation of AUX/IAA proteins. *Nature, 414*, 271. doi:10.1038/35104500

Greenwood, A. I. (2014). *The interaction between the EVH1 domain of VASP and Proline-rich sequences: significance of isomerization, phosphorylation, and a secondary binding site.* (PhD of Biophysics), Cornell University. (2014-02-25T18:39:59Z)

Greenwood, A. I., Rogals, M. J., De, S., Lu, K. P., Kovrigin, E. L., & Nicholson, L. K. (2011). Complete determination of the Pin1 catalytic domain thermodynamic cycle by NMR lineshape analysis. *J Biomol NMR, 51*(1-2), 21-34. doi:10.1007/s10858-011-9538-9

Hanes, S. D. (2015). Prolyl isomerases in gene transcription. *Biochim Biophys Acta, 1850*(10), 2017-2034. doi:10.1016/j.bbagen.2014.10.028

Harbeck, B., Huttelmaier, S., Schluter, K., Jockusch, B. M., & Illenberger, S. (2000). Phosphorylation of the vasodilator-stimulated phosphoprotein regulates its interaction with actin. *J Biol Chem, 275*(40), 30817-30825. doi:10.1074/jbc.M005066200

Hsu, T., McRackan D Fau - Vincent, T. S., Vincent Ts Fau - Gert de Couet, H., & Gert de Couet, H. (2001). Drosophila Pin1 prolyl isomerase Dodo is a MAP kinase signal responder during oogenesis. (1465-7392 (Print)).

Kang, B., Zhang, Z., Wang, L., Zheng, L., Mao, W., Li, M., . . . Mo, X. (2013). OsCYP2, a chaperone involved in degradation of auxin-responsive proteins, plays crucial roles in rice lateral root initiation. *Plant J, 74*(1), 86-97. doi:10.1111/tpj.12106

Krause, M., Leslie, J. D., Stewart, M., Lafuente, E. M., Valderrama, F., Jagannathan, R., . . . Gertler, F. B. (2004). Lamellipodin, an Ena/VASP Ligand, Is Implicated in the Regulation of Lamellipodial Dynamics. *Developmental Cell, 7*(4), 571-583. doi:https://doi.org/10.1016/j.devcel.2004.07.024

Langridge, J. (1957). Effect of Day-length and Gibberellic Acid on the Flowering of Arabidopsis. *Nature, 180*, 36. doi:10.1038/180036a0

Lu, K. P., Finn, G., Lee, T. H., & Nicholson, L. K. (2007). Prolyl cis-trans isomerization as a molecular timer. *Nat Chem Biol, 3*(10), 619-629. doi:10.1038/nchembio.2007.35

Machner, M. P., Urbanke, C., Barzik, M., Otten, S., Sechi, A. S., Wehland, J., & Heinz, D. W. (2001). ActA from Listeria monocytogenes can interact with up to four Ena/VASP homology 1 domains simultaneously. *J Biol Chem, 276*(43), 40096-40103. doi:10.1074/jbc.M104279200

Mai, Y. X., Wang L Fau - Yang, H.-Q., & Yang, H. Q. (2011). A gain-of-function mutation in IAA7/AXR2 confers late flowering under short-day light in Arabidopsis. (1744-7909 (Electronic)).

Maruoka, M., Sato, M., Yuan, Y., Ichiba, M., Fujii, R., Ogawa, T., . . . Watanabe, N. (2012). Abl-1-bridged tyrosine phosphorylation of VASP by Abelson kinase impairs association of VASP to focal adhesions and regulates leukaemic cell adhesion. *Biochem J, 441*(3), 889-899. doi:BJ20110951 [pii] 10.1042/BJ20110951

Nechama, M., Kwon, J., Wei, S., Kyi, A. T., Welner, R. S., Ben-Dov, I. Z., . . . Lu, K. P. (2018). The IL-33-PIN1-IRAK-M axis is critical for type 2 immunity in IL-33-induced allergic airway inflammation. *Nat Commun, 9*(1), 1603. doi:10.1038/s41467-018-03886-6

Pastorino, L., Sun, A., Lu, P.-J., Zhou, X. Z., Balastik, M., Finn, G., . . . Lu, K. P. (2006). The prolyl isomerase Pin1 regulates amyloid precursor protein processing and amyloid-β production. *Nature, 440*, 528. doi:10.1038/nature04543

https://www.nature.com/articles/nature04543#supplementary-information

Petit, M. M., Fradelizi, J., Golsteyn, R. M., Ayoubi, T. A., Menichi, B., Louvard, D., . . . Friederich, E. (2000). LPP, an actin cytoskeleton protein related to zyxin, harbors a nuclear export signal and transcriptional activation capacity. *Mol Biol Cell, 11*(1), 117-129.

Rogals, M. J., Greenwood, A. I., Kwon, J., Lu, K. P., & Nicholson, L. K. (2016). Neighboring phosphoSer-Pro motifs in the undefined domain of IRAK1 impart bivalent advantage for Pin1 binding. *The FEBS Journal, 283*(24), 4528-4548. doi:10.1111/febs.13943

Tan, X., Calderon-Villalobos, L. I., Sharon, M., Zheng, C., Robinson, C. V., Estelle, M., & Zheng, N. (2007). Mechanism of auxin perception by the TIR1 ubiquitin ligase. *Nature, 446*(7136), 640-645. doi:10.1038/nature05731

Wang, Y., Liu C Fau - Yang, D., Yang D Fau - Yu, H., Yu H Fau - Liou, Y.-C., & Liou, Y. C. (2010). Pin1At encoding a peptidyl-prolyl cis/trans isomerase regulates flowering time in Arabidopsis. (1097-4164 (Electronic)).

Yao, J. L., Kops O Fau - Lu, P. J., Lu Pj Fau - Lu, K. P., & Lu, K. P. (2001). Functional conservation of phosphorylation-specific prolyl isomerases in plants. (0021-9258 (Print)).

Zhang, Y., Tu, Y., Gkretsi, V., & Wu, C. (2006). Migfilin interacts with vasodilator-stimulated phosphoprotein (VASP) and regulates VASP localization to cell-matrix adhesions and migration. *J Biol Chem, 281*(18), 12397-12407. doi:10.1074/jbc.M512107200

Zheng, Z., Yang, X., Fu, Y., Zhu, L., Wei, H., & Lin, X. (2017). Overexpression of PvPin1, a Bamboo Homolog of PIN1-Type Parvulin 1, Delays Flowering Time in Transgenic Arabidopsis and Rice. *Frontiers in Plant Science, 8*, 1526.

Zhu, Z.-X., Liu, Y., Liu, S.-J., Mao, C.-Z., Wu, Y.-R., & Wu, P. (2012). A gain-of-function mutation in OsIAA11 affects lateral root development in rice. *Molecular Plant, 5*(1), 154-161.

Zhu, Z. X., Liu, Y., Liu, S. J., Mao, C. Z., Wu, Y. R., & Wu, P. (2012). A gain-of-function mutation in OsIAA11 affects lateral root development in rice. *Mol Plant, 5*(1), 154-161. doi:10.1093/mp/ssr074

Zimmermann, J., Labudde, D., Jarchau, T., Walter, U., Oschkinat, H., & Ball, L. J. (2002). Relaxation, Equilibrium Oligomerization, and Molecular Symmetry of the VASP (336-380) EVH2 Tetramer. *Biochemistry, 41*, 11143-11151.

APPENDIX

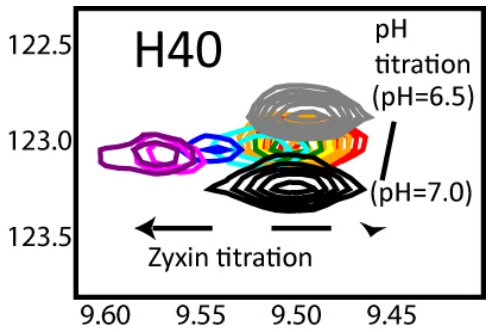

Appendix Figure 2.1. pH titration compared to Zyxin titration. Overlay of the ^{15}N-^{1}H HSQC H40 region at pH=6.5 (gray), pH=6.67 (red) and pH=7.0 (black), as well as the titration with Zyxin$^{41-140}$ at pH=6.67 (orange, yellow, green, cyan, blue, magenta, purple).

The proximity of H40 to the secondary binding site and the fact that experiments were acquired at pH 6.67 (within the typical His sidechain pKa range) raises the possibility that chemical shift changes at the secondary site during Zyxin$^{41-140}$ titration could be due to slight changes in pH. To rule out this possibility, peak trajectories were mapped for pH titration in the range of 6.65 to 7.0. Reassuringly, the pH-dependent peak trajectories differ completely from those induced by titration with Zyxin$^{41-140}$, as exemplified by H40 (Fig. S1), demonstrating that the chemical shift changes observed in the Zyxin$^{41-140}$ titration are not due to potential changes in pH during the titration.

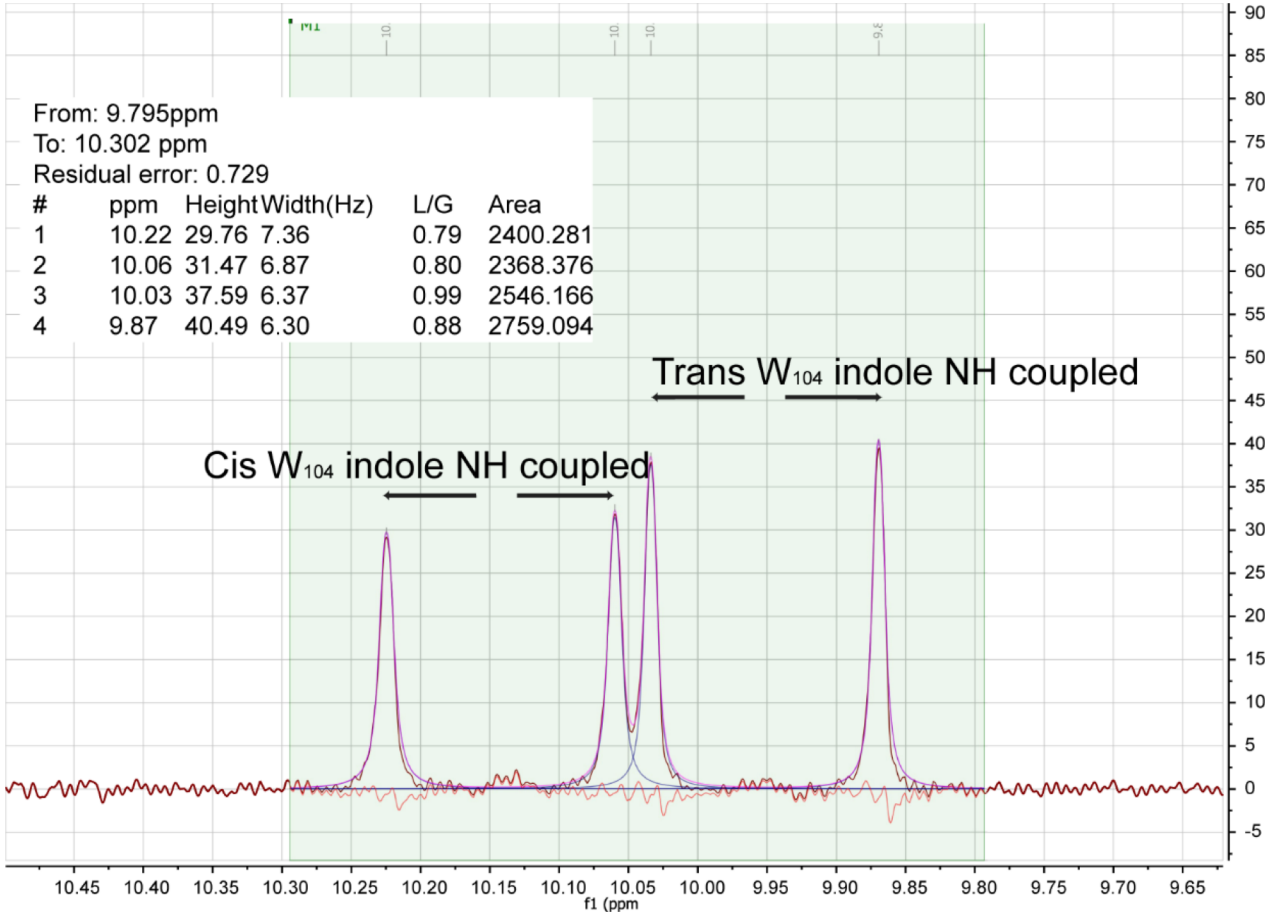

Appendix Figure 4.1. ^{1}D-Integration Lorentzian using MNOVA software to calculate the equilibrium constant between free trans and free cis isomer of ^{104}W-P^{105}. Water gate pulse was used, NH coupled.

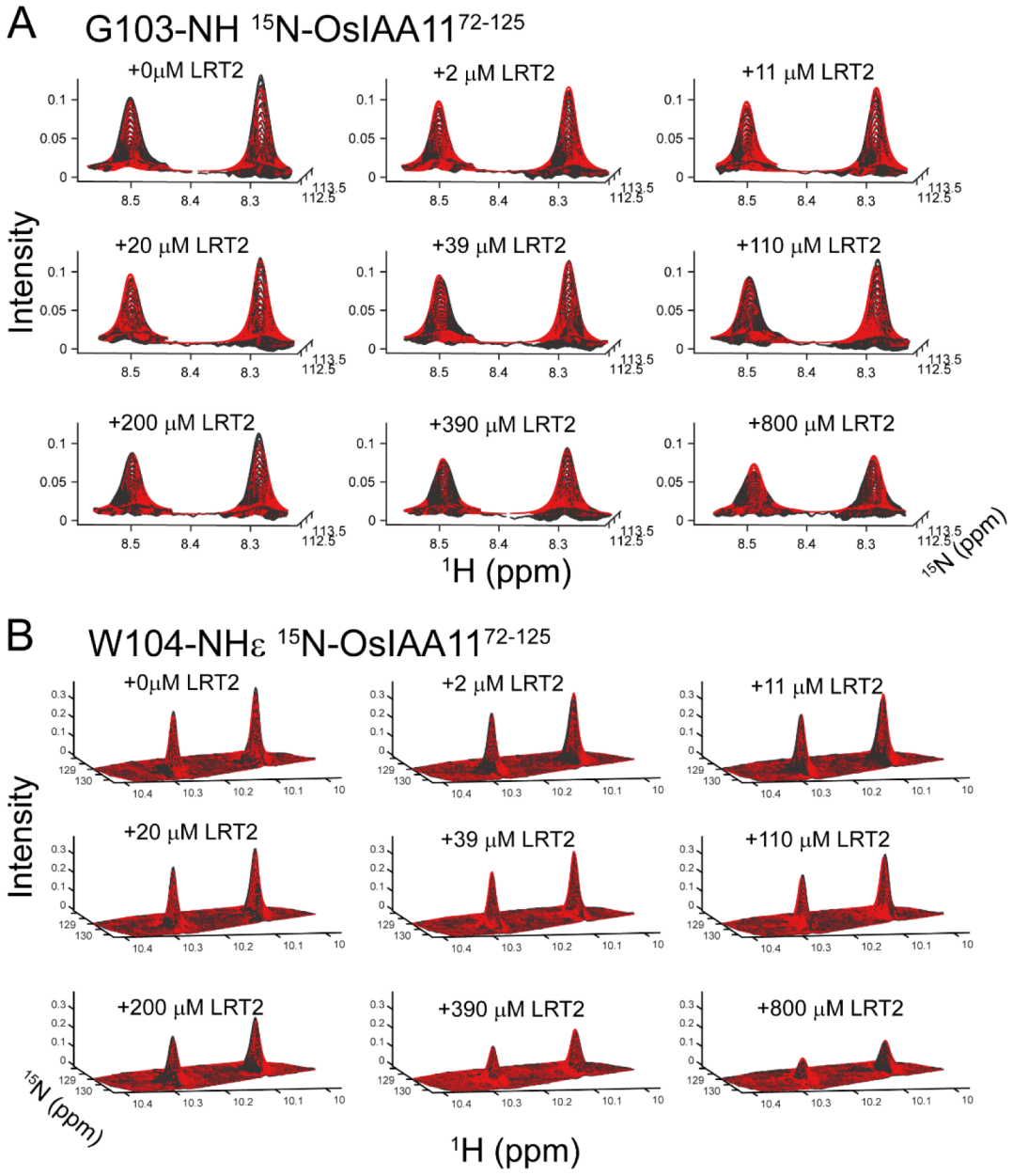

Appendix Figure 4.2 2D Lineshape simulation for ^{15}N-OsIAA11$^{72-125}$ upon titration with unlabeled LRT2, analysis with TITAN. A. ^{15}N-^{1}H-HSQC of G103 HN lineshape for varying amount of LRT2, data (black) compare to simulated with scalar coupling between HN and Ha of 6.5 Hz and found microscopic kinetic rates (red). **B.** ^{15}N-^{1}H-HSQC of W104 HN indole lineshape for varying amount of LRT2, data (black) compare to simulated with scalar coupling between HN indole and Hδ of 3 Hz and found microscopic kinetic rates (red).

Appendix Table 5.1. Primers used for mutagenesis of LRT2

Primer Name	Primer Sequence 5' to 3'
LRT2-NdeI-FW	ACTAATCATATGATGTCGAACACGAGGGTGTTCTTCGAC ATGACCGTCGGCGG
LRT2-HindIII-Rev	AACATAAAGCTTCTAGGAGAGCTGGCCGCAGTCGGCGA TGACGACCGGCTTGGC
H61Q LRT2 FW	AGC ACC TTC CAA CGC GTG ATC
H61Q LRT2 Rev	GAT CAC GCG TTG GAA GGT GCT
R62A LRT2 FW	AGC ACC TTC CAC GCA GTG ATC
R62A LRT2 Rev	GAT CAC TGC GTG GAA GGT GCT
G72A LRT2 FW	ATG TGC CAG GGC GCA GAC TTC A
G72A LRT2 Rev	TT GCC GCG GGT GAA GTC TGC GCC
Q118A LRT2 FW	ACT AAC GGG TCC GCG TTC TTC ATC
Q118A LRT2 Rev	GAT GAA GAA CGC GGA CCC GTT AGT
F120A LRT2 FW	TCC CAG TTC GCC ATC TGC A
F120A LRT2 Rev	GCA GGG CAC GGT GCA GAT GGC GAA
P125K LRT2 FW	ATC TGC ACC GTG AAA TGC AGC TGG CT
P125K LRT2 Rev	CCC GTC CAG CCA GCT GCA TTT CAC
V124A/P125K/C126T/S127E LRT2 FW	CAG TTC TTC ATC TGC ACC GCG AAA ACC GAA TGG
V124A/P125K/C126T/S127E LRT2 Rev	GTC CAG CCA TTC GGT TTT CGC GGT GCA GAT GAA
W128A LRT2 FW	AGC GCG CTG GAC GGG AAG CAC GTC GTG TTC
W128A LRT2 Rev	TC CAG CGC GCT GCA GGG CAC
H133Q LRT2 FW	TG GAC GGG AAG CAA GTC GTG TT
H133Q LRT2 Rev	AA CAC GAC TTG CTT CCC GTC CA